63-2-4

296 020

Office of Naval Research
Contract Nonr-3639(00)
Task No. NR 099-363

A STUDY PROGRAM ON CESIUM VAPOR-FILLED THERMIONIC CONVERTERS HAVING IRIDIUM EMITTERS

Yearly Summary Report

1 November 1961 - 31 October 1962

MND - 2934

BY:

M. E. Talaat
D. S. Trimmer
A. J. Kennedy

Approved by:

M. E. Talaat

M. E. Talaat, Manager
Energy Conversion R&D Laboratories
Nuclear Division

Martin Marietta Corporation
Baltimore 3, Maryland
December 1962

FOREWORD

This report presents the work accomplished under Contract Nonr-3639(00) for the period 1 November 1961 to 31 October 1962.

The research was carried out in the Energy Conversion R&D Laboratories of the Martin Marietta Corporation, Nuclear Division. The laboratories are under the direction of Dr. M. E. Talaat.

The program was carried out under the auspices of the Power Branch of the Office of Naval Research and was sponsored by Comdr. John J. Connelly.

ABSTRACT

An extensive mapping of the performance of cesium vapor-filled energy conversion devices was obtained for the high vacuum work function emitter materials, iridium and rhenium, for the interelectrode gap of .030". Characteristic current-versus-voltage curves and summaries of the output power density and efficiency are given for the emitter temperature range of 1550-2000°K and the cesium temperature range of 475-600°K. The data shows a systematic superiority of iridium to rhenium.

Tests with a platinum emitter device confirm the trend of good performance in cesium vapor with high vacuum work function emitter materials.

Data is given showing a highly precise agreement between two iridium filament emitter devices and an electron bombardment heated device with iridium emitter. At the emitter temperature of 1700°K, liquid cesium temperature of 525°K, and interelectrode gap of .030", the output power density of the three devices was 5.6 ± 0.2 w/cm^2 and the energy conversion efficiency was 14.25 ± 1.25%.

The program includes a theoretical study of cesium adsorption phenomena on the electrode surfaces and of plasma phenomena in the interelectrode gap. The theory is used to predict the characteristic voltage-current curve in the volume ionization mode of operation, and is applied to the test data.

TABLE OF CONTENTS

I. INTRODUCTION

The objective of this program is the study of the performance of cesium vapor-filled thermionic energy conversion devices which utilize, as the emitter material, the high vacuum work function metals iridium, rhenium, platinum, and rhodium. Particular emphasis was placed on the study of the iridium emitter which, on the basis of tests conducted in this laboratory prior to the initiation of this contract, had been judged to be of particular importance in attaining the objective of research in thermionic energy conversion, namely, the realization of output power densities of the order of 10 watts/sq cm and conversion efficiencies over 13% at emitter temperatures and interelectrode spacings which are compatible with reliable performance and long life.

For the purpose of fulfilling this objective, a program having three parts was carried out. In one part tests were made with filament devices to provide a mapping of the performance of the energy conversion device as a function of emitter temperature and liquid cesium temperature. In another part, a theoretical program contributed to the understanding of the physical phenomena underlying the performance of thermionic energy converters. The theoretical program considered two subjects of interest, namely, the plasma phenomena in the interelectrode gap and the adsorption phenomena on the electrode surfaces. The third part of the program entailed the design, fabrication, and test of a large-area, electron bombardment heated cylindrical device with iridium as the emitter material. This device provided an important corroboration of some of the test results obtained with the iridium emitter filament device.

II. SUMMARY

The tests with filament devices provided extensive mapping of the performance of thermionic energy conversion devices having iridium and rhenium as the emitter material. The devices had nickel collectors and an interelectrode gap of 0.030". Characteristic current vs voltage curves, in the emitter temperature range of 1550-2000°K and in the cesium temperature range of 475-600°K, were measured for iridium and rhenium and are presented in Section IV. Since the devices used were identical except for the emitter material, a systematic comparison of the performance of iridium to that of rhenium was obtained. The data shows a slight, though clearly systematic, superiority of iridium to rhenium.

A device with platinum emitter was also tested. The test indicated that the performance of the platinum emitter is comparable to that of iridium and rhenium, thus confirming that platinum continues the trend of good performance, in cesium vapor, with high vacuum work function emitter materials.

In testing the fourth emitter material, rhodium, difficulties were encountered due to the problem of maintaining a rhodium filament in tension and in alignment.

The theoretical part of the program treated the two principal aspects of the theory of vapor-filled thermionic energy converters. First, there is the study of the plasma phenomena in the interelectrode gap. This study is concerned with the transport of the charge carriers from the emitter to the collector under the conditions of space charge sheaths, either positive or negative, near the electrodes, and a quasi-neutral plasma which fills the major portion of the interelectrode gap. The theory clearly differentiates two modes of operation, namely, the surface ionization mode in which ions are generated mainly at the emitter surface, and the volume ionization mode in which the performance of the device is characterized by the ionization of cesium in the interelectrode gap by energetic electrons of the plasma.

The second subject for theoretical study has been the adsorption of cesium on the electrode surfaces. A relatively simple model of the adsorbed cesium was shown to be in quantitative agreement with the experiment of Taylor and Langmuir on the adsorption of cesium on tungsten. Application of this model to high vacuum work function material in cesium vapor shows clearly the basis for the large electron emission at relatively low values of cesium pressure which is fundamental to the superior performance of the high vacuum work function emitter materials.

A discussion of the theoretical studies is given in Section VII. Specific calculations, relating theory to measured performance in the volume ionization mode of operation, are given.

The third principal part of this program was concerned with the development and test of an electron bombardment heated device. The emitter of this device was a hollow cylinder of iridium; a wire was strung inside the hollow cylinder and served as a radiation and electron bombardment heater.

A leak developed, as a result of an embrittlement in the expansion joints, before the device could be tested over a full range of the parameters. However,

an important corroboration of the data of the filament devices was obtained. This discussion is in Section VI of this report, and a characteristic curve is given which shows highly precise agreement between the data of two filament emitter devices and this large area electron bombardment heated device at the liquid cesium temperature of approximately 525°K and the emitter temperature of 1700°K. The output power density at this operating point is 5.6 ± 0.2 watts/sq cm and the conversion efficiency is 14.25 ± 1.25%. Also of importance is the fact that the characteristic curve at the operating power was not affected by a difference of collector temperature from 603°K to 783°K.

III. CONCLUSIONS AND RECOMMENDATIONS

The primary conclusion which may be drawn from the program is the desirability of the materials iridium and rhenium for use as the emitter of cesium vapor-filled thermionic energy conversion devices. Of particular significance is the fact that the power densities from a few watts/sq cm to over ten watts/sq cm and energy conversion efficiencies of 10-17% were obtained at the relatively large interelectrode gap of 30 mils. The ability to use such a spacing (as opposed to conventional spacings of 1-5 mils) will be a key factor when a useful application requires the fabrication of hundreds or thousands of individual cells. The wide interelectrode spacing and the consequent coarse tolerance on the spacing will be essential to the production of large numbers of units with a requirement of extremely high reliability.

A second conclusion of great importance is brought out in Section VI, where the characteristic curves of three different iridium emitter devices are matched with very good agreement at a practical operating point. Lack of reproducibility of performance, due to microscopic differences in emitter surface between one device and another, have often characterized thermionic measurement. In this case, very good agreement was obtained between two devices having iridium filaments as the emitter and a third device whose iridium emitter was fabricated from a solid piece of iridium which had been prepared by sintering.

The ultimate goal of research in thermionic energy conversion is the development of energy conversion units having the extremely high reliability necessary for application in useful, nuclear fueled systems. Mindful of this goal, the following two factors should be given prominence in further experimental research with the high vacuum work function emitter materials.

A. Dependence of Performance on Interelectrode Spacing - This program emphasized tests at the relatively large interelectrode spacing of .030". As remarked above, the ability to use wide spacing is of great importance in obtaining a capability of fabricating reliable devices. Nevertheless, the dependence of performance on spacing must be carefully examined.

B. Reproducibility of the Data - Sound engineering of a reliable system will require thermionic data which has been reproduced, over and over again, with many test devices. Though the agreement which has been shown with three iridium devices makes an important contribution to the study of the reproducibility and reliability of the data, it must be recognized that this is just a first step toward the compilation of data with precisely known reliability. In this connection, it should be pointed out that the corroboration of the test results of the filament devices with data from large area devices has thus far been carried out over only a part of the range of the parameters emitter temperature and cesium temperature.

Both of these areas of study will be given prominence in the continuation of this program. Flat plate, variable spacing devices will be used to study the performance of the iridium and rhenium emitter over a range of spacings from .010" to .050". Though the scope of the next year's program does not allow a thorough investigation of the reproducibility of the thermionic data, the testing of additional devices will nevertheless contribute to the resulution of the problem of reproducibility.

IV. TEST RESULTS WITH FILAMENT EMITTER DEVICES

A. Introduction

Tests with metal enveloped filament emitter devices, identical except for the emitter material, were made. These tests showed excellent performance in cesium vapor with both iridium and rhenium emitters, and a systematic superiority of iridium to rhenium was indicated over a wide range of emitter temperatures and cesium pressures. Tests made with a glass enveloped device having a platinum emitter also gave indications that the performance in cesium vapor of the platinum emitter may be comparable to the performance obtained with the rhenium and iridium.

In this section the data obtained with three devices is presented. The devices are:

Emitter	Collector	Interelectrode Gap	Envelope
Iridium	Nickel	.030	Metal
Rhenium	Nickel	.030	Metal
Platinum	Nickel	.030	Glass

Detailed summaries of the dependence of output power density and efficiency on the emitter temperature and cesium temperature have been obtained for iridium and rhenium. These summaries have been obtained for both the volume ionization mode of operation and the surface ionization mode of operation and are given in Section IV.E.

A detailed description of the devices is contained in Section VIII, "Procedure." The procedure section also discusses the testing procedure and various other factors relevant to the obtaining of the data.

B. Iridium Emitter

Characteristic current vs voltage curves for the iridium emitter device are given in Figs. 1-6. Each figure shows a family of curves taken at a liquid cesium temperature. Though a certain degree of scatter is apparent in the experimental data, a smooth variation in the performance with changes in emitter temperature is clearly shown in each figure.

The characteristic curves show the two modes of operation which characterize the performance of the plasma thermionic energy converter, namely the volume ionization mode of operation and the surface ionization mode of operation.

In some instances, particularly at the lower emitter temperature (see, for example, Fig. 4) abrupt transitions from the surface ionization mode to the volume ionization mode are observed. In these measurements, the output voltage is decreased from its open circuit valve and the transition from the surface ionization mode to the volume ionization mode is represented on the figure by a dashed line.

At the higher values of emitter temperature the two modes tend to merge into a combined mode of operation and the transition is seen as a change in the slope of the characteristic curve.

The curves are shown on a semi-logarithmic scale which does not include explicitly the open circuit voltage. For this reason, the measured open circuit voltage is shown on the bottom axis of the scale, and is connected by a dashed line to the lowest measured value of output current density.

Figures 1 and 2 show the liquid cesium temperatures of 474°K and 498°K. These temperatures are well below optimum and the output power density of the device is quite low. Note the crossing of the curves near short circuit. Such behavior at these low cesium vapor pressures are typical of the S-type performance of the cesium covered emitter. The emitter work function is a function of cesium coverage, hence a function of emitter temperature. Under some conditions, the reduction in work function, with reduction of emitter temperature, is sufficiently large that the emission current density increases as the emitter temperature is decreased.

Figure 3 shows the characteristic curves at a liquid cesium temperature of 525°K. Though the temperature is well below optimum in regard to output power density, the characteristic curves show performance which would be appropriate for application to useful systems. In particular, the output voltages tend to be higher than those obtained at the optimum liquid cesium temperature (viz., 575°K).

Figure 4 shows the characteristic curves at the liquid cesium temperature of 556°K. The output power densities have increased over those obtained at 525°K.

Figure 5 shows the characteristic curves at the liquid cesium temperature of 575°K. These curves show the best output power density which was obtained in the testing of this device. Note that the curves stop at an output current density of about 30 amps/cm^2 (as discussed in the section on procedure, this was done because of a limit on the input power which can be applied to a filament emitter.) The curves suggest that even higher values of output power density are obtainable at this cesium temperature at the emitter temperature of 1740°K and below. The curves at the higher values of emitter temperature, however, show a tendency to approach a saturation value.

Figure 6, the characteristic curves taken at the liquid cesium temperature of 596°K, shows performance at a higher liquid cesium temperature than the optimum. No saturation is indicated at current densities of 30 amp/cm^2 or lower. Nevertheless, the voltage at which the current rises sharply is now considerably lower than the voltage at the lower liquid cesium temperature.

In summary, the following trends in the behavior of the characteristic curves are consistently observed as the liquid cesium temperature is increased from 525°K to 596°K.

1. The surface ionization mode of operation is clearly distinguishable from the volume ionization mode of operation particularly for emitter temperatures of 1740°K or lower. At higher emitter temperatures there is a tendency for the two modes to merge together indicating that the device operates in a combined mode at these emitter temperatures.

2. At each liquid cesium temperature the characteristic curves are generally translated to higher output voltages as the emitter temperature is increased.

3. The slope of the characteristic curves in the volume ionization mode of operation becomes steeper as the liquid cesium temperature is increased.

4. The characteristic curves are generally translated to lower output voltages as the liquid cesium temperature is increased.

As discussed in Section VII, these trends are in general agreement with the theory.

C. Rhenium Emitter

The characteristic current vs voltage curves for the rhenium emitter are shown in Figs. 7-12. The rhenium data was obtained for the same emitter temperature region, and at approximately the same values of liquid cesium temperature, as was the iridium data.

The trends shown by the data are quite similar to those of the iridium data, Figs. 1-6. The best liquid cesium temperature was again 575°K. Generally, at all liquid cesium temperatures the output voltages, hence the output power densities, of the rhenium emitter device are somewhat lower, particularly at the lower emitter temperatures, than those obtained with the iridium emitter device. (See Section IV.E in which the output power density and efficiency of the two devices are given as a function of the emitter temperature and liquid cesium temperature.)

Note that even at the relatively low liquid cesium temperature of 525°K saturation currents of over 10 amps/cm^2 are obtained. The fact that there are high saturation currents at relatively low cesium pressures is of great importance in the performance of the rhenium emitter device at the large interelectrode gap of 30 mil. The emitter work function is a function of cesium pressure and can be lowered, even to values below 2 ev, merely by increasing the cesium pressure; however, an increase in pressure will ultimately result in a degeneration of performance due to power losses in the interelectrode gap (see Section VII on Theory). This is shown by the characteristic curves at a liquid cesium temperature of 598°K, which shows a drop in output voltage from that at 575°K. With this rhenium emitter saturation currents in excess of 10 amps/cm^2 are obtained at the liquid cesium temperature of 525°K, and at 575°K the saturation currents are in excess of 30 amps/cm^2. It can be presumed that the high power densities, obtained with an interelectrode gap of 30 mil, are a result of the fact that large saturation currents can be obtained at liquid cesium temperatures sufficiently low so that the power losses in the interelectrode gap are not significant.

The characteristic curves for rhenium can also be seen to generally follow the trends emmerated in the discussion of the results on the iridium emitter device.

D. Platinum Emitter

The testing of the platinum device followed a somewhat different procedure than the testing of the iridium and rhenium devices. In the first place, the device had guard rings, thereby assuring that the output current of the device was obtained

from a section of the filament emitter with well-defined area. In the second place, the method of obtaining the characteristic curve was different. For this method of taking data, the load was varied by means of a 60 cps sweep voltage in the external circuit, and the simultaneous values of output current and output voltage were recorded by photographing the trace on an X-Y oscilloscope.

Figure 36 shows a typical photograph of a characteristic curve obtained in this manner. The picture shows the rise of current as the output voltage is decreased from open circuit to short circuit, and also shows the retracing of the curve as the voltage is again increased to the open circuit condition. Note that the curve does not retrace itself exactly, but shows the double valued behavior typical of the transition from the surface ionization mode of operation to the volume ionization mode of operation.

Figure 32 shows a family of characteristic current vs voltage curves taken at the liquid cesium temperature of 487°K. The best output power density shown in these curves is of the order of 1.75 w/cm^2 which occurs at the emitter temperature of 1765°K. Figure 34 shows another family of curves taken at the liquid cesium temperature of 568°K. At 1765°K a power density of the order of 4.4 w/cm^2 was obtained.

These characteristics do not show the best power density which can be obtained under these conditions, since the output current density was still rising with voltage at the lowest value of output voltage at which measurements were made. In Fig. 35 the performance at an emitter temperature of 1765°K and at a liquid cesium temperature of 569°K is shown to have an output power density of the order of 8.8 w/cm^2.

Figure 35 also provides a test of the validity of the data taken with a 60 cps sweep. Since the curves are shown to be independent of the magnitude of the sweep it is indicated that transient responses do not significantly affect the performance of the device.

Figure 33 was the characteristic curve obtained at the emitter temperature of 1655°K at the liquid cesium temperature of 514°K. The output power density of the order of 3 w/cm^2 which was obtained in this run is particularly significant because of the relatively low value of emitter temperature.

E. Summary of Output Power Density and Efficiency

The curves presented in this section give a detailed summary of the dependence of the output power density and energy conversion efficiency on the emitter temperature and the liquid cesium temperature. The curves are drawn through experimentally measured values of output power density; the values of the efficiency at measured output points were determined according to the procedure given in Section VIII.

In general, the trends shown by the data are the same for the iridium and rhenium emitter materials. Nevertheless, a slight, though clearly systematic superiority of iridium to rhenium is indicated throughout the range of emitter temperature and liquid cesium temperature. Figure 28 compares the best observed values of the output power density and efficiency of iridium to those obtained with rhenium.

The curves give summaries for both the volume ionization and the surface ionization modes of operation. The high levels of output power density and efficiency occur in the volume ionization mode of operation. The data for the surface ionization mode of operation is also of interest since it displays smooth trends in the

dependence of performance on emitter temperature and liquid cesium temperature.

1. Volume Ionization Mode of Operation

The following figures are given for the volume ionization mode of operation:

Iridium Emitter

Figure 13 - Output power density versus emitter temperature, parametric in liquid cesium temperature

Figure 14 - Efficiency versus emitter temperature, parametric in liquid cesium temperature

Figure 15 - Output power density versus liquid cesium temperature, parametric in emitter temperature

Figure 16 - Efficiency versus liquid cesium temperature, parametric in emitter temperature

Rhenium Emitter

Figure 17 - Output power density versus emitter temperature, parametric in liquid cesium temperature

Figure 18 - Efficiency versus emitter temperature, parametric in liquid cesium temperature

Figure 13, output power density versus emitter temperature, parametric in liquid cesium temperature, shows that an optimum cesium temperature, in the neighborhood of 575°K, is indicated for the iridium. This is presumably a characteristic of the 30 mil interelectrode gap.

Note that, at the lower values of cesium temperature, the output power density decreases with increasing emitter temperature. This is typical of the performance at low cesium vapor pressures, since an increase in emitter temperature results in a lowering of the work function which, in some ranges of cesium pressure and emitter temperature, results in a lowering of the thermionic current.

The curve at the liquid cesium temperature of 596°K, a temperature above the optimum value, rises sharply with emitter temperature, crossing the other curves. This is typical of the behavior at high vapor pressures. The curve suggests that at the high emitter temperatures the optimum liquid cesium temperature is above 575°K.

Figure 14, efficiency versus emitter temperature, parametric in liquid cesium temperature, shows that these efficiency curves display the same trends as the power density curves. However, the efficiency curves do not show as sharp a sensitivity to the liquid cesium temperature as do the output power density curves. Thus, at liquid cesium temperatures at which the power density is considerably reduced from its best value, the energy conversion efficiency remains greater than 10%, i.e., in a region which is suitable for practical application.

Figure 15 shows the output power density versus cesium temperature, parametric in emitter temperature. These curves contain the same information as those

of Fig. 13; however, the different manner of plotting displays more clearly the dependence on cesium temperature. The curves are quite close together and show a clear crossing at about 525°K. Below this temperature the output power density decreases with increasing emitter temperature, while above this temperature the output power density is increased with increasing emitter temperature.

A note on the internal consistency of the data is appropriate at this point. The data was not taken in the order of increasing liquid cesium temperature; in fact, the data at the liquid cesium temperature of 525°K was the last to be taken. At this liquid cesium temperature the output power density falls where it is expected, not only with regard to the magnitude (4-6 w/cm^2), but also with regard to the dependence of output power density on emitter temperature (it tends to be the cross-over point, at which the output power density is only slightly dependent on emitter temperature).

Figure 16 shows the efficiency versus liquid cesium temperature, parametric in emitter temperature. These curves tend to display the same trends as the curves of output power density, Fig. 15.

For the rhenium emitter device, Fig. 17 shows the output power density and Fig. 18 the energy conversion efficiency, plotted versus emitter temperature, parametric in liquid cesium temperature.

In general, the same trends are displayed by the rhenium data as by the iridium data. The best performance was measured at the liquid cesium temperature of 575°K. The curve at the liquid cesium temperature of 597°K suggests that, for the higher emitter temperature, the optimum liquid cesium temperature may be higher than 575°K. The performance of the rhenium emitter device is rather lower than that of the iridium emitter device and this can be seen well on comparison of the efficiency curves, Figs. 14 and 18. The range of emitter temperature and liquid cesium temperature for which the energy conversion efficiency is greater than 10% is considerably narrower for the rhenium than it is for the iridium.

2. Surface Ionization Mode of Operation

The following families of curves are given for the surface ionization mode of operation.

Iridium Emitter

Figure 19 - Output power density versus emitter temperature, parametric in liquid cesium temperature

Figure 20 - Efficiency versus emitter temperature, parametric in liquid cesium temperature

Figure 21 - Output power density versus liquid cesium temperature, parametric in emitter temperature

Rhenium Emitter

Figure 22 - Output power density versus emitter temperature, parametric in liquid cesium temperature

Figure 23 - Output power density versus liquid cesium temperature, parametric in emitter temperature

Figure 24 - Efficiency versus emitter temperature, parametric in liquid cesium temperature

Consistent trends in the dependence of performance on emitter temperature and on liquid cesium temperature are displayed in these families of curves. Figure 19 shows output power density versus emitter temperature for the iridium. At each liquid cesium temperature, the curve of output power density tends to reach a maximum (though at the lowest liquid cesium temperature, this maximum is indicated to be at a lower emitter temperature than the lowest at which measurements were made). The emitter temperature at which this maximum occurs tends to be higher as the liquid cesium temperature is increased. The best value of output power density increases with increasing emitter temperature, but it appears that there may be an optimum at the emitter temperature of 1840°K.

Generally, similar trends as those discussed for the iridium emitter device in the previous paragraph are also shown for the rhenium emitter device, Figs. 22 and 23. In the case of the rhenium emitter, however, an optimum emitter temperature is not indicated and the best values of output power density and efficiency are obtained at the highest emitter temperature.

Figure 21 gives the output power density versus liquid cesium temperature, parametric in emitter temperature for the iridium emitter device. The envelope of this family of curves gives a clear picture of the dependence of output power density on emitter temperature and liquid cesium temperature for the surface ionization mode of operation. At the liquid cesium temperature of 472°K, the best output power density is obtained at the lowest emitter temperature, 1581°K. As the liquid cesium temperature is increased above 472°K, the curves indicate that the best output power density increases, and is obtained successively at 1633°K and at 1686°K. As higher liquid cesium temperatures are considered, the tendency for the curves to cross continues, and the best output power density occurs at an emitter temperature which increases with increasing liquid cesium temperature.

Figure 21, for the iridium device, shows a maximum power density for the surface ionization mode of operation at the emitter temperature of 1833°K at the liquid cesium temperature of 526°K. For the rhenium data, Fig. 24, the best output power density is found at the highest emitter temperature, 2000°K. There is still an optimum value of liquid cesium temperature, however, as for the rhenium, this is indicated to be in the neighborhood of 547°K.

V. ELECTRON BOMBARDMENT HEATED DEVICE

A. Description of Device

Figure 37 is a sketch of this device showing the important features. The iridium emitter had an outside diameter of 0.315 inch and a length of 0.500 inch; thus, the iridium emitter area was 3.18 cm^2. The inside diameter of the emitter was 0.120 inch. This resulted in a heavy wall thickness (0.0975 inch) which, during operation, helped to maintain a constant temperature over the entire surface of the emitter. The nickel collector had an inside diameter of 0.375 inch; thus the interelectrode gap was 0.030 inch. The collector had a sapphire window attached so that the emitter temperature could be measured optically. This measurement was made by observing into a hohlraum hole (.015 inch diameter and .060 inch deep) placed in the emitter surface. The radiation from the hole is approximately black-body radiation, and therefore the observations are not dependent on the emissivity of the surface. The collector had two large conically shaped fins which permitted the heat delivered to the collector to be dissipated at a fairly low temperature (approximately 700 - 800°K). The device used two ceramic seals to insulate the emitter from the collector. The design of the seals has been used before on other devices, with only slight changes made on the ends of the seals to accomodate changes in configuration. The seal was a columbium metal to aluminum oxide seal using a vanadium braze developed in the Nuclear Division of the Martin Company. The bellows used to take up the differential expansion were fabricated from 0.002 inch thick fansteel #82 (an alloy of tantalum and columbium). Aluminum oxide spacers were used to maintain the alignment of the emitter. Attached to these spacers were radiation shields which were introduced to decrease heat losses due to radiation from the tantalum extensions from the iridium emitter. Two side arms were provided; one was used to evacuate the device while the other held the cesium ampule. Figure 38 shows a view of the completed device.

B. Testing Procedure

1. General

Figure 39 is a photograph of the device ready for test. Most of the device is hidden by a heater surrounding the collector fins, however below this can be seen the end of one of the ceramic seals and the two side-arms.

The electron bombardment heater for this device is simply a short length of tungsten wire supported between two heavy rods whose diameter is 4 to 5 times that of the wire. This structure is held in position by a molybdenum coil spring at the upper end. The heater must be well insulated from the emitter so that high voltage electron bombardment power can be used to heat the emitter. The length of the tungsten wire must be determined by optimizing the efficiency of the device. A length of 1.25 inch was found to work well (not necessarily optimum since not enough data was obtained to determine this parameter).

Emitter heaters with both .010" and .020" diameter tungsten wire were used without any noticeable change in performance. Aluminum oxide sleeves were used on the support rods to help maintain the alignment of the heater.

The tungsten wire is heated to a temperature of about 2600°K with an A.C. voltage. A high positive D.C. voltage (with respect to the heater) is applied to the emitter in order to collect the current emitted by the heater. This supplies the electron bombardment power. The total input power is the sum of this electron bombardment power and the joule heating of the tungsten wire.

Thermocouples were used to monitor the temperature at various places such as collector, outer edge of fin, ceramic seal, cesium ampule, and pump lead. The emitter temperature was monitored with the Shawmeter. The output of the Shawmeter was fed into a controller and recorder. The controller operated a magnetic amplifier saturable reactor system which was placed in the input circuit to the high voltage electron bombardment supply. Thus the emitter temperature was held constant by an automatic control of the electron bombardment voltage, controlled through optical measurement of the emitter temperature.

2. Vacuum Testing

The device is operated in vacuum to thoroughly outgas and clean all parts of the device and to age the emitter.

The device was evacuated using an oil diffusion pump system with a liquid nitrogen cold trap. This system was capable of a pressure of 5×10^{-8} mm Hg. With the device mounted on a bell jar plate, the outside of the device was evacuated to 5×10^{-5} mm Hg. At this point the heater could be turned on and the emitter was brought up to temperature very slowly. As the emitter was heated, gas began to evolve both inside and outside the device. After a total of twelve hours operation (eight hours at $T_E = 1925°K$) the pressure had recovered to 7×10^{-8} mm Hg inside the device.

Before the device was sealed, the capsule was broken by collapsing the thin metal walls around the glass ampule. The cesium was heated slightly to drive off any adsorbed gases. The pressure was still at 7×10^{-8} mm Hg and at this point the device was sealed off from the vacuum system. After the cesium was distilled into the upper portion of the side-arm, the portion of this arm containing the glass from the ampule was removed by use of a welding operation. At this point the device was ready for operation in cesium vapor.

3. Test with Cesium Vapor

The procedure for heating the emitter, and measuring and controlling its temperature, was the same for tests in cesium vapor as it was for the vacuum tests.

The liquid cesium temperature was controlled by means of a heater, placed around the side-arm containing the liquid cesium pool, which was controlled by a controller - saturable reactor system. A thermocouple on the cesium pool was used as the sensing element to control the cesium heater. This temperature, as well as other thermocouples readings, were recorded on a six-point strip chart recorder.

During the operation of the device, the output power was recorded using an ammeter and a voltmeter. The input power was measured at many of the data points by use of a wattmeter for the joule heating of the heater and a voltmeter and ammeter for the electron bombardment power. The load was varied by use of a 50 ampere capacity D.C. power supply.

C. Test Data

Figure 25 shows the characteristic current vs voltage curves which were obtained with this device. The data was obtained at the emitter temperature of 1700°K with the liquid cesium temperature in the range of 413 to 538°K.

These curves show a clear increase of performance with increasing liquid cesium temperature. Note, however, that the voltage of ignition of the volume ionization mode of operation decreases with increasing liquid cesium temperature.

Figure 26, based on the current versus voltage data, displays the output power density as a function of output voltage for the emitter temperature of 1700°K for the various values of liquid cesium temperature.

Figure 27 shows the overall efficiency of this device, i.e. the total output power divided by the total input power. The best values of the overall efficiency are in excess of 9%. Estimates of the thermal efficiency of the device indicate that these overall efficiencies correspond to thermionic efficiencies of (13-15%).

A comparison of the data obtained with this device to that obtained with the filament emitter iridium device is contained in section VI, reproducibility of data.

VI. REPRODUCIBILITY OF DATA

Figure 29 shows a characteristic current-vs-voltage curve for the iridium emitter, with experimental points taken from these devices:

	T_E	T_L	T_C	Gap	P_{out}
MC 1	1686	526	603	.030	5.5
C 1	1700	518	783	.030	5.6
G 14	1718	530	780	.030	5.8

MC 1: Metal enveloped, filament device, discussed in section IV.

C 1: Electron bombardment heated device, discussed in section V.

G 14: Glass enveloped, guard ring, filament device, similar in design to the platinum device geometry discussed in section IV.

The close agreement of the three devices is a most important indication of the reproducibility of the data. At this operating point, at the emitter temperature of 1700 ± 20°K, the output power density is 5.6 ± 0.2 w/cm^2. The overall efficiency of 9.3% which was obtained with the electron bombardment heated device is in close correspondence with the thermionic efficiency of 14.25 ± 1.25% which was obtained with the filament devices.

In addition to the general reliability of the data which can be inferred from fig. 29, three specific factors are shown not to have a substantial effect on the performance of the device. These are:

Collector temperature - Note that the collector temperature of MC 1 is over 175 degrees lower than that of C 1 and G 14. Though the devices show some difference in the surface mode of operation, and the device with the low collector temperature has the highest open circuit voltage, nevertheless the volume ionization mode of operation of the three devices is substantailly the same, independent of collector temperature. (Note, in this connection, that the measurements in the surface mode of operation may not be as accurate as the measurements in the volume ionization mode of operation. This is because a leak resistance, i.e. a high resistance short across one of the seals, would affect the measurement at low values of current but would be insignificant at the high currents obtained in the volume ionization mode of operation).

Geometry - Though the interelectrode gap is the same for the three devices, the geomtry is quite different. In the filament device, the ratio of collector to emitter area is 4 to 1, whereas in the electron bombardment heated device, this ratio is 1.2 to 1. Thus, the geomtry of the electron bombardment heated device, though nominally cylindrical, is a close approximation to that of a flat-plate device.

Note, however, that effects due to geometry may be a function of the cesium pressure. As discussed below, there are discrepancies between the performance of the filament device and that of the electron bombardment heated device at low values of cesium pressure.

Surface Preparation - Since thermionic properties are primarily surface phenomena, involving the orientation of the crystal faces on the surface of the material, one might expect a difference in performance between the filament emitter and the high-density sintered iridium of the electron bombardment heated device. That such differences do not occur indicates that the aging of the emitter, which is carried out in vacuum at high temperature, prior to the introduction of the cesium, has been adequate to provide a surface which has consistent thermionic properties.

Figures 30 and 31 compare data of the filament device with that of the electron bombardment heated device at the relatively low liquid cesium temperature of 473 and 493°K. Note that the performance of the electron bombardment heated device is somewhat higher than that of the filament at 493°K, and is substantially higher at 473°K. Thus, the remarkable agreement at the liquid cesium temperature of 525°K which is shown in fig. 29 is not repeated at the lower liquid cesium temperature.

A plausible explanation for the lack of agreement at low pressure may be the removal of ions from the plasma due to diffusion more readily at the lower pressures than at the high pressures. Consider an ion which leaves the plasma by following a path parallel to the emitter surface. The plasma region of the device is in the form of a right cylinder, where the outer surface is the collector, and the "top" and "bottom" surfaces provide areas for the ions to diffuse out of the plasma. Now the ratio of this area to the emitter area is 0.300 in the case of the filament device, and 0.13 in the case of the electron bombardment heated device. On this basis, the superior performance of the electron bombardment heated device over that of the filament device at the liquid cesium temperatures of 473 and 493°K, corresponding to ion mean free paths of .272 cm and .219 cm, respectively, may be explained qualitatively by the fact that ions may escape the plasma region more readily in the case of the filament device. At the liquid cesium temperature of 525°K, the mean free path is much smaller, .044 cm, and such diffusion effects may be expected to be smaller. It should be noted here that the gap is 0.076 cm.

It is to be noted that the agreement shown by fig. 29 is at a liquid cesium temperature of 525°K, well below the optimum for the filament devices. Data with electron bombardment heated devices was not obtained at higher liquid cesium temperatures, and so the high levels of output power density and efficiency, which were obtained with the filament device at the liquid cesium temperature of 550, 575 and 598°K, remain uncorroborated by the data obtained with large area devices. To examine this operating region with large area, electron bombardment heated devices is the primary objective of the work of the laboratory in the immediate future. Before such corroboration the filament devices near the optimum value of cesium pressure must be regarded as being of a preliminary character. Nevertheless, the operation point of

5.6 ± .2 watts/cm^2, at the emitter temperature of 1700°K and at the relatively wide interelectrode gap of .030", has been strongly substantiated from measurements on three different devices and is of great importance in the reliable applications of thermionic energy conversion to a useful nuclear fueled system.

VII. THEORY

A. GENERAL

There are two principal aspects of the theory of the cesium vapor filled thermionic energy conversion devices. The first aspect is the problem of cesium adsorption on refractory metals, and is concerned with the determination of the work function of the emitter surfaces as a function of emitter temperature and cesium pressure. The second aspect is the theory of plasma phenomena in the interelectrode gap. This problem is concerned with the determination of the characteristic current versus voltage curve, given the emitter temperature, collector temperature, emitter work function, collector work function, cesium pressure, and geometry.

Detailed discussion of the theoretical work which has been carried out in this laboratory is given in references 1, 2 and 3. This work has been supported in part by this contract.

The work may be summarized as follows:

1. Plasma Theory. The theory of the plasma phenomena which underlies the performance of the vapor filled thermionic energy converter has been considered for both the volume ionization mode of operation and the surface ionization mode of operation. The use of the theory and its application to some of the measurements made in this program is given in section B below.

2. Adsorption Theory. A model of the adsorbed cesium is used to compute the energy of evaporation of cesium from a refractory metal surface as a function of the cesium coverage. The theoretical values of the quantity are shown to be in close agreement with the experimental values of Taylor and Langmuir for cesium on tungsten. The model brings out the importance of the vacuum work function to the cesium coverage and shows the basis for the large coverage, (Hence, large work function reduction), at relatively low vapor pressures which is responsible for the superior performance in cesium vapor of the high vacuum work function materials such as iridium and rhenium.

B. HOW TO PREDICT THE VOLTAGE-CURRENT CHARACTERISTIC CURVE OF THE THERMIONIC PLASMA ENERGY CONVERTER WHEN OPERATING IN THE VOLUME IONIZATION MODE OF OPERATION AND COMPARISON WITH THE TEST RESULTS

The salient equations presented in Refs. 1 and 2 for the volume ionization mode of operation which are used in the calculations are represented here for the convenience of the readers. First, it should be remembered that the mode diagram, used in the theoretical treatment of the volume ionization mode of operation, is that shown here in Fig. 42 (also see Fig. 4, Ref. 2 and Fig. 1, Ref. 1). In that diagram ϕ_E and ϕ_C are the emitter and collector work functions, respectively, V_{SE} and V_{SC} are the emitter and collector sheath potentials, V_{SS} is the voltage drop from the emitter sheath edge to the collector sheath edge (i.e., across the interelectrode plasma region), and V is the output voltage. In the following equations I_e is the output electron current density, I_{eE} is the emitter saturation current density, I_p is the diffusion ion current density and I_{ep} is the plasma random electron current density.

The basic equations can now be presented on the basis of this mode diagram as follows:

1. The Voltage Balance Equation, viz.,

$$V = \phi_E - (V_{SE} + V_{SS}) + V_{SC} - \phi_C \ , \tag{1}$$

which can be derived readily by inspection of the mode diagram (also see Ref. 1).

2. The Current Balance Equations

The current balance equation at the emitter is given by

$$I_e = I_{eE} - I_{ep}\exp(-V_{SE}/E_e) \ , \tag{2}$$

which physically states that since the emitter sheath is positive the net electron current from the emitter is the difference between the saturation current, I_{eE}, from the emitter surface minus the current due to the Maxwellian plasma electrons possessing enough energy to overcome the emitter sheath potential barrier, V_{SE}, viz., $I_{ep}\exp(-V_{SE}/E_e)$ where I_{ep} is the random electron current in the plasma, and is given by

$$I_{ep} = en_e \sqrt{\frac{eE_e}{2\pi m_e}} \tag{3}$$

(with n_e = the electron density, E_e = the electron temperature in volts (see Eq. 7) and m_e = electron mass).

Similarly the current balance equation at the collector is given by

$$I_e = I_{ep}\exp(-V_{SC}/E_e) \ , \tag{4}$$

which physically states that the electron current reaching the collector is primarily made of the Maxwellian plasma electrons possessing enough energy to overcome the collector sheath potential barrier, V_{SC}, viz., $I_{ep}\exp -V_{SC}/E_e$.

3. The Energy Balance Equation, viz.,

$$I_{eE}(\phi_E + 2E_T) - (I_{eE} - I_e)(\phi_E + 2E_e) = I_e(V + \phi_C + 2E_e + V_{SS}) \ , \tag{5}$$

which physically states that the net electron cooling of the emitter (the left hand side of the equation) is equal to the output power, I_eV, plus the power lost in the electron heating of the collector, $I_e(\phi_C + 2E_e)$, plus the power lost due to the plasma voltage drop, I_eV_{SS}.

By using the voltage balance equation (Eq. 1) in the energy balance equation (Eq. 5) we arrive at the following interesting relation between the plasma electron temperature, E_e, and the sheath potential difference $(V_{SE} - V_{SC})$, viz.,

$$I_{eE}(2E_e - 2E_T) = I_e(V_{SE} - V_{SC}) \tag{6}$$

where

$$E_e = (kT_e/e) \ , \tag{7}$$

$$E_T = (kT_E/e) \ . \tag{8}$$

T_e and T_E are the electron and emitter temperatures in °K, k = Boltzmann constant, and e = electronic charge.

4. The Electron Temperature, E_e

Equations (2) and (4) when solved for the sheath potential difference in terms of the electron temperature and load current yield the following relation

$$V_{SE} - V_{SC} - E_e\ln\frac{I_{ep}}{I_{eE} - I_e} - E_e\ln\frac{I_{ep}}{I_e} = E_e\ln\frac{I_e}{I_{eE} - I_e} \tag{9}$$

This relation in conjunction with the energy balance relation derived in Eq. (3) yield an expression from which the electron temperature can be determined for any chosen electron load current density

$$E_e\left(2 - \left(\frac{I_e}{I_{eE}}\right)\ln\frac{I_e}{I_{eE} - I_e}\right) = 2E_T \ . \tag{10}$$

If we designate by γ the ratio of the emitter temperature to the electron temperature, $\gamma = (E_T/E_e)$, and by z the ratio of the electron load current density to the emitter saturation current, $z = (I_e/I_{eE})$, we get the normalized relation between the electron load current density and the electron temperature

$$\gamma = 1 - 0.5z\ln\frac{z}{1-z} \tag{11}$$

which can be readily used to calculate γ once z is chosen.

5. The Plasma Voltage Drop, V_{SS}

The rate of energy fed per unit area of the emitter surface to the plasma through the voltage drop, V_{SS}, across the interelectrode plasma region (viz., $I_e V_{SS}$) must equal the sum of the rate of elastic P_{el} and inelastic P_{in} energy losses resulting from collisions with the ions and neutrals which the electrons undergo in traversing the interelectrode plasma region. Thus,

$$I_e V_{SS} = P_{el} + P_{in} , \tag{12}$$

where the electron energy lost in elastic collisions with the cesium neutrals and ions is given by

$$P_{el} = g n_e \int_o^\infty f_{el}\left(\tfrac{1}{2}m_e v^2\right) \nu_c f(v)dv , \tag{13}$$

where for a Maxwellian distribution of electron velocities the function f(v)dv is given by

$$f(v)dv = \frac{4}{\sqrt{\pi}}\left(\frac{v}{v_o}\right)^2 \exp\left(-\left(\frac{v}{v_o}\right)^2\right) d\left(\frac{v}{v_o}\right) . \tag{14}$$

f_{el} is the fraction of the electron energy lost in elastic collision which is given by the expression

$$f_{el} = \frac{2m_e}{m_p}\left(1 - \frac{E_g}{E_e}\right) \tag{15}$$

for any electron temperature, E_e, and gas temperature

$$E_g = \frac{kT_g}{e} . \tag{16}$$

ν_c is the collision frequency of the electrons and is given by

$$\nu_c = \frac{v}{\lambda_e} \tag{17}$$

and v_o is the most probably random electron velocity, viz.,

$$v_o = \sqrt{2eE_e/m_e} \quad . \tag{18}$$

We now take the electron collision frequency with cesium to be a constant over the electron temperature range of interest, viz.,

$$\nu_c = \frac{v_o}{\lambda_e} = v_o(q_n n_n + q_p n_e) \tag{19}$$

[In this equation,

$$q_n = \frac{230}{E_e} \times 10^{-20} \text{ sq m} \tag{20}$$

is the cross section of the neutral cesium atom for $0.1 \leq E_e \leq 1$, and

$$q_p = 248 \times 10^{-20} \frac{1}{E_e^2} \ln \frac{1.55 \times 10^{13} E_e^{3/2}}{n_e^{\frac{1}{2}}} \text{ sq m} \tag{21}$$

is the cross section of the cesium ion as derived by equating the conductivity formula when the vapor becomes a fully ionized gas, viz.,

$\sigma_e = \frac{e^2 n_e}{m_e v_o q_p n_e}$, to Spitzer conductivity formula for a fully ionized gas, viz,

$$\sigma_e = \frac{4\sqrt{2}\,\gamma_E (4\pi\varepsilon_o)^2}{\pi\sqrt{\pi}\sqrt{em_e}\ln\Lambda} E_e^{3/2} \quad .$$

Thus,

$q_p = \frac{\pi\sqrt{\pi}}{8\gamma_E}\left(\frac{e}{4\pi\varepsilon_o}\right)^2 \frac{\ln\Lambda}{E_e^2}$, where ε_o = permitivity of free space and

$\gamma_E = 0.582$ as given by Spitzer for singly ionized particles and

$$\Lambda = \frac{3}{2\sqrt{\pi n_e}}\left(\frac{4\pi\varepsilon_o E_e}{e}\right)^{3/2}.]$$

Integrating Eq. (13) we get the following expression for the rate of electron energy lost, per unit area of the emitter surface, in elastic collisions with

the cesium neutrals and ions of the interelectrode plasma:

$$P_{el} = g n_e \frac{2m_e}{m_p} \left(1 - \frac{E_g}{E_e}\right) \frac{v_o}{\lambda_e} \left(\frac{3}{2} e E_e\right) . \tag{22}$$

The rate of inelastic energy lost per unit emitter area can be estimated by assuming that the inelastic excitation collisions do not remove energy from the plasma and that the required rate of generation of ions in the volume is $(= \alpha_i n_e)$ where α_i is the net rate of generation of ions per electron. Based on these assumptions the rate of electron energy which is lost in inelastic ionizing collisions per unit emitter area is given by

$$P_{in} = e(V_i + 1.5E_e)\ (\alpha_i n_e) g , \tag{23}$$

with V_i being the ionization potential and $1.5eE_e$ the mean electron energy.

6. The Diffusion Equations for Electrons and Ions and Continuity Equation

The diffusion equations for electrons and ions and continuity equation given in Ref. 2 are represented here, respectively, as follows:

$$I_e = -en_e K_e \frac{dV}{dx} + \frac{d}{dx}(en_e K_e E_e) , \tag{24}$$

$$I_p = -en_e K_p \frac{dV}{dx} - \frac{d}{dx}(en_e K_p E_g) , \tag{25}$$

$$-\frac{dI_e}{dx} = \frac{dI_p}{dx} = en_e(\alpha_i - \alpha_r n_e) , \tag{26}$$

where K_e is the electron mobility and is given (for Maxwellian distribution of electron velocity) by

$$K_e = \frac{e}{3m_e} \int_0^\infty \frac{4}{\sqrt{\pi}} \epsilon^{-(v/v_o)^2} \frac{d}{d(v/v_o)}(1/\nu_c)(v/v_o)^3 d(v/v_o) = \frac{e}{m_e \nu_c} = \frac{e\lambda_e}{m_e v_o} \tag{27}$$

when the collision frequency, ν_c, is a constant $= (v_o/\lambda_e) = v_o(q_n n_n + q_p n_e)$ as in Eq. (19).

K_p is the Compton ion mobility for cesium ions in cesium vapor and is given by

$$K_p = 1.06 \frac{e\lambda_o}{m_p v_g} \quad , \tag{28}$$

where $\lambda_o = (1/q_o n_o)$. (29)

n_o is the total neutral and ion particle density and is given by

$$n_o = \frac{p}{kT_g} \quad , \text{ where p is the vapor pressure;} \tag{30}$$

q_o is the collision cross section for cesium ions in cesium vapor and is given by $q_o = \pi(1.69 + 2.62)^2 \times 10^{-20} = 58.3 \times 10^{-20}$ sq m (1.69×10^{-10}m is the Pauling cesium ion radius and 2.62×10^{-10}m is the cesium atom radius); m_p is the mass of the cesium atom or ion = 2.2×10^{-25}Kg; v_g is the random neutral velocity at an average gas temperature, T_g, and is given by

$$v_g = (2eE_g/m_p)^{1/2} \quad , \quad (E_g = kT_g/e) \; ; \tag{31}$$

α_r is the volume recombination coefficient for cesium.

Solution of the diffusion and continuity equations subject to (a) Poisson's equation when $n_e = n_p$, viz., $(d^2V/dx^2) = 0$, (b) when the recombination term is negligible, (c) when the emitter and collector sheath widths are negligible with respect to the interelectrode gap, g, and (d) when n_e is a maximum n_{eo} near the collector, yields a sinusoidal distribution function for the electrons, viz.,

$$n_e = n_{eo} \cos \alpha (g - x), \tag{32}$$

where

$$\alpha^2 = \alpha_i/(E_e + E_g)K_p \quad . \tag{33}$$

The expression for the diffusion ion current may now be obtained by integrating the continuity equation for ions, viz.,

$$I_p = \int_o^g en_e \alpha_i dx = en_{eo} \alpha_i g \left[\frac{-\sin \alpha g}{\alpha g}\right] \tag{34}$$

(the negative sign being due to the fact that the ion current is in the direction of the negative x axis). We should note here that the ratio $(\sin \alpha g)/(\alpha g)$ is not too far from unity (within a maximum error of 10%) when $0 \leq \alpha g \leq \frac{\pi}{4}$ and is $= \frac{2}{\pi}$ when $\alpha g = \frac{\pi}{2}$. Thus, for the sake of simplicity in this treatment we will take an average value of $(\sin \alpha g)/(\alpha g) = 0.818$, we will neglect the charge concentration gradient term in the diffusion equation (Eqs. 24 and 25) and we will take

$$\frac{dV}{dx} = \frac{V_{SS}}{g} \tag{35}$$

(i.e., neglect the sheaths' thicknesses with respect to the interelectrode spacing.) Thus, the simplified diffusion equation for the electron current, I_e, is given by

$$I_e = en_e K_e (V_{SS}/g) = en_e \frac{e\lambda_e}{m_e v_o} (V_{SS}/g) = I_{ep} \frac{\lambda_e \sqrt{\pi}}{g} \frac{V_{SS}}{E_e} \tag{36}$$

and the simplified ion current balance equation is given by equating the simplified ion current diffusion equation (when the charge concentration gradient term is neglected), viz., $I_p = en_e K_p (V_{SS}/g)$, which is also the rate per unit emitter area at which ions are removed from the plasma, to the rate at which ions are generated per unit emitter area from Eq. (34) (when an average value of $(\sin \alpha g)/(\alpha g) \approx \frac{1}{2}(1 + \frac{2}{\pi}) = 0.818$ is taken), viz., $I_p = en_e(0.818 \alpha_i g)$. The result is the following relation which defines the rate of generation of ions per electron (α_i) in terms of the ion mobility, K_p, the voltage drop across the interelectrode plasma region, V_{SS}, and the interelectrode spacing, g, viz.,

$$\alpha_i = 1.22 K_p (V_{SS}/g^2) = \frac{e(1.3\lambda_o)}{m_p v_g g} (V_{SS}/g). \tag{37}$$

7. The Voltage V_{SS} in Terms of Electron Temperature, E_e

By substituting the expression of α_i in Eq. (37) into the expression for the inelastic collision losses as given by Eq. (23) we get the following expression for the inelastic collision losses in terms of (V_{SS}/g), the ion mobility, K_p, the electron temperature, E_e, the electron density, n_e, and the ionization potential, V_i, viz.,

$$P_{in} = en_e(V_i + 1.5E_e)\ 1.22K_p(V_{SS}/g) . \tag{38}$$

If we now substitute the expression for the elastic collision losses given by Eq. (22) and the expression for the inelastic collision losses given by Eq. (38) into the expression for (V_{SS}/g) given by Eq. (12) and use for I_e in Eq. (12) the simplified diffusion equation, viz., Eq. (36), we get a quadratic equation in (V_{SS}/g) in terms of the electron temperature, E_e, the gas or ion temperature, E_g, the electron mean free path, λ_e, the ion mean free path, λ_o, in the ion mobility equation, the interelectrode spacing, g, the ionization potential, V_i, the ion mass, m_p, and the electron mass, m_e, viz.,

$$\left(\frac{V_{SS}}{g}\right)^2 = \frac{6m_e}{m_p}\frac{E_e(E_e - E_g)}{\lambda_e^2} + \left(\frac{V_{SS}}{g}\right)\left(\frac{V_i + 1.5E_e}{g}\right)\left(\frac{1.3\lambda_o}{\lambda_e}\right)\sqrt{\frac{m_e E_e}{m_p E_g}} \qquad (39)$$

Solution of the quadratic equation (39) for (V_{SS}/g) yields

$$\frac{V_{SS}}{g} = \left(\frac{V_i + 1.5E_e}{g}\right)\left(\frac{0.65\lambda_o}{\lambda_e}\right)\left(\frac{m_e E_e}{m_p E_g}\right)^{0.5}\left[1 + \left(1 + 6\left(\frac{g}{\lambda_e}\right)^2 \frac{E_g(E_e - E_g)}{(V_i + 1.5E_e)^2}\left(\frac{\lambda_e}{0.65\lambda_o}\right)^2\right)^{0.5}\right] \qquad (40)$$

The physical significance of Eq. (40) can be clearly appreciated by inspection of terms. In the first place, if the elastic losses are negligible by comparison to the inelastic losses, as in the case of a relatively low pressure converter, the voltage drop across the interelectrode plasma region, V_{SS}, is then given by

$$V_{SS} = (V_i + 1.5E_e)\left(\frac{1.3\lambda_o}{\lambda_e}\right)\left(\frac{m_e E_e}{m_p E_g}\right)^{0.5} \quad \text{(when the inelastic losses are dominant as in low pressure cases)} \qquad (41)$$

and it can be clearly seen that the voltage drop across the interelectrode plasma region, V_{SS}, is independent of the interelectrode spacing, is approximately directly proportional to the ionization potential of the gas, V_i, to the square root of the electron to ion mass ratio, to the square root of the electron temperature to gas temperature and to the ratio of the ion to electron mean free path (and thus is practically independent of the vapor pressure).

In the second place, if the inelastic losses are negligible by comparison to the elastic losses as in the case of a high pressure converter the voltage drop across the interelectrode spacing, V_{SS}, is then given by

$$V_{SS} = \frac{g}{\lambda_e}\left(\frac{3}{2}E_e\right)\sqrt{\frac{8}{3}\frac{m_e}{m_p}\left(1 - \frac{E_g}{E_e}\right)} \quad \text{(when the elastic losses are dominant as in high pressure cases)} \qquad (42)$$

and it can be readily seen that the voltage drop across the interelectrode plasma region, V_{SS}, is directly proportional to the spacing, the electron temperature, E_e (which from Eq. 10 is a function of the electron load current), the square root of

the electron to atom mass ratio, $\frac{m_e}{m_p}$, the square root of the ratio of the temperature difference between the electrons and atoms to the electron temperature $(E_e - E_g)/E_e$, and is inversely proportional to the electron mean free path (and thus is practically directly proportional to the gas pressure).

Obviously, for intermediate pressures the voltage drop across the interelectrode plasma region, V_{SS}, as can be calculated from Eq. (40) is influenced by all the factors discussed in connection with the special cases given by Eqs. (41) and (42), but is not as sharply dependent on these factors as in the case of relatively low pressure or relatively high pressure cases.

We now have all the equations to compute the voltage-current characteristic equation as indicated in the following procedure.

8. Program for the Prediction of the Voltage-Current Characteristic Curve

a. Choose the ratio of electron load current density to emitter saturation current density, viz., $z = (I_e/I_{eE}) \leq 0.875$ *

b. Calculate the electron temperature from Eq. (10), viz.,

$$E_e = \frac{E_T}{1 - 0.5 \ln\left(\frac{z}{1 - z}\right)}$$

where $E_T = \frac{T_E}{11600}$ volt, where T_E is the emitter temperature in °K.

c. Calculate the electron mean free path, λ_e, for low ionization, viz.,

$$\lambda_e = \frac{1}{q_n n_o} \quad \text{where } n_o = \frac{p}{kT_g} = 0.725 \times 10^{16}(p/T_g) \text{ atoms/cc}$$

where p, for cesium, is given in dynes/sq cm by Langmuir's formula

$$p = \text{antilog}_{10}\left[14.178 - 1.35 \log_{10} T_g - \frac{4041}{T_L}\right],$$

where T_L is the liquid cesium temperature in °K,

$$T_g = \frac{4}{9} T_E \left(\frac{1 + \sqrt{b} + b}{1 + \sqrt{b}}\right)^2,$$

where $b = \frac{T_C}{T_E}$, T_C = collector temperature in °K,

---

* Eq. (10) poses a theoretical upper limit on $z = 0.90183$ when $E_e \to \infty$ or $\gamma = 0$ in Eq. (11). When $z = 0.875$, $\gamma = 0.1487$ or $E_e = 6.72(E_T)$. Note that the resultant voltage to satisfy this electron temperature may become negative (i.e., converter operation with an externally applied voltage).

$q_n = \frac{230}{\sqrt{E_e}} \times 10^{-16}$ sq cm, $\quad k = 1.38 \times 10^{-16}$ erg/°K .

d. Calculate (g/λ_e).

e. Calculate the ion mean free path $\lambda_o = \frac{1}{q_o n_o}$,

where $q_o = 58.3 \times 10^{-16}$ sq cm.

f. Calculate (λ_o/g) .

g. Calculate $0.65\lambda_o/\lambda_e$.

h. Calculate $E_g = (T_g/11600)$ volt and obtain the ratio $\frac{E_e}{E_g}$.

i. Calculate $E_e - E_g$.

j. Calculate

$$V_{SS} = \left(\frac{V_i + 1.5E_e}{A}\right)\left(\frac{0.65\lambda_o}{\lambda_e}\right)\sqrt{\frac{E_e}{E_g}}\left[1 + \left(1 + \left(\frac{g}{\lambda_e}\right)^2 \frac{6(E_e - E_g)E_g}{(V_i + 1.5E_e)^2}\left(\frac{\lambda_e}{0.65}_o\right)^2\right)^{0.5}\right],$$

where $A = \sqrt{(m_p/m_e)}$.

k. Calculate $(\phi_E - \phi_C) - V = E_e \ln \frac{z}{1 - z} + V_{SS}$.

l. Calculate $y = \frac{I_{ep}}{I_e} - z\left(\frac{g}{\lambda_e\sqrt{\pi}}\right)\left(\frac{E_e}{V_{SS}}\right)$.

m. Calculate $\psi = \frac{1}{\delta} \ln \frac{y}{1 - z}$.

n. Calculate $V_{SE} = \psi E_T$.

o. Calculate $V_{SC} = E_e \ln \frac{y}{z}$.

p. Knowing $I_{eE} = 120.4\, T_E^2 \exp - \frac{\phi_E}{E_T}$, calculate $I_e = zI_{eE}$.

q. Knowing $(\phi_E - \phi_C)$, calculate $V = (\phi_E - \phi_C) - E_e \ln \frac{z}{1 - z} - V_{SS}$.

r. Plot I_e versus V .

J. Example of Calculations

The presented program of calculations is now applied in the prediction of the voltage-current characteristics curve for the volume ionization mode of operation with the following conditions:

$T_E = 1718^oK$

$T_C = 780^oK$

$T_L = 530^oK$

The calculated curve for an effective emitter work function $\phi_E = 2.48$ volts (obtained from the saturation current) and for a collector work function $\phi_C = 1.75$ volts is plotted and compared with the results obtained on 3 different devices with an iridium emitter and nickel collector. The comparison is given in Fig. 43 and the conditions for the various tests are indicated on the figure.

Comparison of the solid theoretical line with the experimental points from these three different devices show good agreement particuarly with the data points of device MNEC-C14 and MNEC-MC1.

VIII. PROCEDURE

A. Description of Filament Devices

The devices used for the testing of iridium, rhenium, and platinum consist of a .020" filament as the emitter, maintained in tension by a molybdenum spring. The iridium and rhenium emitter devices each has a stainless steel envelope, with a nickel collector which contains a sapphire window for optical temperature measurements.

A sketch of the metal enveloped thermionic energy converter with directly heated emitter is shown in Figure 40. The emitter consists of the central 0.500 inch portion of a 0.020 inch diameter wire which has a total length of 1.500 inches. The emitter area facing the nickel collector is 0.203 cm^2. The interelectrode gap is 0.030 inch. End effects are minimized in this design by enlarging the gap adjacent to the collector to 0.300 inch. Thus, the current collected tends to be restricted to that coming from the central .203 cm^2 of the emitter and this value was taken as the nominal emitter area used in analysis of the data. The temperature distribution along the emitter also tends to minimize these end effects.

The platinum device was a glass enveloped, guard ring device, as shown in figure 41. Holes drilled through the nickel collector enable optical temperature measurement of the emitter. The collector has a length of 1"; the emitter area facing the collector is .405 sq cm. The guard rings assure that the measured current is obtained from the central portion of the emitter.

B. Testing

1. Vacuum Testing

Prior to testing with cesium vapor, the device is operated on a vacuum system for the purpose of aging and outgassing the emitter and also outgassing the envelope. The vacuum system used is a Veeco system with a 200 l.p.s. mechanical forepump and a 85 l.p.s. oil diffusion pump used in conjunction with a liquid nitrogen cold trap.

The outgassing of the emitter and envelope is carried out at a temperature above the maximum temperature which the device will be operated in cesium vapor. The envelope of the device is heated in an oven to a temperature of 400°C. This outgassing is carried out for approximately six to eight hours until the ionization gauge indicates that no further outgassing takes place.

The outgassing of the emitter was done for 8 hours at 2200°K for iridium, 8 hours at 2500°K for rhenium and 8 hours at 1800°K for platinum. The devices were also operated in vacuum for over 16 hours at lower temperatures. These times were determined by the requirement that the vacuum thermionic performance of the devices become stable.

An important advantage of a filament device is the fact that the filament can readily be outgassed, thus assuring a clean thermionic surface and virtually eliminating the possibility of spureous thermionic data due to a contaminated emitter surface.

At the conclusion of the tests the cesium ampule is opened and then the device is removed from the vacuum system. For these devices, the vacuum at the time of seal-off was $2 - 5 \times 10^{-7}$ mm Hg.

2. Test with Cesium Vapor

The cesium vapor pressure is controlled by placing the device in an environmental oven. The oven is capable of maintaining temperature constant to within $\pm 0.5^{\circ}$K. The temperature of the cesium reservoir, as well as the collector temperature and the temperature at several points on the envelope, are recorded with chromel-alumel thermocouples.

The emitter temperature is measured by means of a Shawmeter, a two color, direct reading, optical pyrometer. This instrument has a field of view of .010". The emitter is sighted through a sapphire window in the case of the metal-enveloped device, and though a hole in the nickel collector in the case of the glass envelope device. As the external load, hence the electron heat transfer from the emitter is varied, the input to the emitter must be varied to maintain a constant emitter temperature. Thus, as large output currents are obtained from the device, the input power must be substantially increased. There is a limit, however, to the amount of power which can be supplied to the filament without risk of overheating the end portions which do not face the collector and, hence, are not cooled by electron heat transfer. In our tests, an upper limit of 6 amps (i.e. 30 amps/cm^2) was imposed on the output current. For this reason, characteristics (such as figures 5 and 6) were terminated before short circuit was obtained. Also for this reason, the power densities and efficiencies reported in section IV are not necessarily the optimum but represent the best values which were measured with this limitation on the output current.

3. Heating of Emitter

The emitter is heated directly by passing an electric current through it. A half-wave rectified (60 cps) heating current is used so that there is an "off" half-cycle during which there is no voltage gradient along the emitter due to the heating current. Measurements of performance, therefore, are made during a period of time when there is not electrical input to the emitter.

At large output currents, a voltage gradient still exists in the emitter due to the flow of the output current in the emitter. Analysis of this effect shows that even in the most extreme case (i.e. 30 amps/cm^2), the overestimate of the output voltage caused by this effect should be less than 0.035 v for the iridium emitter device and .05 v for the rhenium emitter device.

C. Efficiency

The following procedure was adopted to estimate the energy conversion efficiency. The input power to the emitter is determined from the sum of two terms, viz. the power required due to the electron cooling of the emitter, and the power required for all other heat losses from the emitter, such as radiation and convection. The I^2R heating of the emitter at open circuit is used as a measure of all these other heat losses except electron cooling. The electron cooling at a given output current is determined under the assumption that the current which reaches the collector comes from a "black-box" of Fermi electrons. Under this assumption, the current density and the emitter temperature can be used, together with the Richardson equation, to give a work function (generally higher than the true surface work function) which gives the net energy removed from the emitter by an electron. Thus, the electron cooling is given by

$$Q_e = J (\phi_e + 2 E_T) \qquad \text{where} \quad E_T = \frac{k}{e} T_E$$

where J is the measured output current density, $2 E_T$ arises from the thermal distribution of the electrons, and ϕ_e, the effective work function for electron cooling, is defined by the Richardson equation, using the measured output current density and the emitter temperature. This estimate for the electron cooling is bound to be greater than or equal to the true electron cooling.

This procedure gives the exact value of the electron cooling term for a vacuum diode operating in either the retarding field, space charge limited, saturation, or Schottky region. Effects due to surface ionization and flow of ion current through the device are neglected, but these are small and are included to some extent by the measure of heat flow at open circuit.

References

1. Talaat, M. E., "Generalized Theory of Thermionic Plasma Energy Converters," AIEE Transaction Paper 62-291, 1961.

2. Talaat, M. E., "The Surface Ionization and Volume Ionization Mode of Operation in the Thermionic Plasma Energy Converter," Proceedings of Thermionic Power Conversion Symposium, Colorado Springs, May 1962.

3. Kennedy, A. J., "Cesium Adsorption on Refractory Metals," Proceedings of Thermionic Power Conversion Symposium, Colorado Springs, May 1962.

Figures

Figures 1 - 6

(section IV. B)

Characteristics current density versus voltage curves for the iridium emitter. Each figure gives families of curves for emitter temperatures in the range of 1580 - 1950°K. The liquid cesium temperatures are:

T_L = 472°K Fig. 1

T_L = 498°K Fig. 2

T_L = 526°K Fig. 3

T_L = 556°K Fig. 4

T_L = 575°K Fig. 5

T_L = 596°K Fig. 6

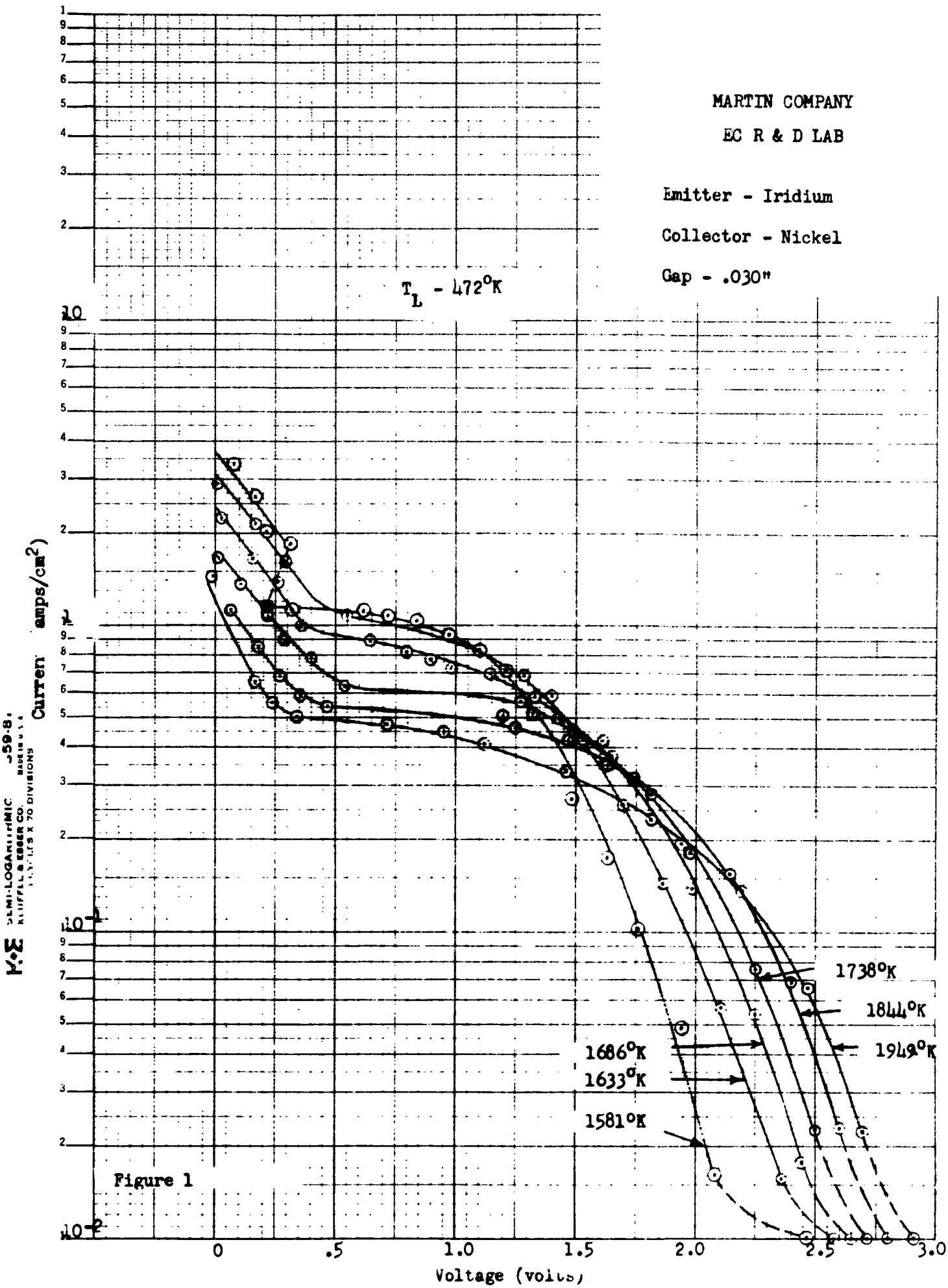
MARTIN COMPANY
EC R & D LAB
Emitter - Iridium
Collector - Nickel
Gap - .030"
T_L - 472°K
1738°K
1844°K
1949°K
1686°K
1633°K
1581°K
Current amps/cm²
Voltage (volts)
0
.5
1.0
1.5
2.0
2.5
3.0

Figure 1

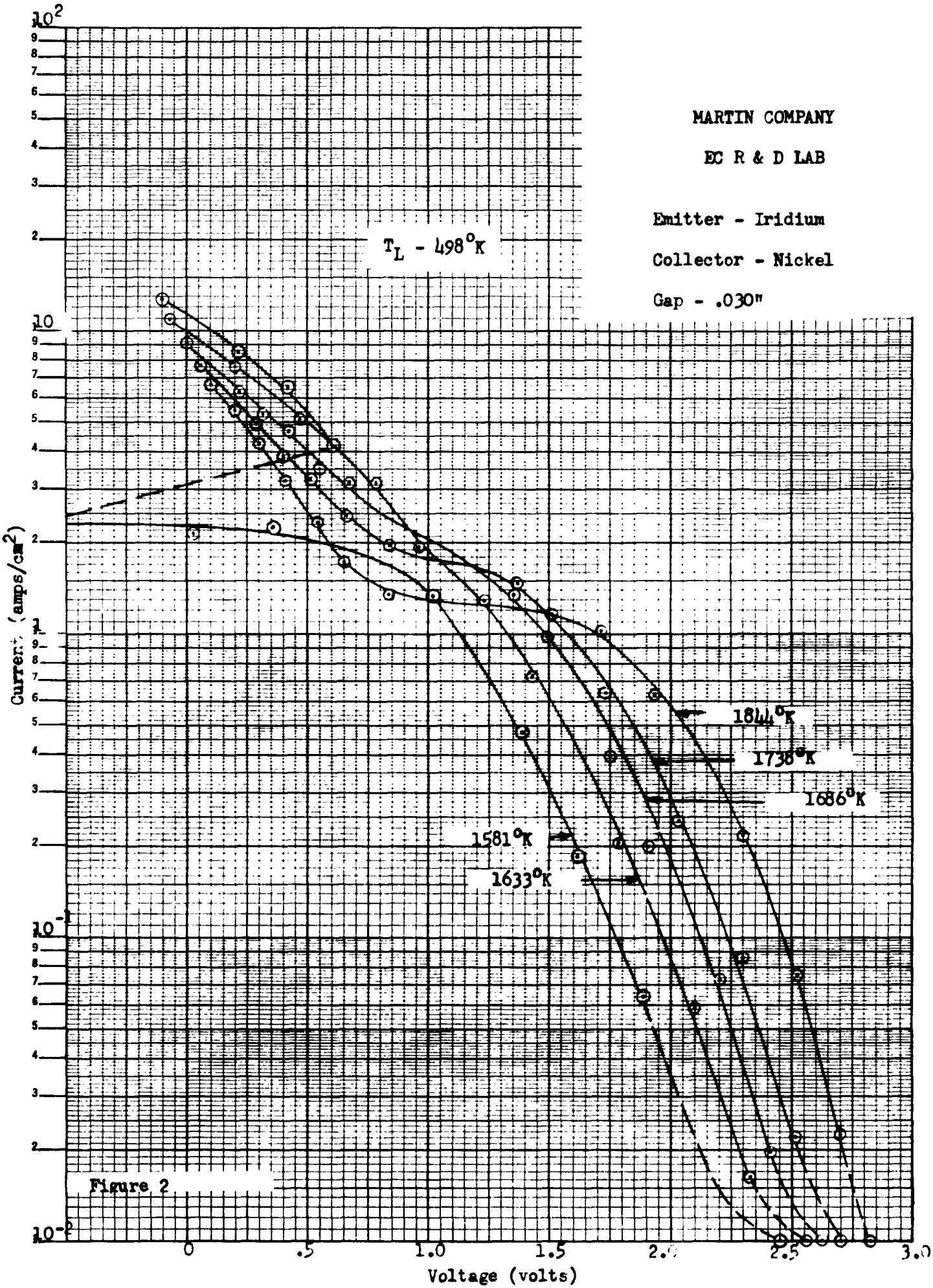
MARTIN COMPANY
EC R & D LAB
Emitter - Iridium
Collector - Nickel
Gap - .030"
T_L - 498°K
1844°K
1738°K
1686°K
1581°K
1633°K
Current (amps/cm²)
Voltage (volts)
0
.5
1.0
1.5
2.0
2.5
3.0

Figure 2

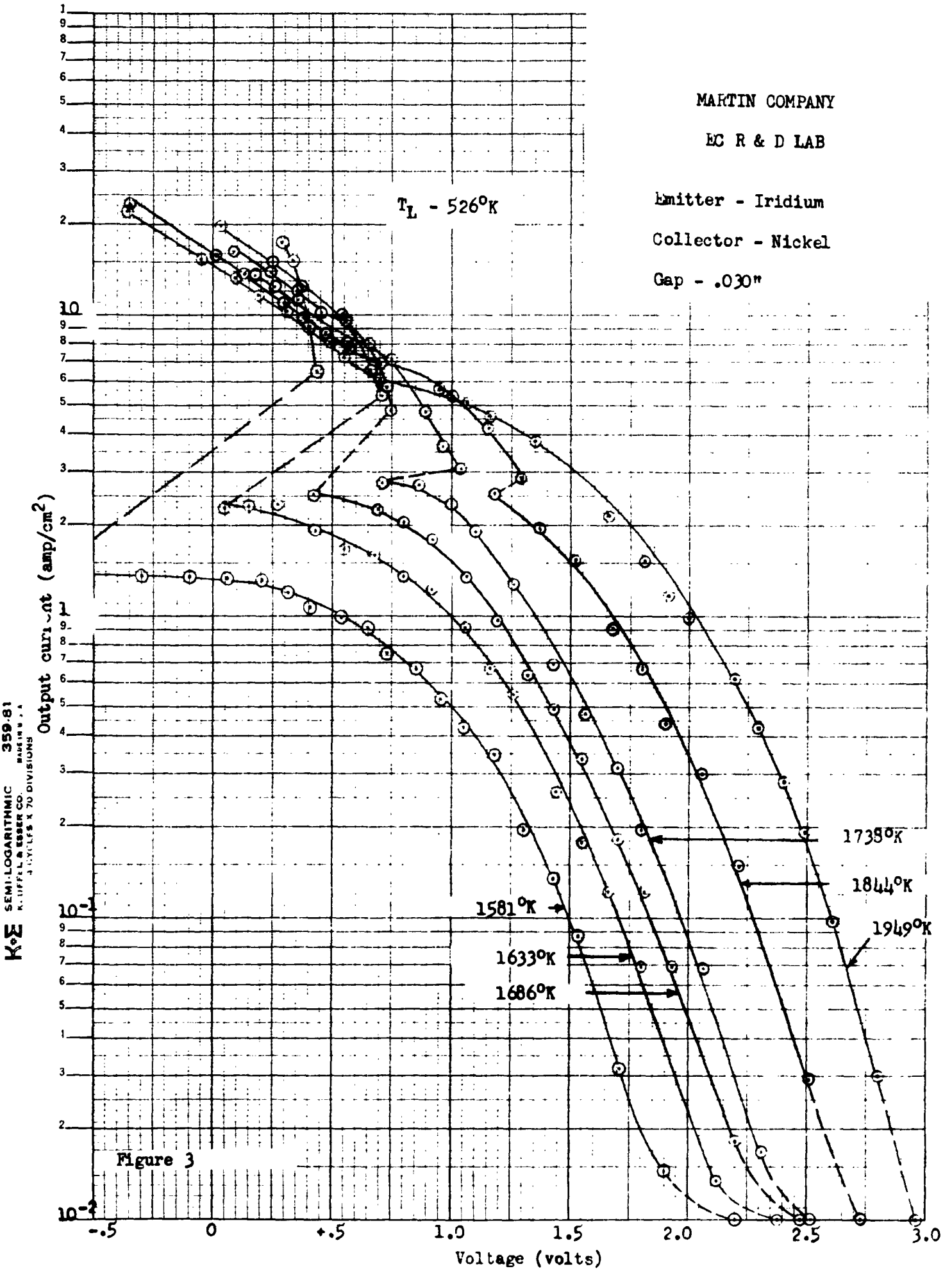
MARTIN COMPANY
EC R & D LAB
Emitter - Iridium
Collector - Nickel
Gap - .030"
T_L - 526°K
1738°K
1844°K
1581°K
1949°K
1633°K
1686°K
Output current (amp/cm²)
Voltage (volts)
-.5
0
+.5
1.0
1.5
2.0
2.5
3.0
10
1
10^{-1}
10^{-2}
K&E SEMI-LOGARITHMIC 359-81
KEUFFEL & ESSER CO.
3 CYCLES X 70 DIVISIONS

Figure 3

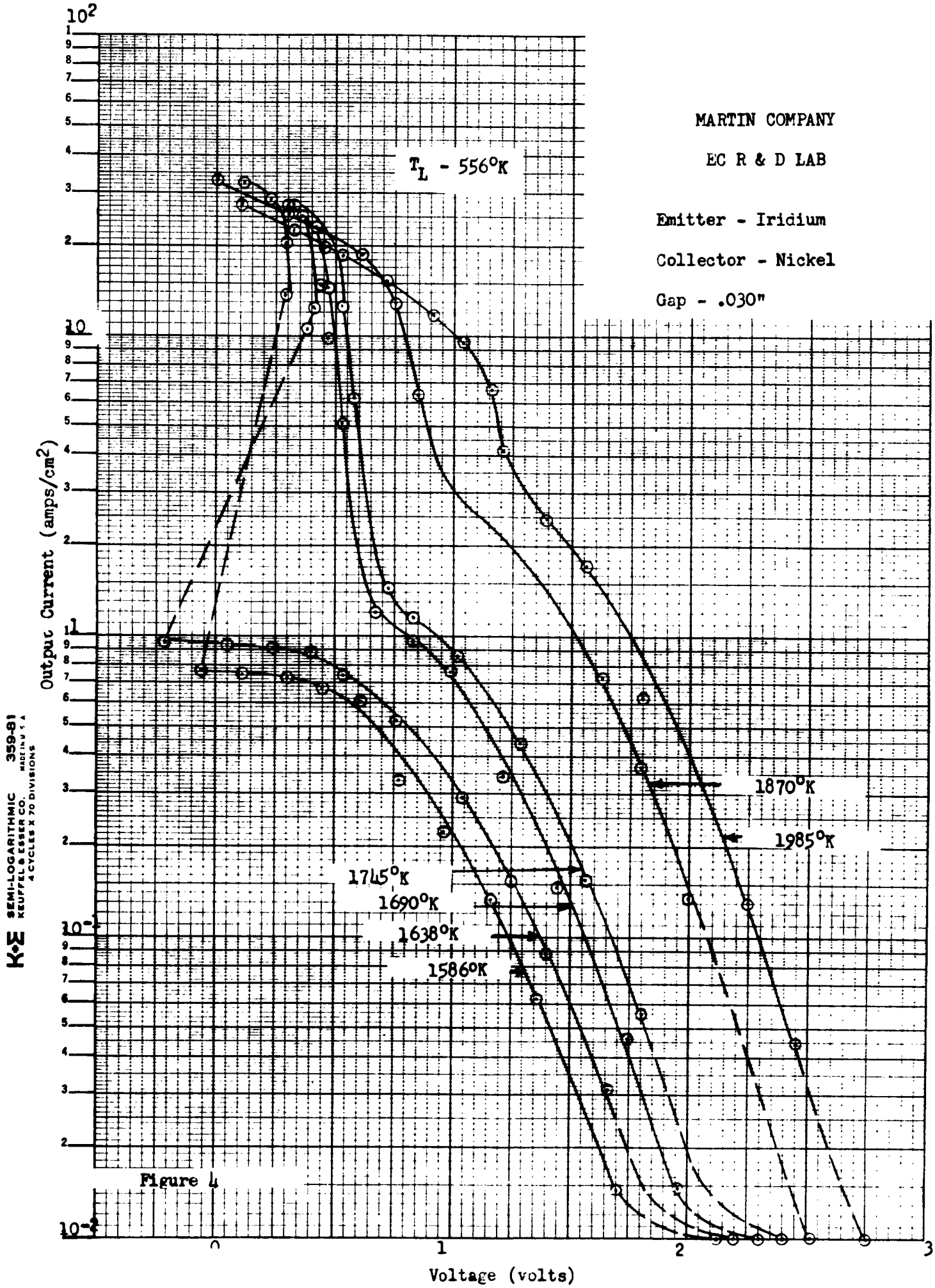
MARTIN COMPANY
EC R & D LAB
Emitter - Iridium
Collector - Nickel
Gap - .030"
T_L - 556°K
1870°K
1985°K
1745°K
1690°K
1638°K
1586°K
Output Current (amps/cm²)
Voltage (volts)
SEMI-LOGARITHMIC 359-81
KEUFFEL & ESSER CO.
4 CYCLES X 70 DIVISIONS

Figure 4

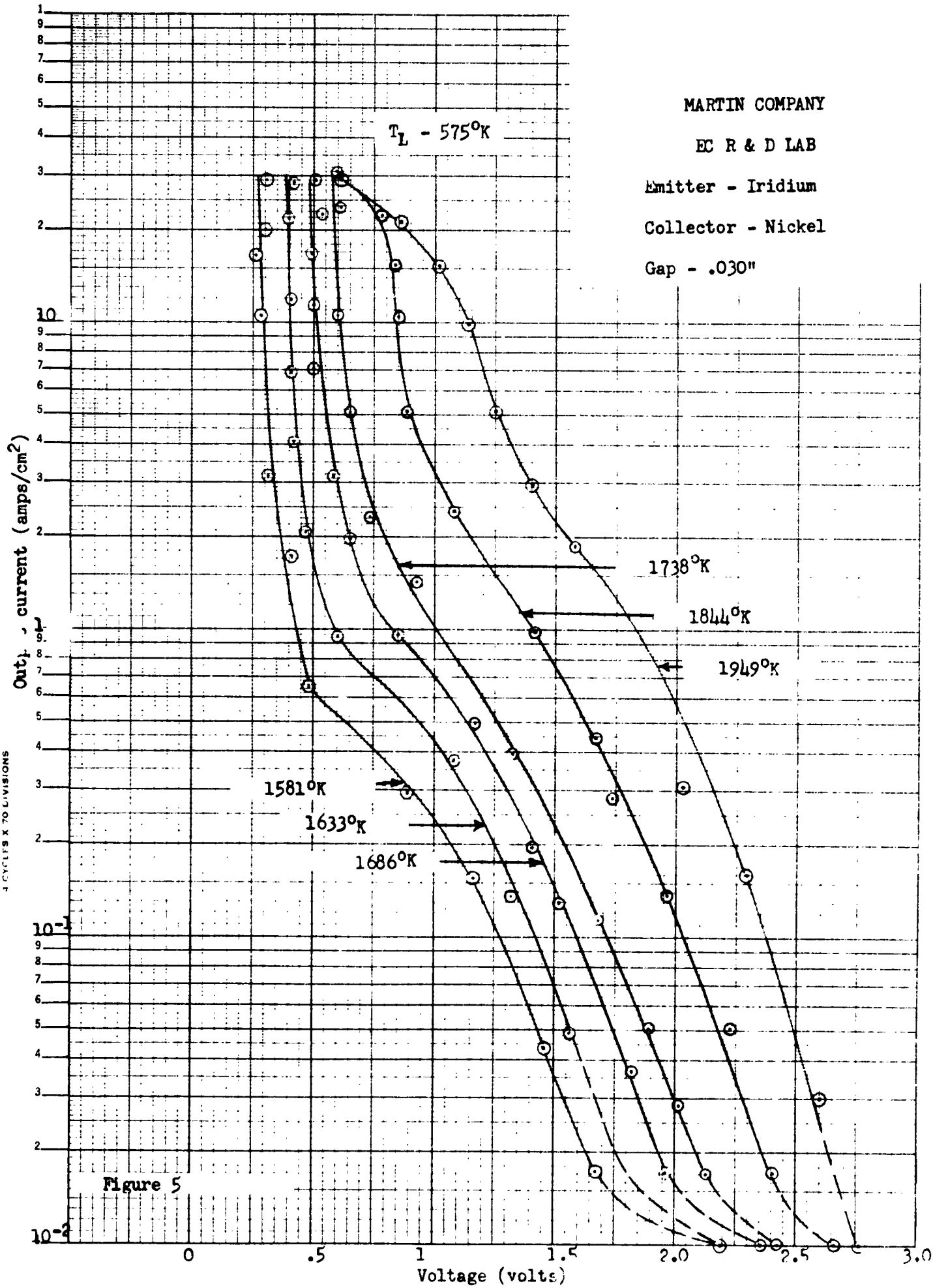
MARTIN COMPANY
EC R & D LAB
Emitter - Iridium
Collector - Nickel
Gap - .030"
T_L - 575°K
1738°K
1844°K
1949°K
1581°K
1633°K
1686°K
Out, current (amps/cm²)
Voltage (volts)
0
.5
1
1.5
2.0
2.5
3.0
SEMI-LOGARITHMIC 359-81
KEUFFEL & ESSER CO.
3 CYCLES X 70 DIVISIONS

Figure 5

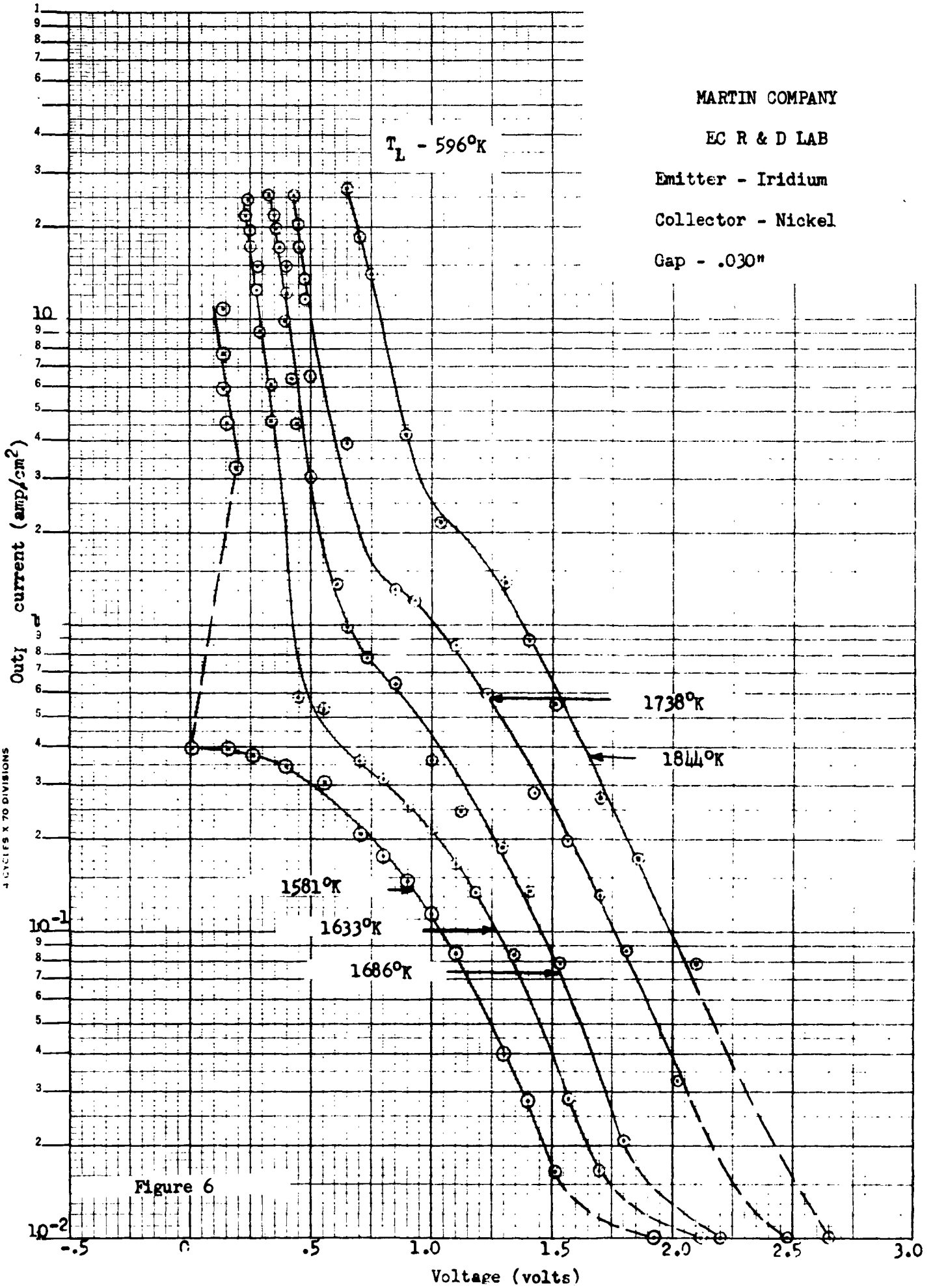
MARTIN COMPANY
EC R & D LAB
Emitter - Iridium
Collector - Nickel
Gap - .030"
T_L - 596°K
1738°K
1844°K
1581°K
1633°K
1686°K
Output current (amp/cm²)
Voltage (volts)
-.5
0
.5
1.0
1.5
2.0
2.5
3.0
10
10^{-1}
10^{-2}

Figure 6

Figures 7 - 12

(section IV. C)

Characteristic current density versus voltage curves for the rhenium emitter. Each figure gives families of curves for emitter temperatures in the range of 1550 - 2000°K. The liquid cesium temperatures are:

T_L = 473°K Fig. 7

T_L = 498°K Fig. 8

T_L = 523°K Fig. 9

T_L = 547°K Fig. 10

T_L = 573°K Fig. 11

T_L = 596°K Fig. 12

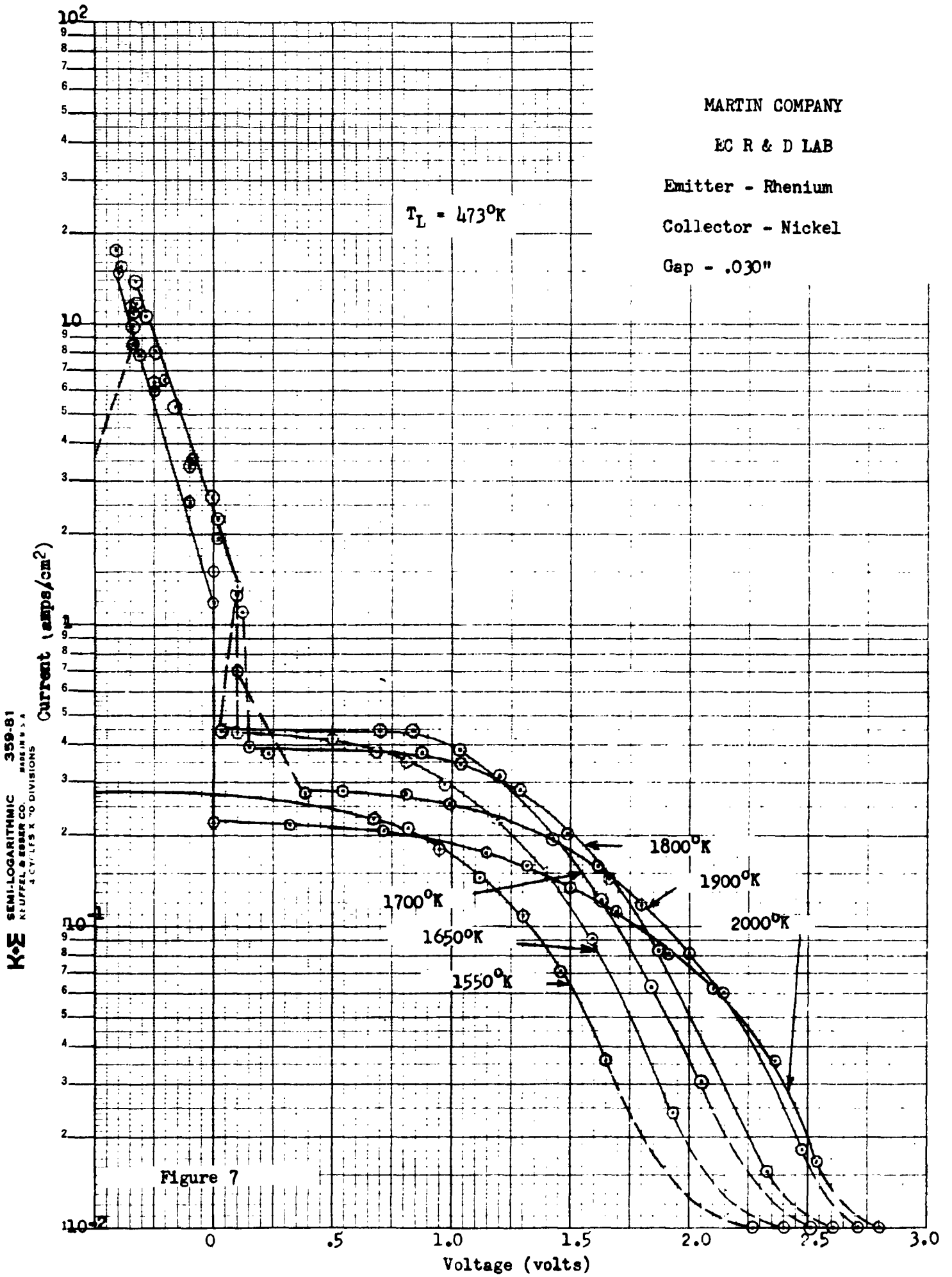
MARTIN COMPANY
EC R & D LAB
Emitter - Rhenium
Collector - Nickel
Gap - .030"
T_L = 473°K
1800°K
1900°K
1700°K
2000°K
1650°K
1550°K
Current (amps/cm²)
Voltage (volts)
0
.5
1.0
1.5
2.0
2.5
3.0
SEMI-LOGARITHMIC 359-81
KEUFFEL & ESSER CO.
4 CYCLES X 10 DIVISIONS

Figure 7

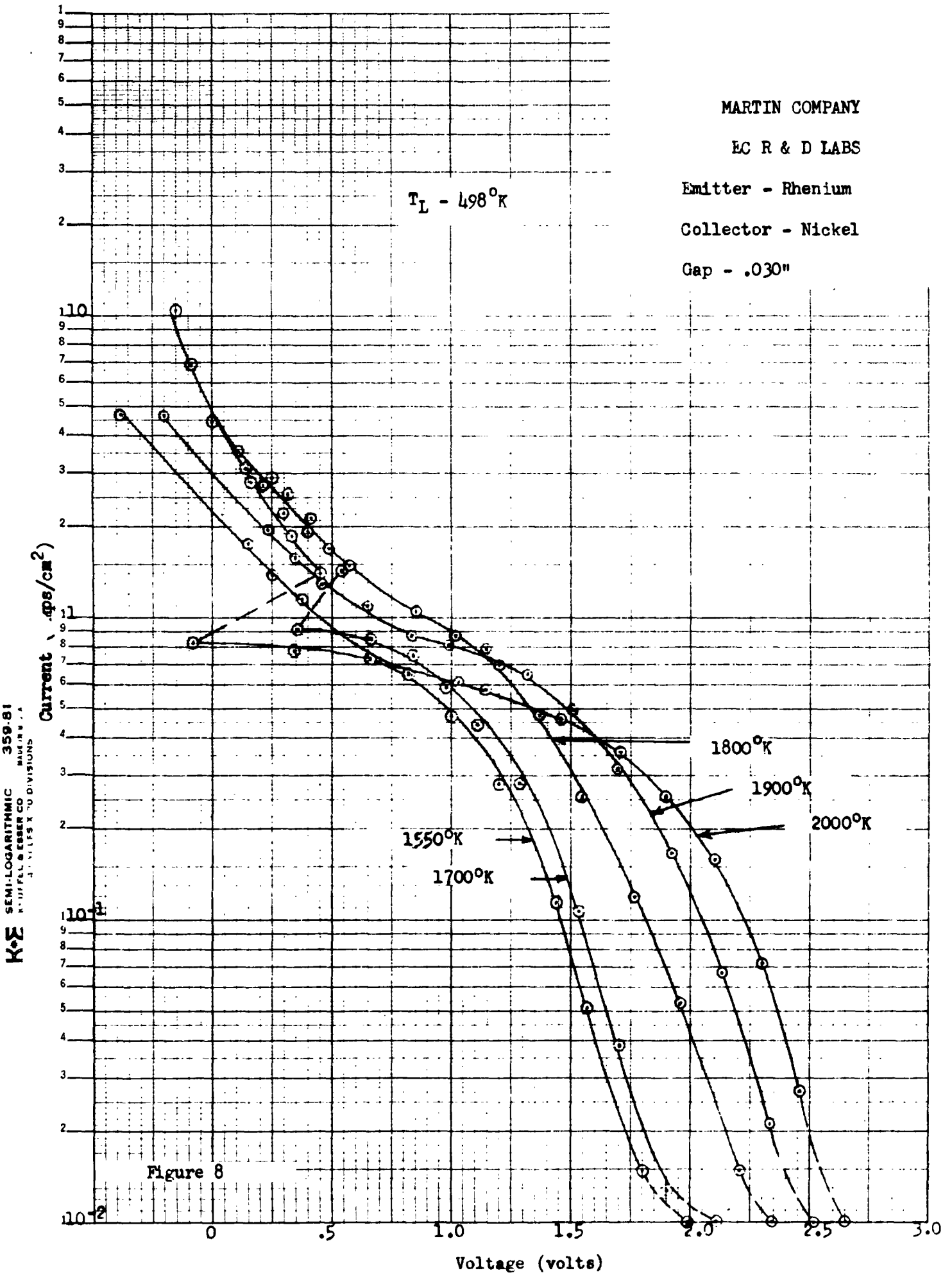
MARTIN COMPANY
EC R & D LABS
Emitter - Rhenium
Collector - Nickel
Gap - .030"
T_L - 498°K
1800°K
1900°K
2000°K
1550°K
1700°K
Current - amps/cm²
Voltage (volts)
0
.5
1.0
1.5
2.0
2.5
3.0
K&E SEMI-LOGARITHMIC 359-81

Figure 8

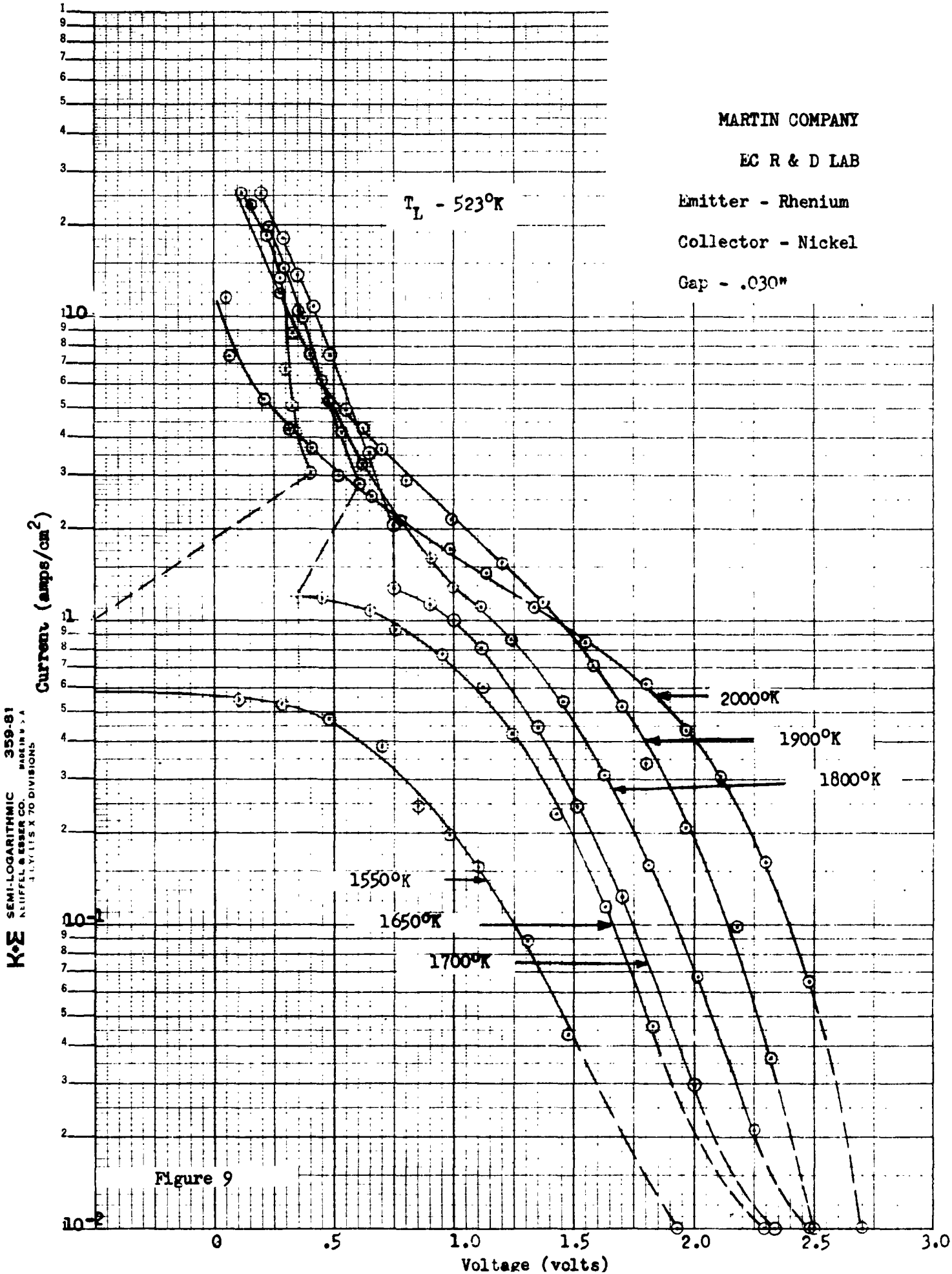
MARTIN COMPANY
EC R & D LAB
Emitter - Rhenium
Collector - Nickel
Gap - .030"
T_L - 523°K
2000°K
1900°K
1800°K
1650°K
1700°K
1550°K
Current (amps/cm²)
Voltage (volts)
0
.5
1.0
1.5
2.0
2.5
3.0
10
1
10⁻¹
10⁻²
K•E SEMI-LOGARITHMIC 359-81
KEUFFEL & ESSER CO.
4 CYCLES X 70 DIVISIONS

Figure 9

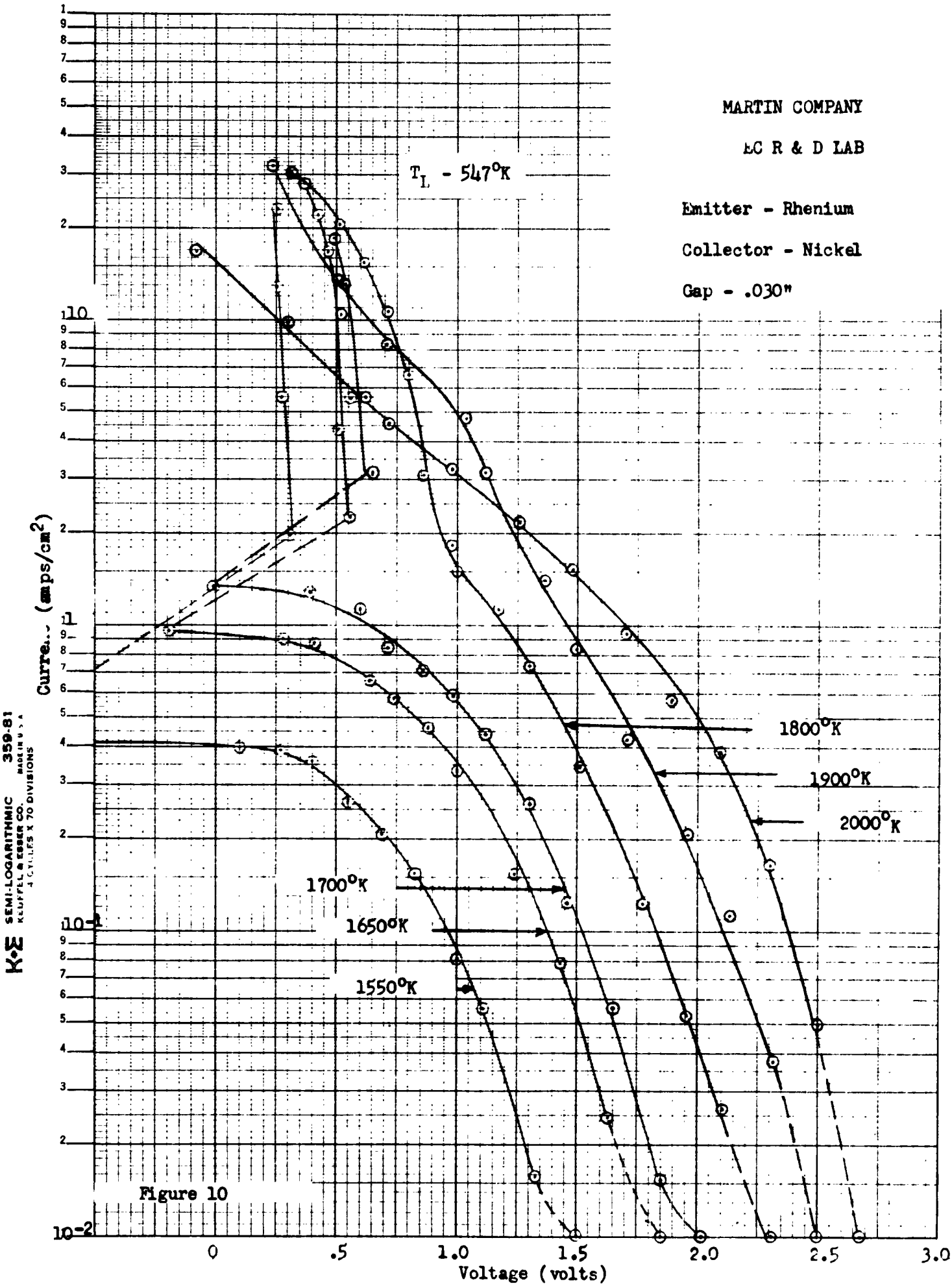
MARTIN COMPANY
EC R & D LAB
Emitter - Rhenium
Collector - Nickel
Gap - .030"
T_L - 547°K
1800°K
1900°K
2000°K
1700°K
1650°K
1550°K
Current (amps/cm²)
Voltage (volts)
0
.5
1.0
1.5
2.0
2.5
3.0
10
1
10^{-1}
10^{-2}
K&E SEMI-LOGARITHMIC 359-81
KEUFFEL & ESSER CO.
4 CYCLES X 70 DIVISIONS

Figure 10

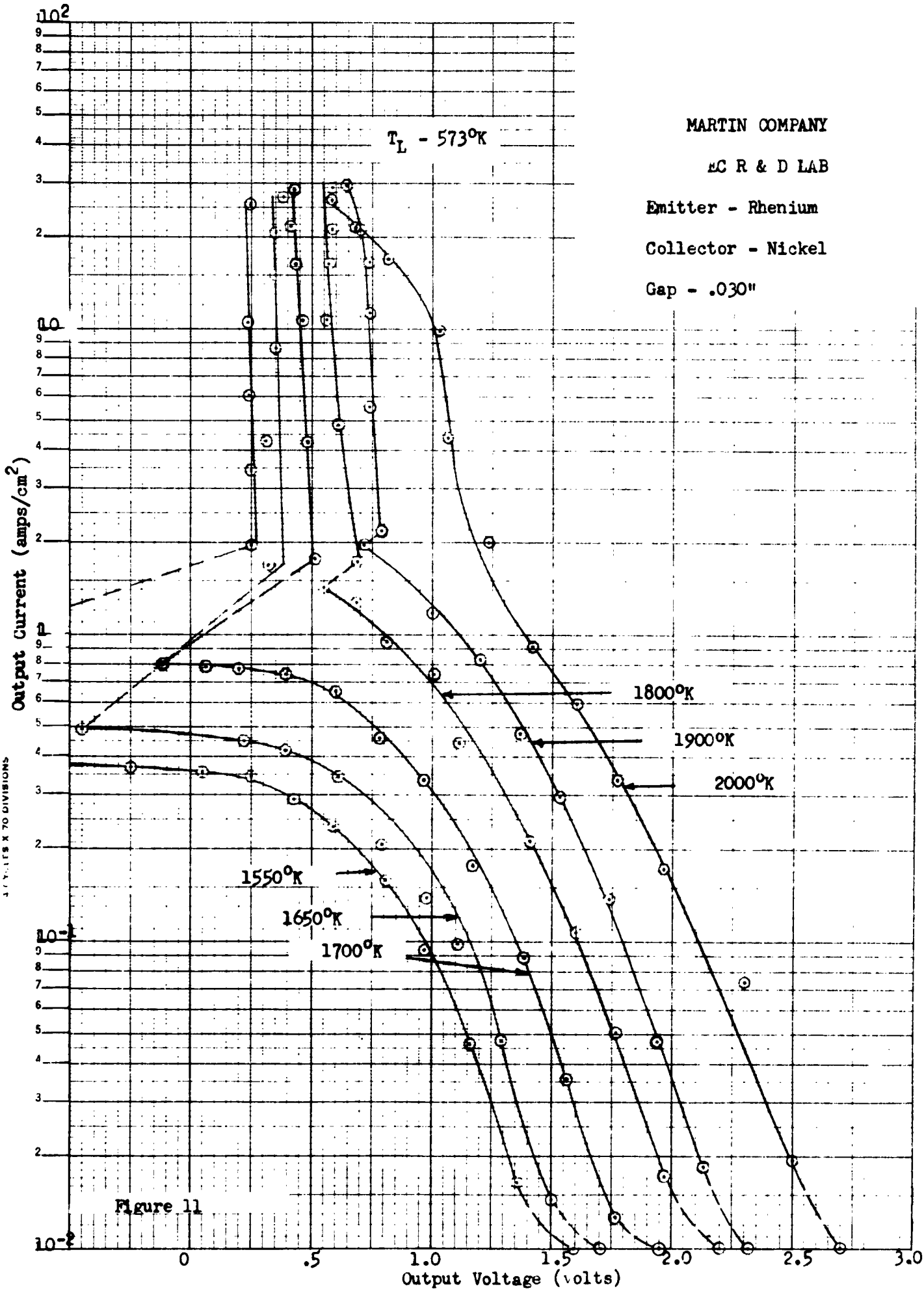
MARTIN COMPANY
RC R & D LAB
Emitter - Rhenium
Collector - Nickel
Gap - .030"
T_L - 573°K
1800°K
1900°K
2000°K
1550°K
1650°K
1700°K
Output Current (amps/cm²)
Output Voltage (volts)
0
.5
1.0
1.5
2.0
2.5
3.0
K•E SEMI-LOGARITHMIC 359-81
KEUFFEL & ESSER CO. MADE IN U.S.A.
5 CYCLES X 70 DIVISIONS

Figure 11

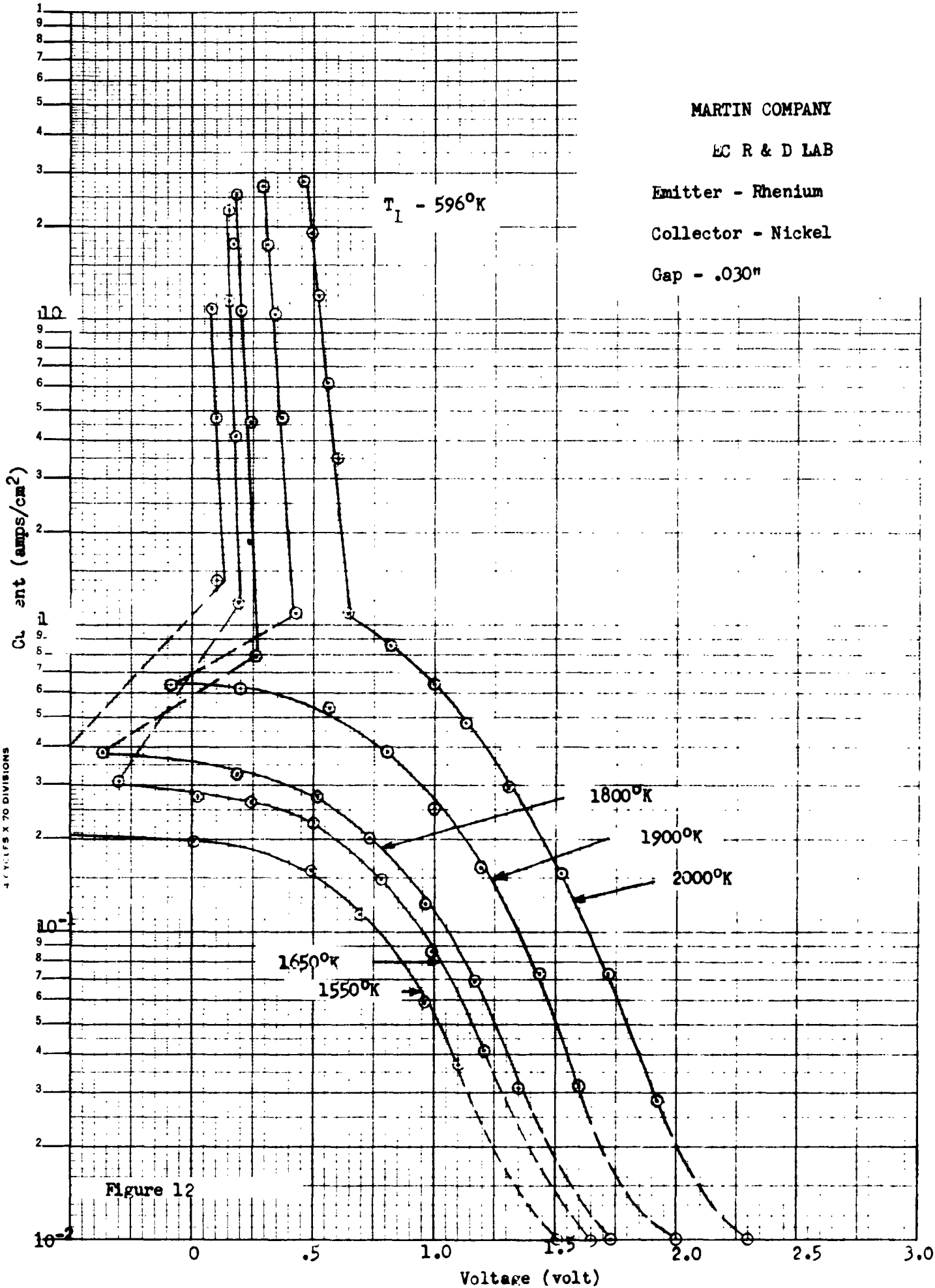
MARTIN COMPANY
EC R & D LAB
Emitter - Rhenium
Collector - Nickel
Gap - .030"
T_I - 596°K
1800°K
1900°K
2000°K
1650°K
1550°K
Current (amps/cm²)
Voltage (volt)
1Ω
1
10^{-1}
10^{-2}
0
.5
1.0
1.5
2.0
2.5
3.0
K+E SEMI-LOGARITHMIC 359-81
KEUFFEL & ESSER CO
4 CYCLES X 70 DIVISIONS

Figure 12

Figures 13 - 24

(Section IV. E)

Summaries of the dependence of the output power density and efficiency on the emitter temperature and liquid cesium temperature for the iridium and rhenium emitter.

Volume Ionization Mode of Operation

Iridium Emitter

Power Density versus Emitter Temperature	Fig. 13
Efficiency versus Emitter Temperature	Fig. 14
Power Density versus Liquid Cesium Temperature	Fig. 15
Efficiency versus Liquid Cesium Temperature	Fig. 16

Rhenium Emitter

Power Density versus Emitter Temperature	Fig. 17
Efficiency versus Emitter Temperature	Fig. 18

Surface Ionization Mode of Operation

Iridium Emitter

Power Density versus Emitter Temperature	Fig. 19
Efficiency versus Emitter Temperature	Fig. 20
Power Density versus Liquid Cesium Temperature	Fig. 21

Rhenium Emitter

Power Density versus Emitter Temperature	Fig. 22
Efficiency versus Emitter Temperature	Fig. 23
Power Density versus Liquid Cesium Temperature	Fig. 24

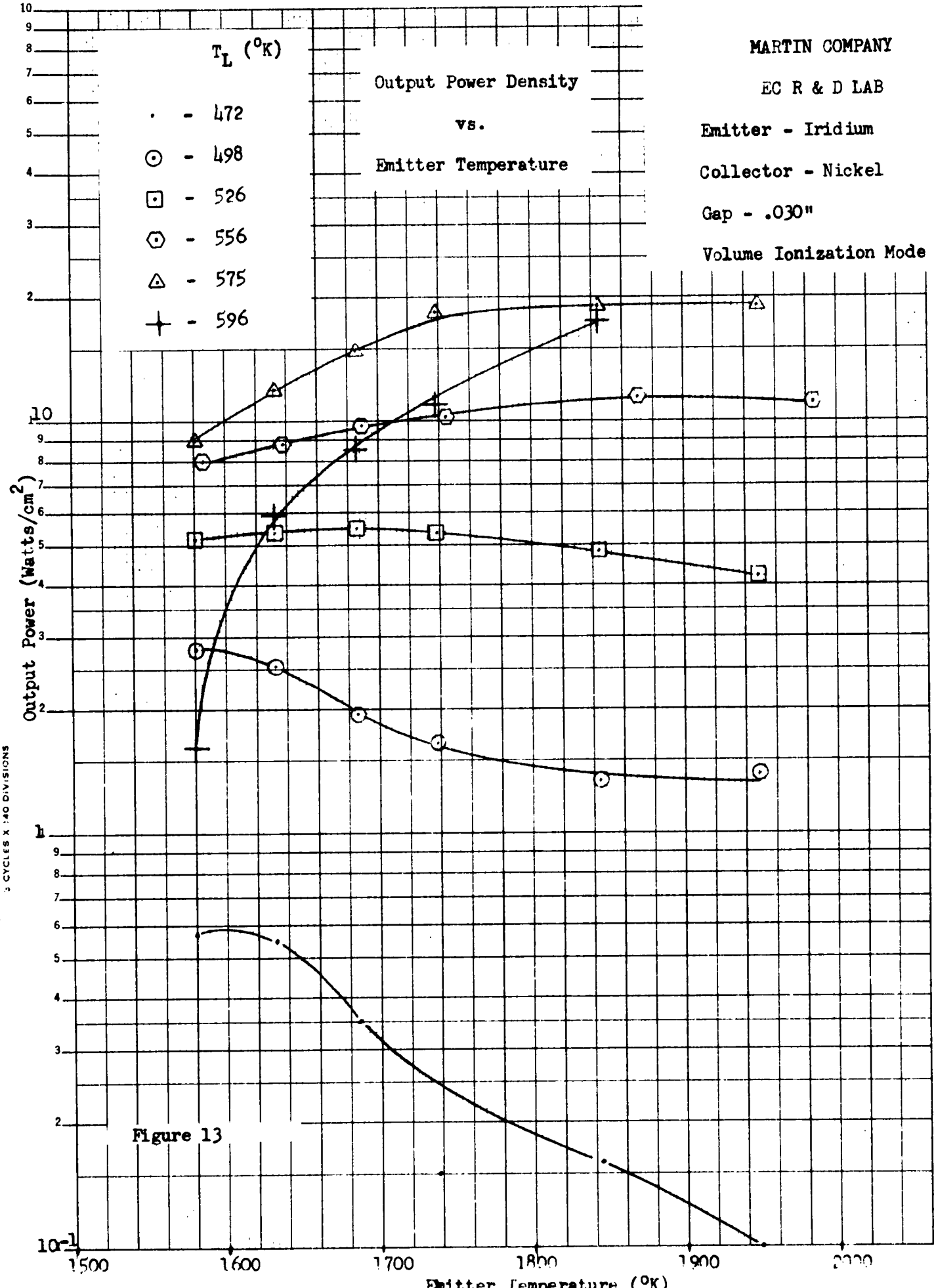
T_L (°K)
· - 472
⊙ - 498
⊡ - 526
⬡ - 556
△ - 575
✦ - 596
Output Power Density
vs.
Emitter Temperature
MARTIN COMPANY
EC R & D LAB
Emitter - Iridium
Collector - Nickel
Gap - .030"
Volume Ionization Mode
Output Power (Watts/cm²)
Emitter Temperature (°K)
1500
1600
1700
1800
1900
10
1
10⁻¹
SEMI-LOGARITHMIC 359-73
KEUFFEL & ESSER CO.
3 CYCLES X 140 DIVISIONS

Figure 13

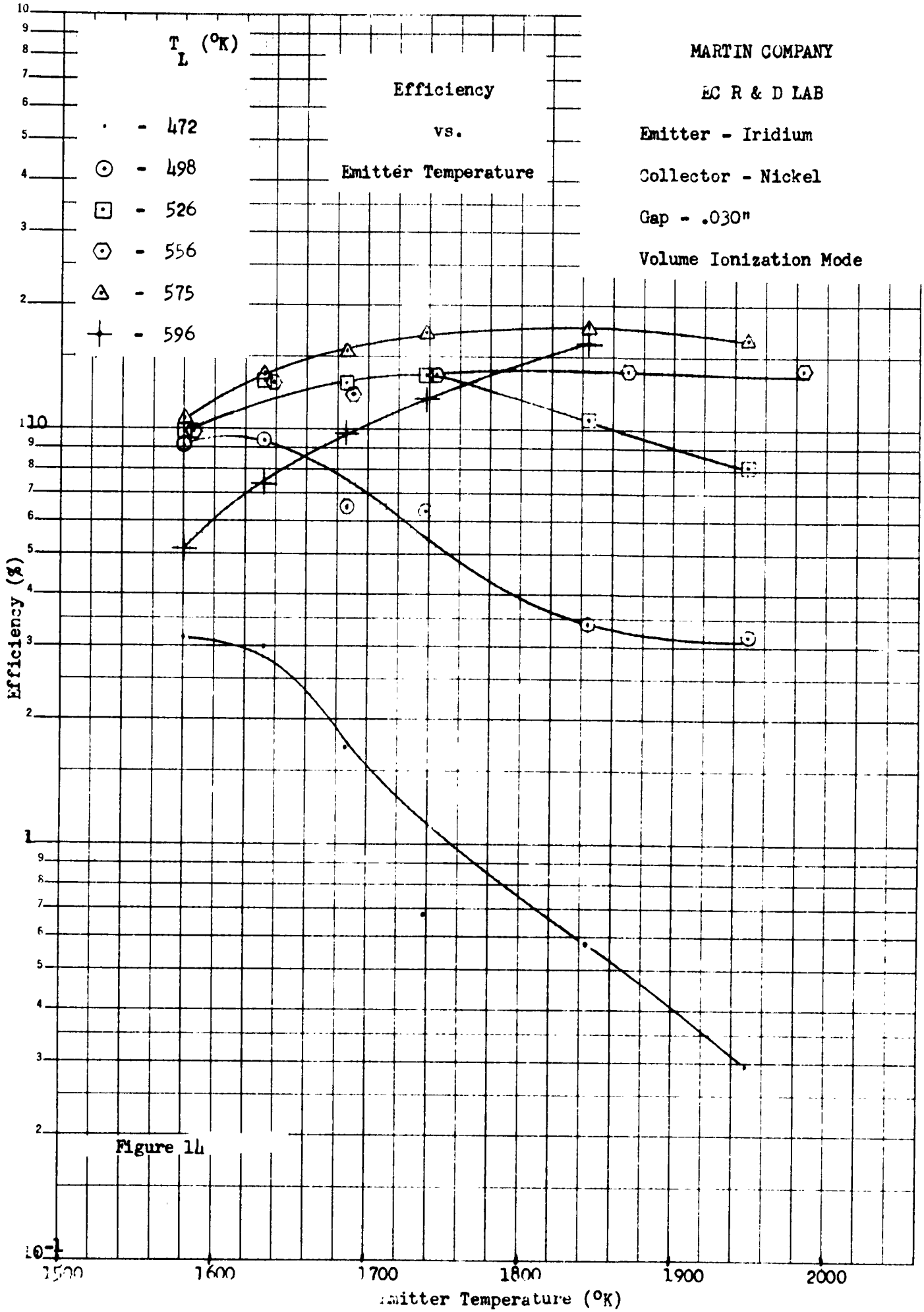
T_L (°K)
· - 472
⊙ - 498
⊡ - 526
⬡ - 556
△ - 575
✦ - 596
Efficiency
vs.
Emitter Temperature
MARTIN COMPANY
EC R & D LAB
Emitter - Iridium
Collector - Nickel
Gap - .030"
Volume Ionization Mode
Efficiency (%)
Emitter Temperature (°K)
1500
1600
1700
1800
1900
2000
SEMI-LOGARITHMIC 359-73
KEUFFEL & ESSER CO.

Figure 14

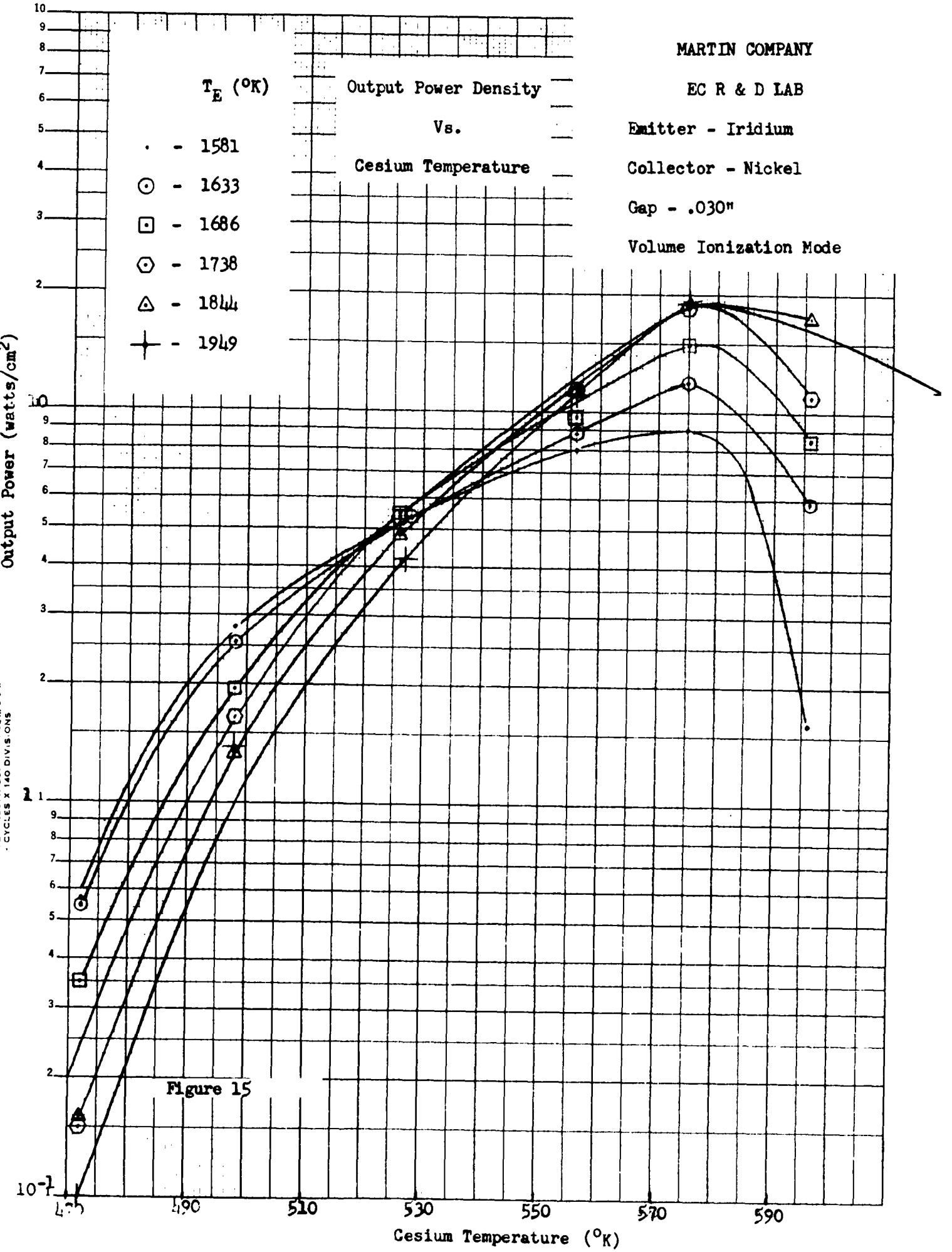
MARTIN COMPANY
EC R & D LAB
Emitter - Iridium
Collector - Nickel
Gap - .030"
Volume Ionization Mode
Output Power Density
Vs.
Cesium Temperature
T_E (°K)
· - 1581
⊙ - 1633
⊡ - 1686
⬡ - 1738
△ - 1844
✦ - 1949
Output Power (watts/cm²)
Cesium Temperature (°K)
10
9
8
7
6
5
4
3
2
1
10⁻¹
490
510
530
550
570
590
KEUFFEL & ESSER CO.
359-73
SEMI-LOGARITHMIC
3 CYCLES X 140 DIVISIONS

Figure 15

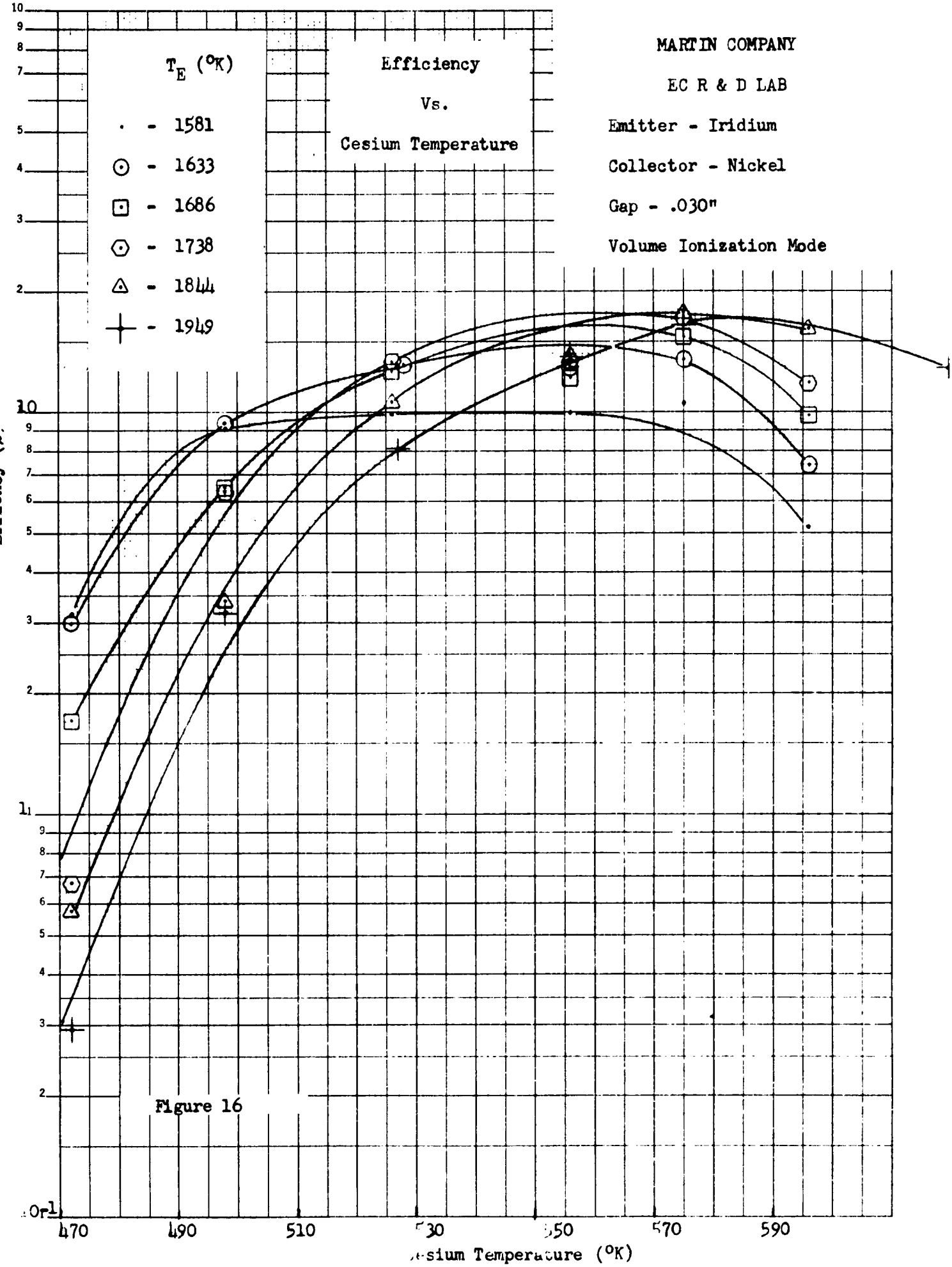
T_E (°K)
· - 1581
⊙ - 1633
⊡ - 1686
⊙ - 1738
△ - 1844
+ - 1949
Efficiency
Vs.
Cesium Temperature
MARTIN COMPANY
EC R & D LAB
Emitter - Iridium
Collector - Nickel
Gap - .030"
Volume Ionization Mode
Effiency (%)
Cesium Temperature (°K)
470
490
510
530
550
570
590

Figure 16

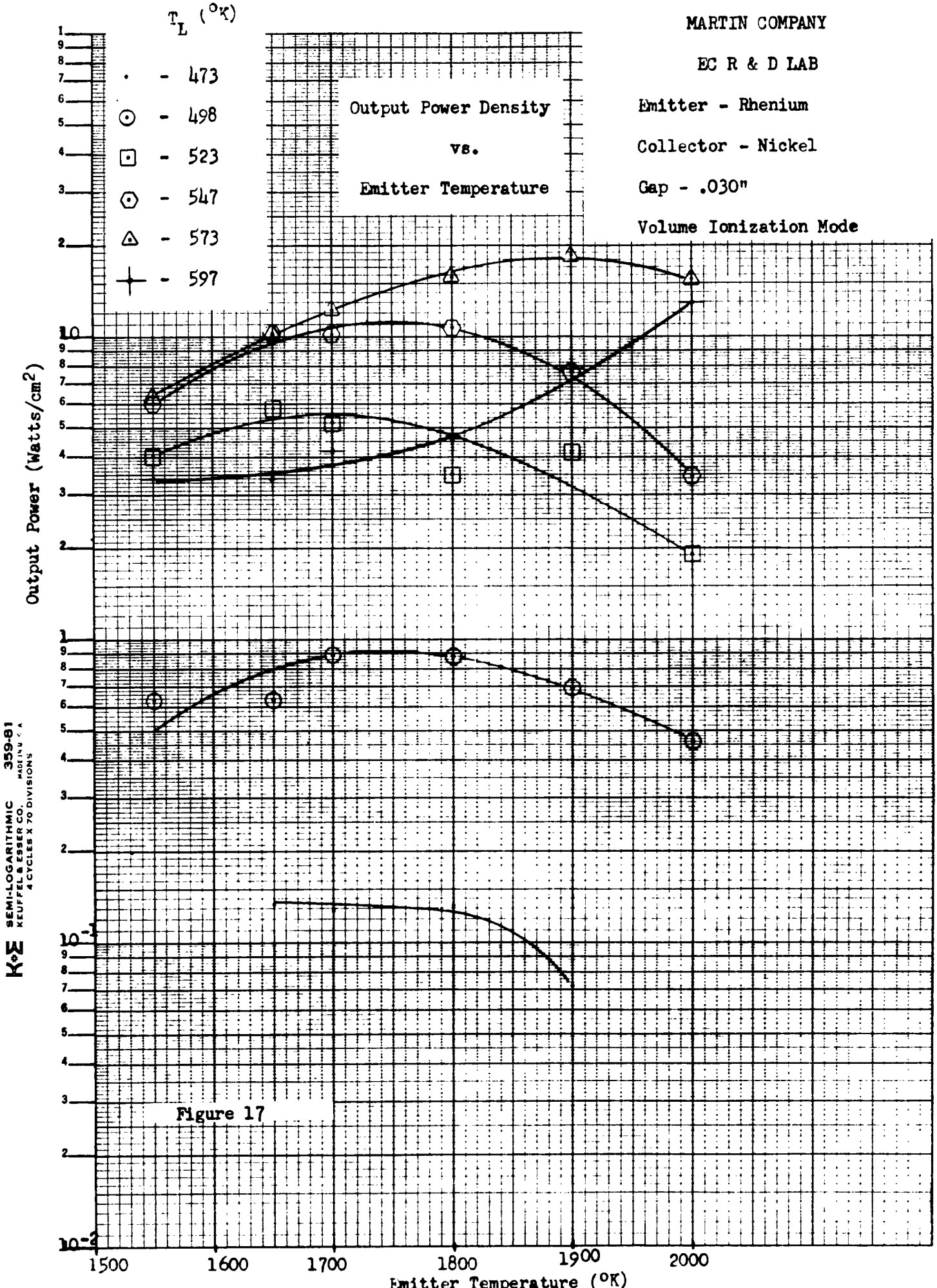
T_L (°K)
· - 473
⊙ - 498
⊡ - 523
⊙ - 547
△ - 573
+ - 597
Output Power Density
vs.
Emitter Temperature
MARTIN COMPANY
EC R & D LAB
Emitter - Rhenium
Collector - Nickel
Gap - .030"
Volume Ionization Mode
Output Power (Watts/cm²)
Emitter Temperature (°K)
1500
1600
1700
1800
1900
2000
SEMI-LOGARITHMIC 359-81
KEUFFEL & ESSER CO.
4 CYCLES X 70 DIVISIONS

Figure 17

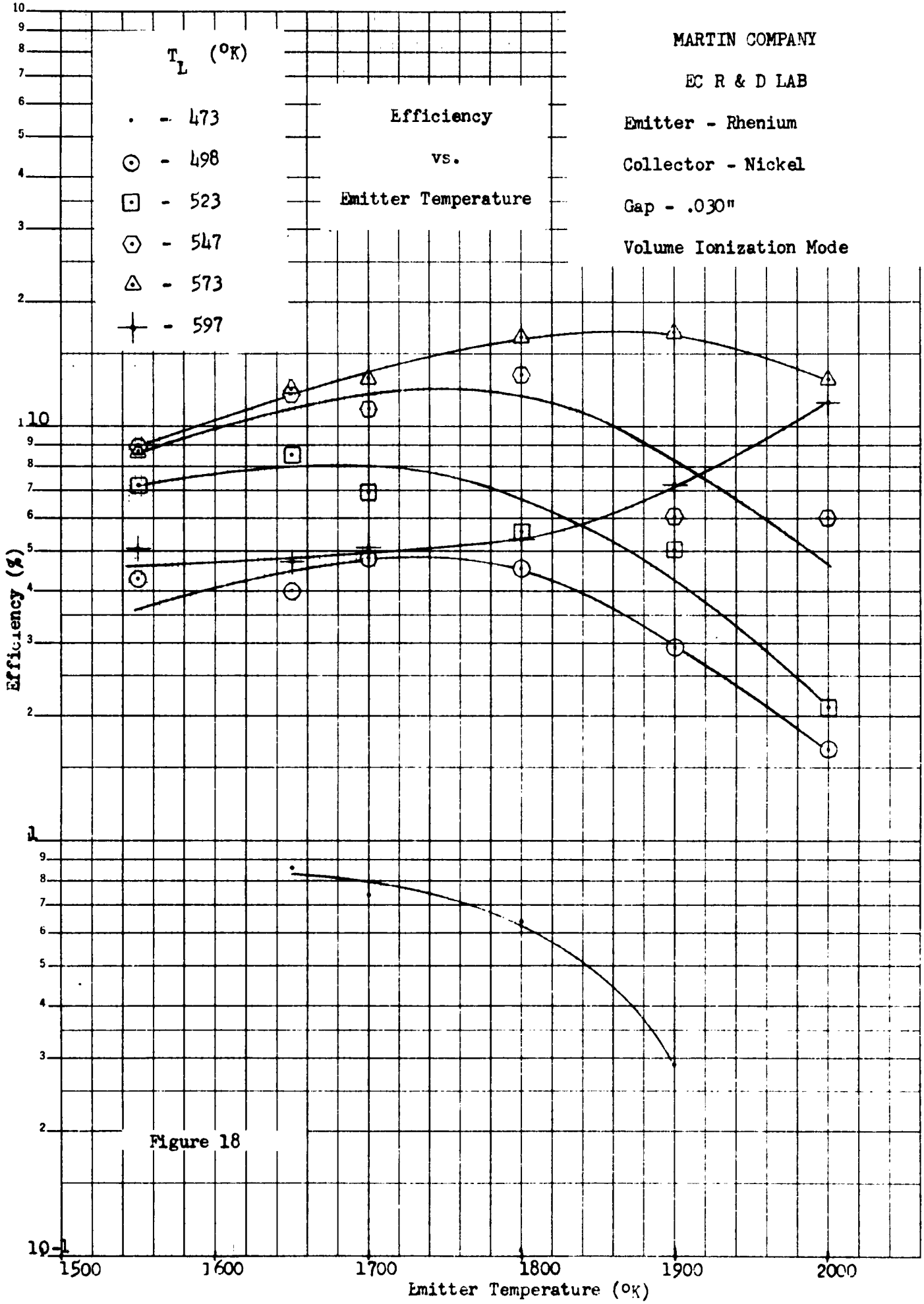
T_L (°K)
· - 473
⊙ - 498
⊡ - 523
⊙ - 547
△ - 573
✦ - 597
Efficiency
vs.
Emitter Temperature
MARTIN COMPANY
EC R & D LAB
Emitter - Rhenium
Collector - Nickel
Gap - .030"
Volume Ionization Mode
Efficiency (%)
Emitter Temperature (°K)
1500
1600
1700
1800
1900
2000
10
1
10-1

Figure 18

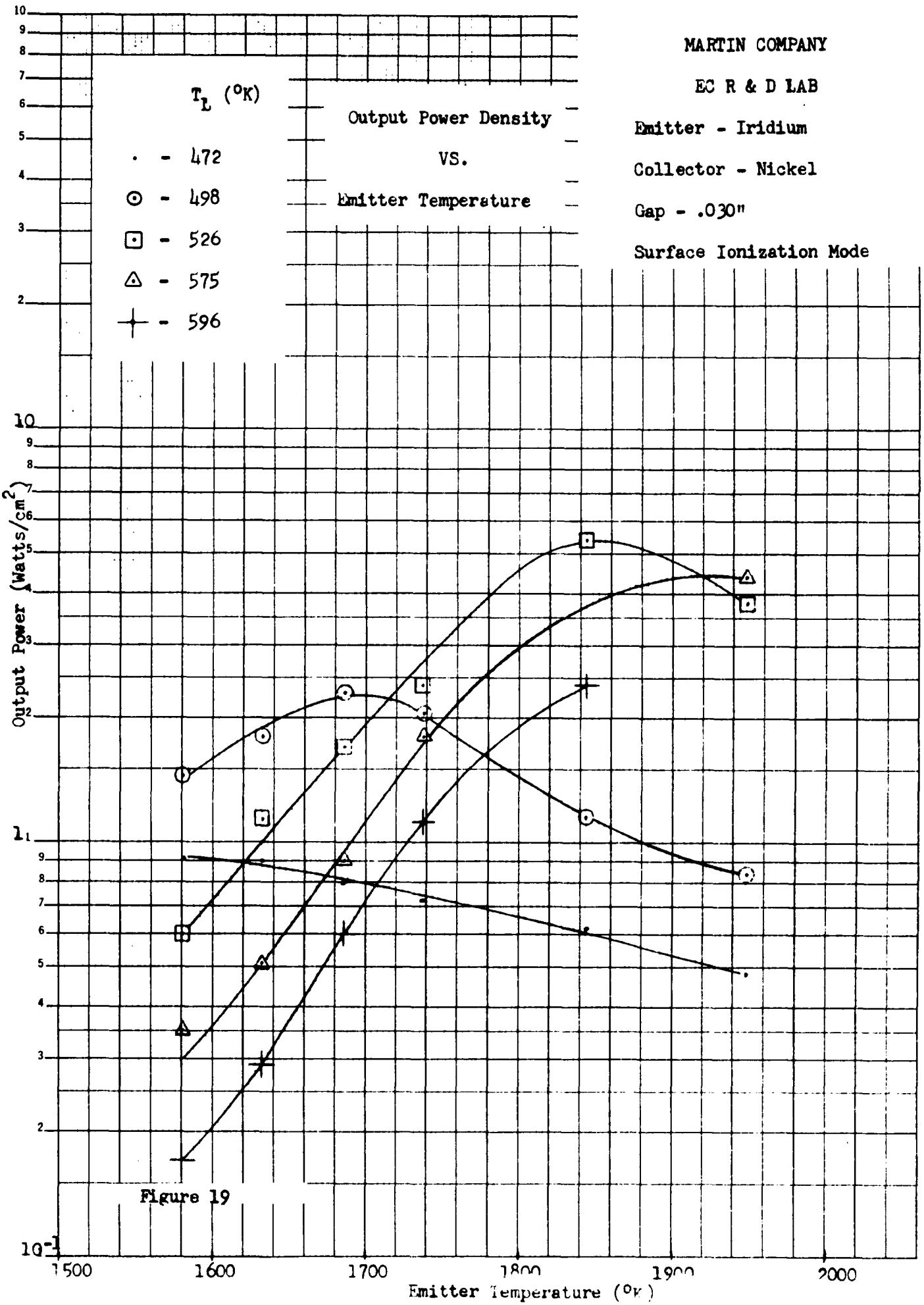
MARTIN COMPANY
EC R & D LAB
Emitter - Iridium
Collector - Nickel
Gap - .030"
Surface Ionization Mode
Output Power Density
VS.
Emitter Temperature
T_L (°K)
· - 472
⊙ - 498
⊡ - 526
△ - 575
✦ - 596
Output Power (Watts/cm²)
Emitter Temperature (°K)
1500
1600
1700
1800
1900
2000
SEMI-LOGARITHMIC 359-73
KEUFFEL & ESSER CO.
3 CYCLES X 140 DIVISIONS

Figure 19

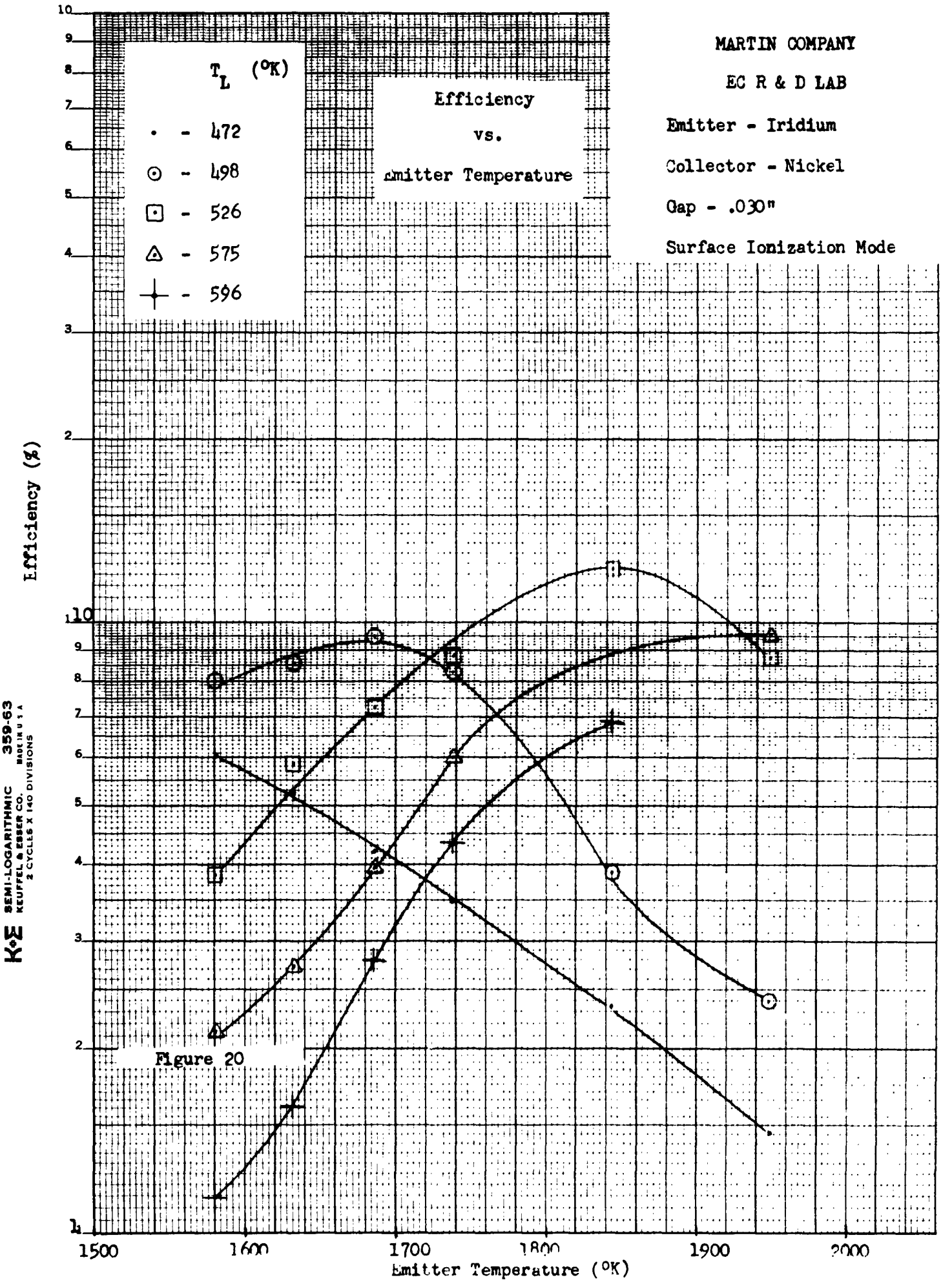
MARTIN COMPANY
EC R & D LAB
Emitter - Iridium
Collector - Nickel
Gap - .030"
Surface Ionization Mode
Efficiency
vs.
Emitter Temperature
T_L (°K)
· - 472
⊙ - 498
⊡ - 526
△ - 575
✦ - 596
Efficiency (%)
Emitter Temperature (°K)
1500
1600
1700
1800
1900
2000
K&E SEMI-LOGARITHMIC 359-63
KEUFFEL & ESSER CO. MADE IN U.S.A.
2 CYCLES X 140 DIVISIONS

Figure 20

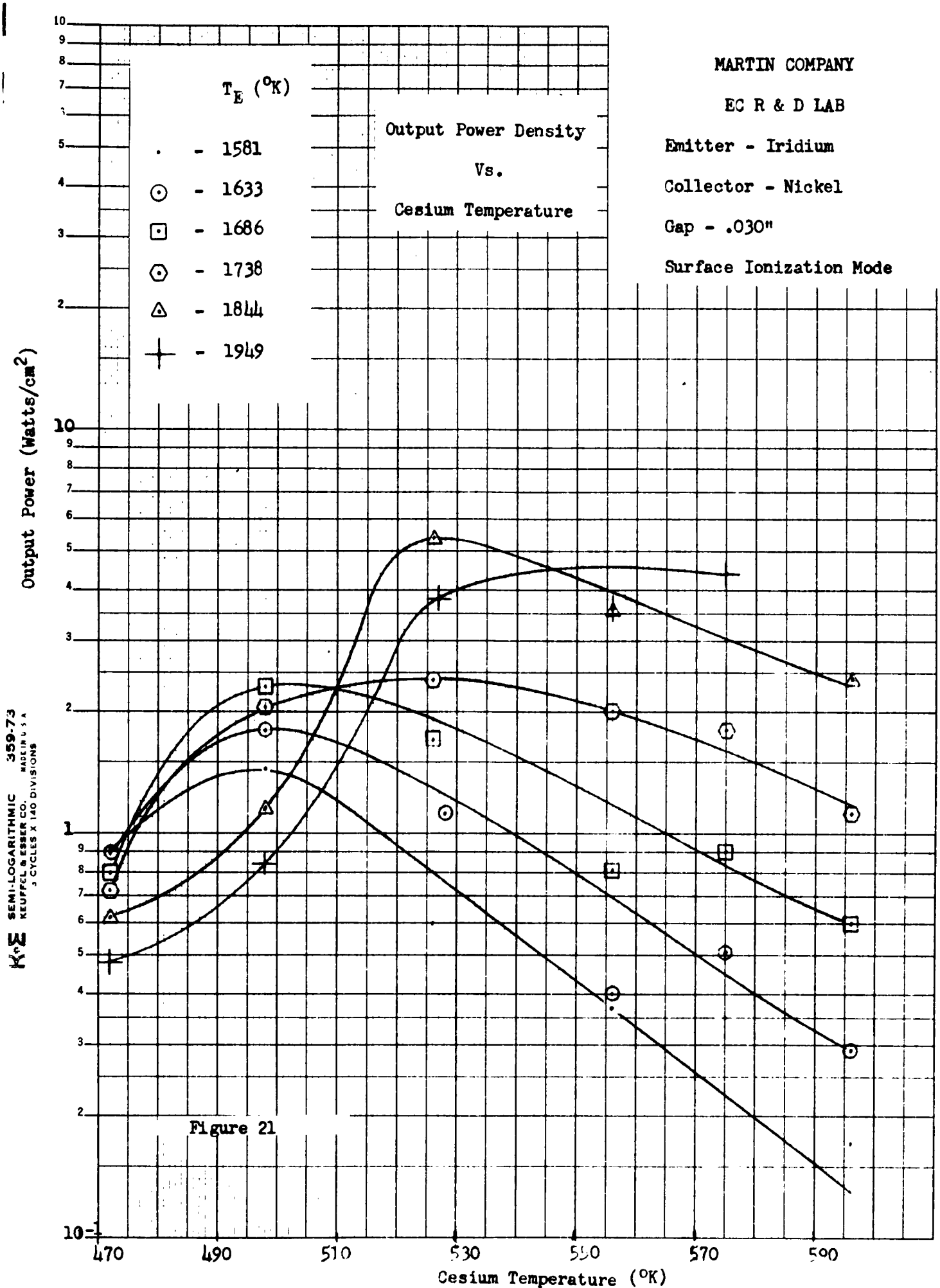
MARTIN COMPANY
EC R & D LAB
Emitter - Iridium
Collector - Nickel
Gap - .030"
Surface Ionization Mode
Output Power Density
Vs.
Cesium Temperature
T_E (°K)
. - 1581
⊙ - 1633
⊡ - 1686
⊙ - 1738
△ - 1844
+ - 1949
Output Power (Watts/cm²)
Cesium Temperature (°K)
470
490
510
530
550
570
590
SEMI-LOGARITHMIC 359-73
KEUFFEL & ESSER CO. MADE IN U.S.A.
3 CYCLES X 140 DIVISIONS

Figure 21

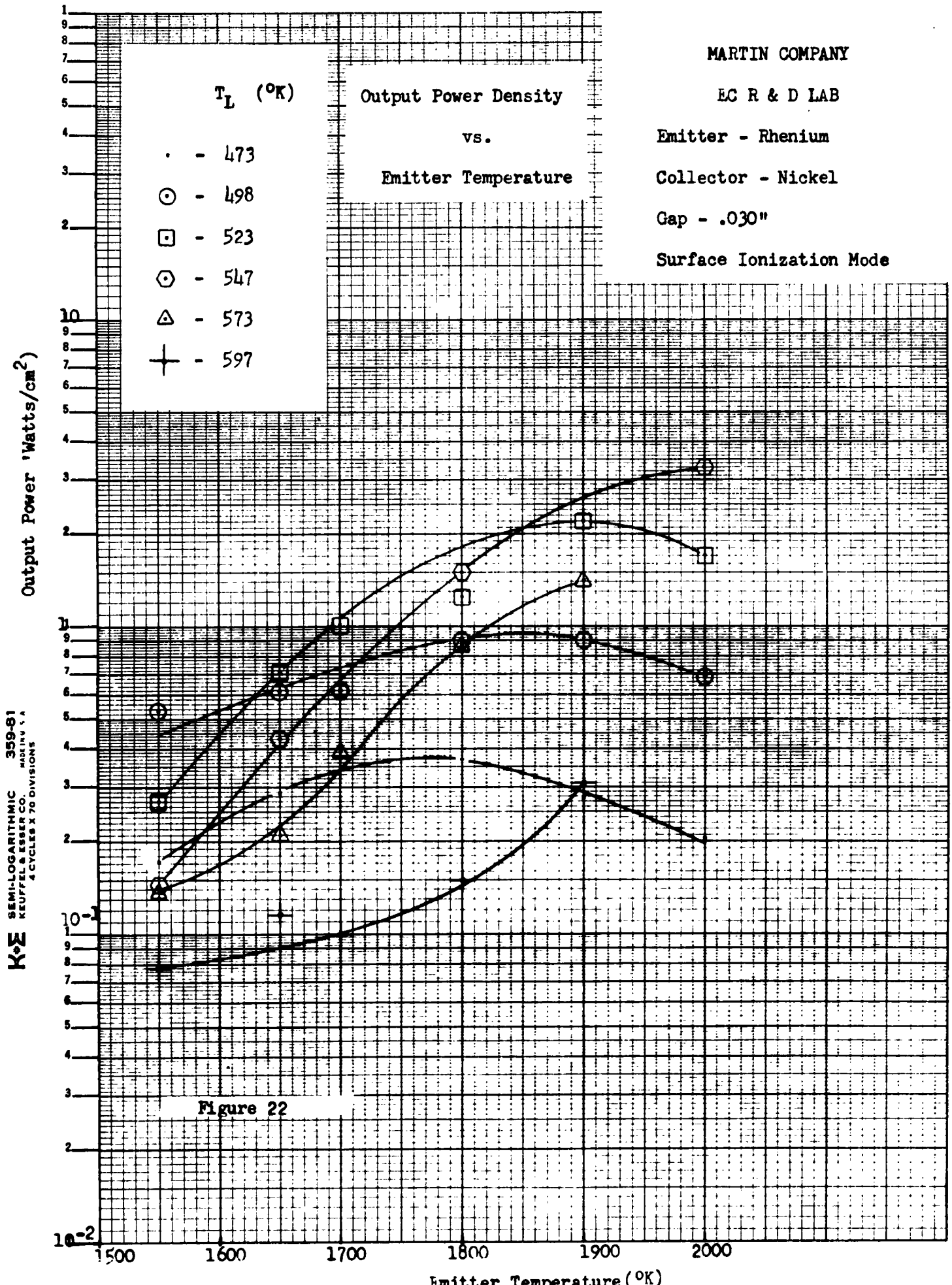
MARTIN COMPANY
EC R & D LAB
Emitter - Rhenium
Collector - Nickel
Gap - .030"
Surface Ionization Mode
Output Power Density
vs.
Emitter Temperature
T_L (°K)
· - 473
⊙ - 498
⊡ - 523
⊙ - 547
△ - 573
+ - 597
Output Power (Watts/cm²)
Emitter Temperature (°K)
1500
1600
1700
1800
1900
2000
SEMI-LOGARITHMIC 359-81
KEUFFEL & ESSER CO.
4 CYCLES X 70 DIVISIONS

Figure 22

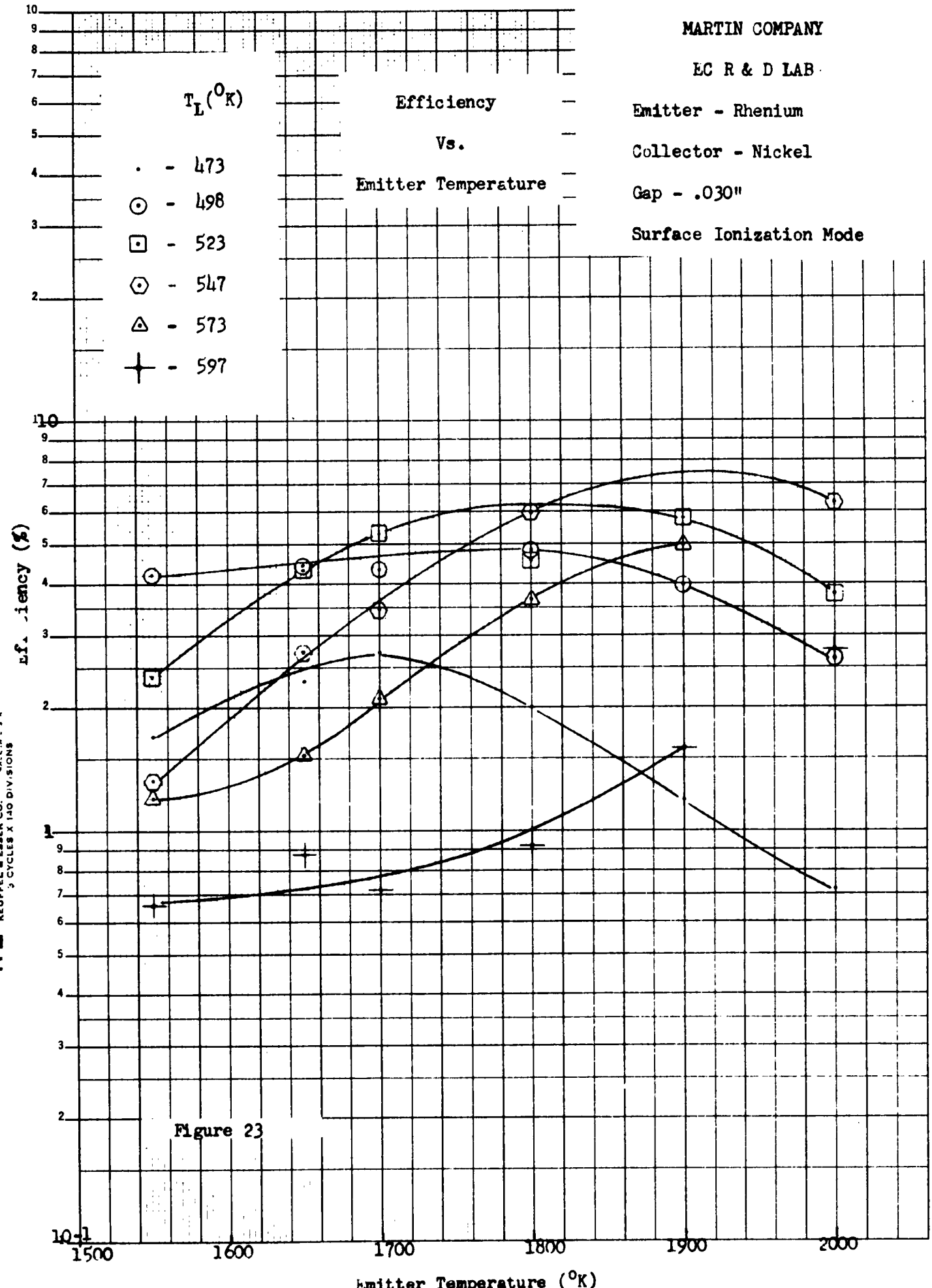
MARTIN COMPANY
EC R & D LAB
Emitter - Rhenium
Collector - Nickel
Gap - .030"
Surface Ionization Mode
Efficiency
Vs.
Emitter Temperature
T_L (^{0}K)
· - 473
⊙ - 498
⊡ - 523
⊙ - 547
△ - 573
+ - 597
Efficiency (%)
Emitter Temperature (^{0}K)
1500
1600
1700
1800
1900
2000
10
1
10-1
SEMI-LOGARITHMIC 359-73
KEUFFEL & ESSER CO.
3 CYCLES X 140 DIVISIONS

Figure 23

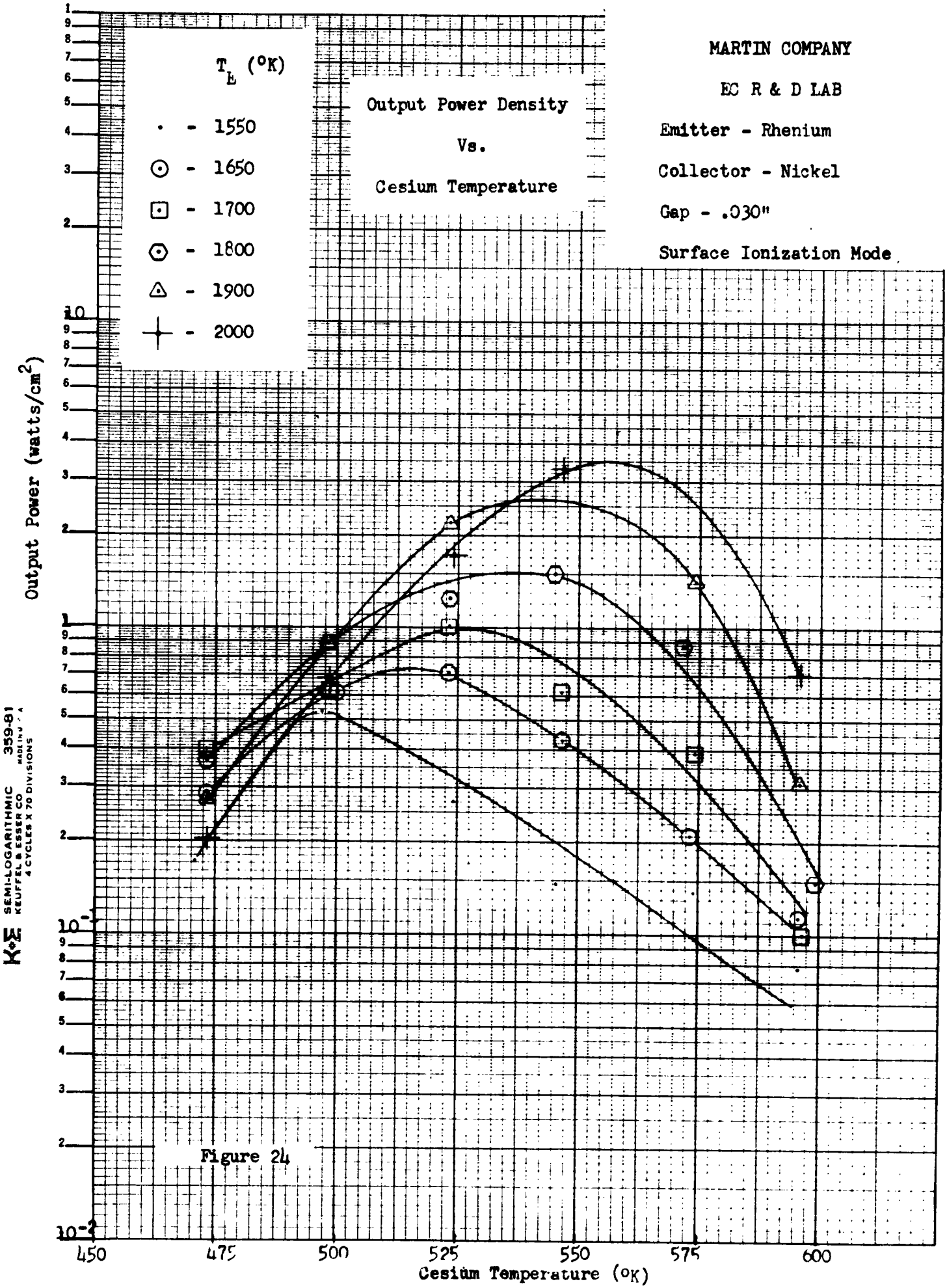
T_E (°K)
· - 1550
⊙ - 1650
⊡ - 1700
⊙ - 1800
△ - 1900
+ - 2000
Output Power Density
Vs.
Cesium Temperature
MARTIN COMPANY
EC R & D LAB
Emitter - Rhenium
Collector - Nickel
Gap - .030"
Surface Ionization Mode
Output Power (watts/cm²)
Cesium Temperature (°K)
450
475
500
525
550
575
600
SEMI-LOGARITHMIC 359-81
KEUFFEL & ESSER CO
4 CYCLES X 70 DIVISIONS

Figure 24

Figures 25 - 27

(section V. C)

Data obtained with the electron bombardment heated iridium emitter device.

Output current density versus voltage	Fig. 25
Output power density versus voltage	Fig. 26
Output power density and efficiency versus liquid cesium temperature. The efficiency in this curve is the overall efficiency, i.e., total output power divided by total input power	Fig. 27

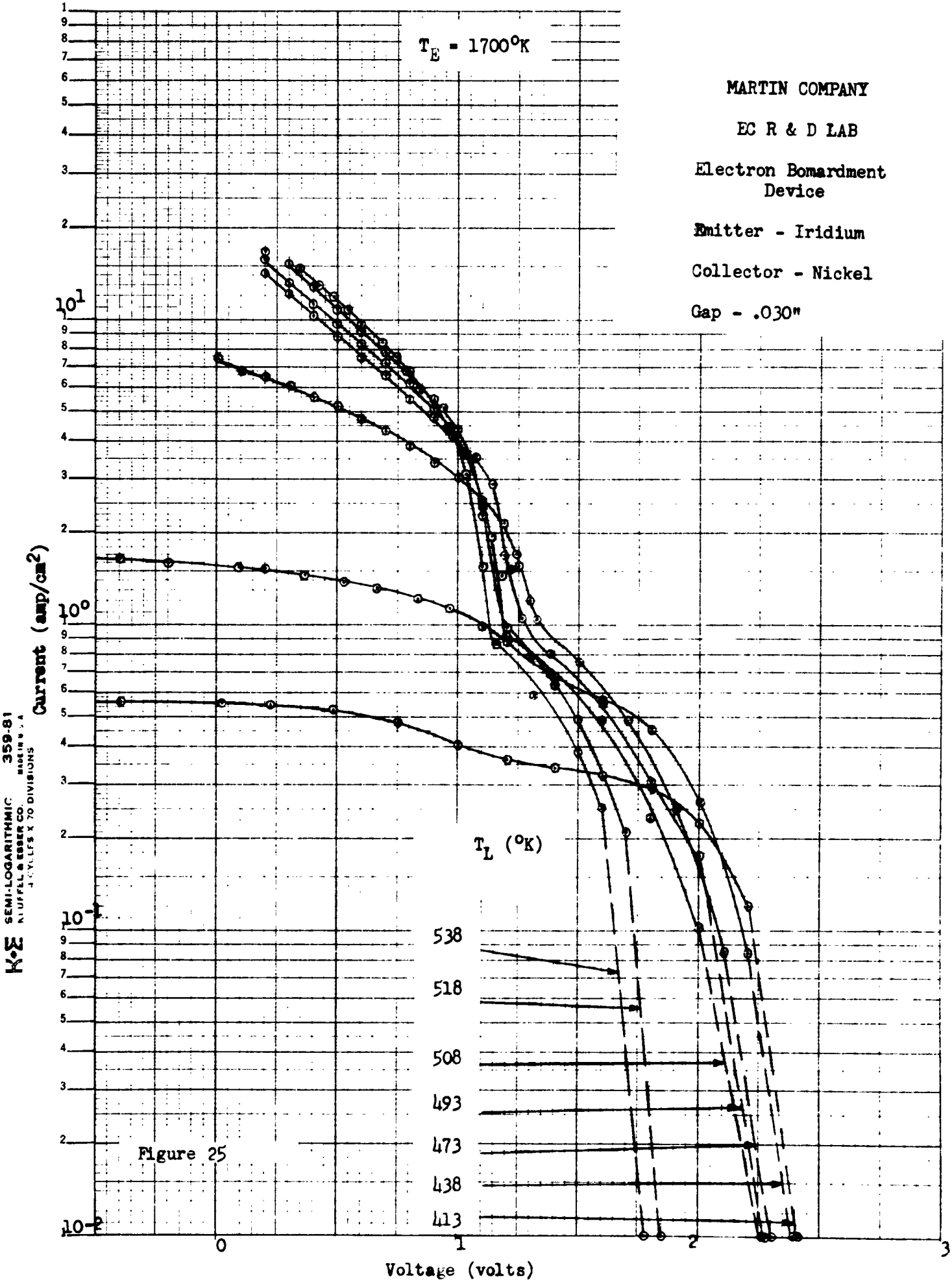
T_E = 1700°K
MARTIN COMPANY
EC R & D LAB
Electron Bomardment Device
Emitter - Iridium
Collector - Nickel
Gap - .030"
Current (amp/cm²)
10^1
10^0
10^{-1}
10^{-2}
T_L (°K)
538
518
508
493
473
438
413
0
1
2
3
Voltage (volts)
K&E SEMI-LOGARITHMIC 359-81
KEUFFEL & ESSER CO.
3 CYCLES X 70 DIVISIONS

Figure 25

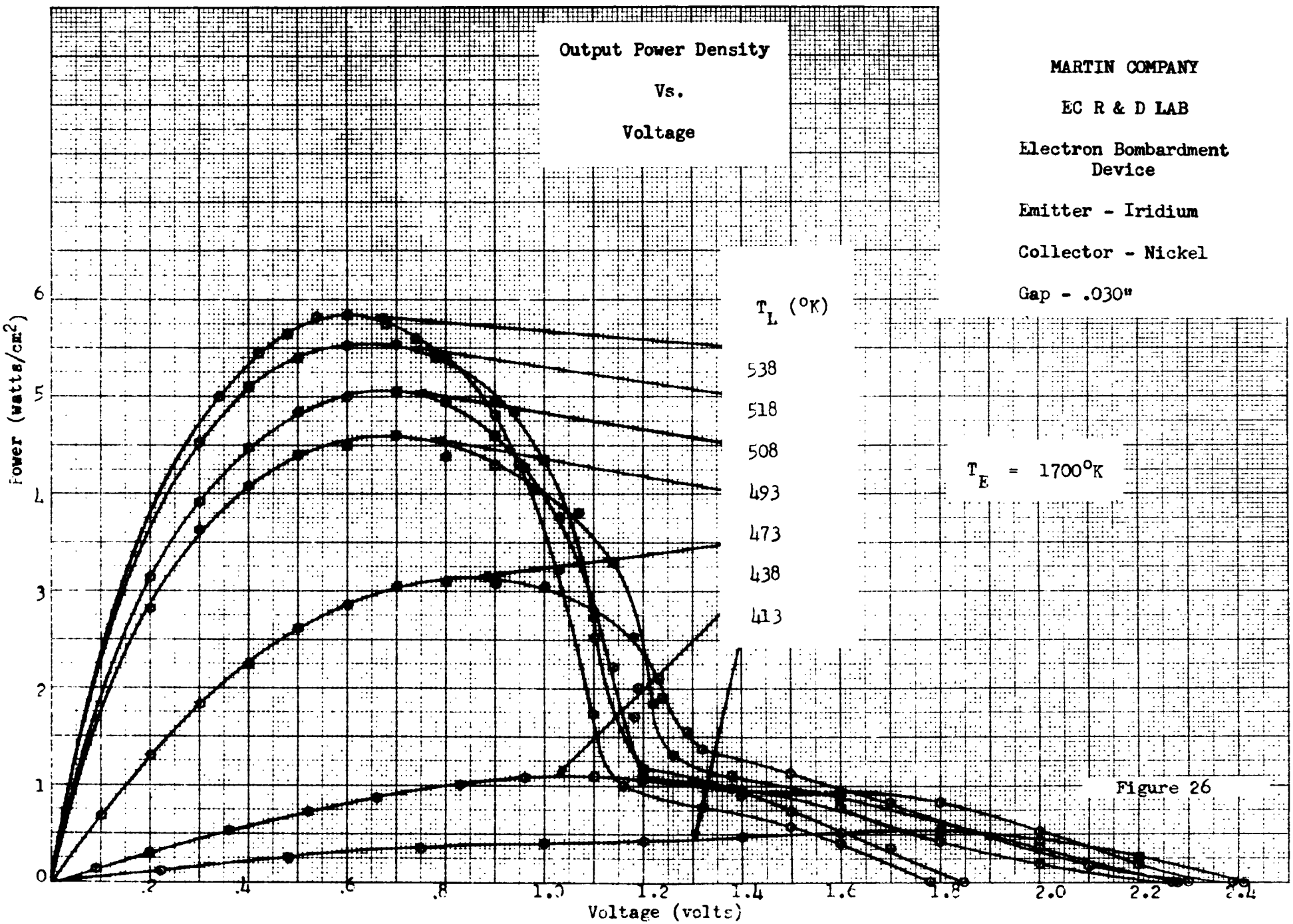

Figure 26

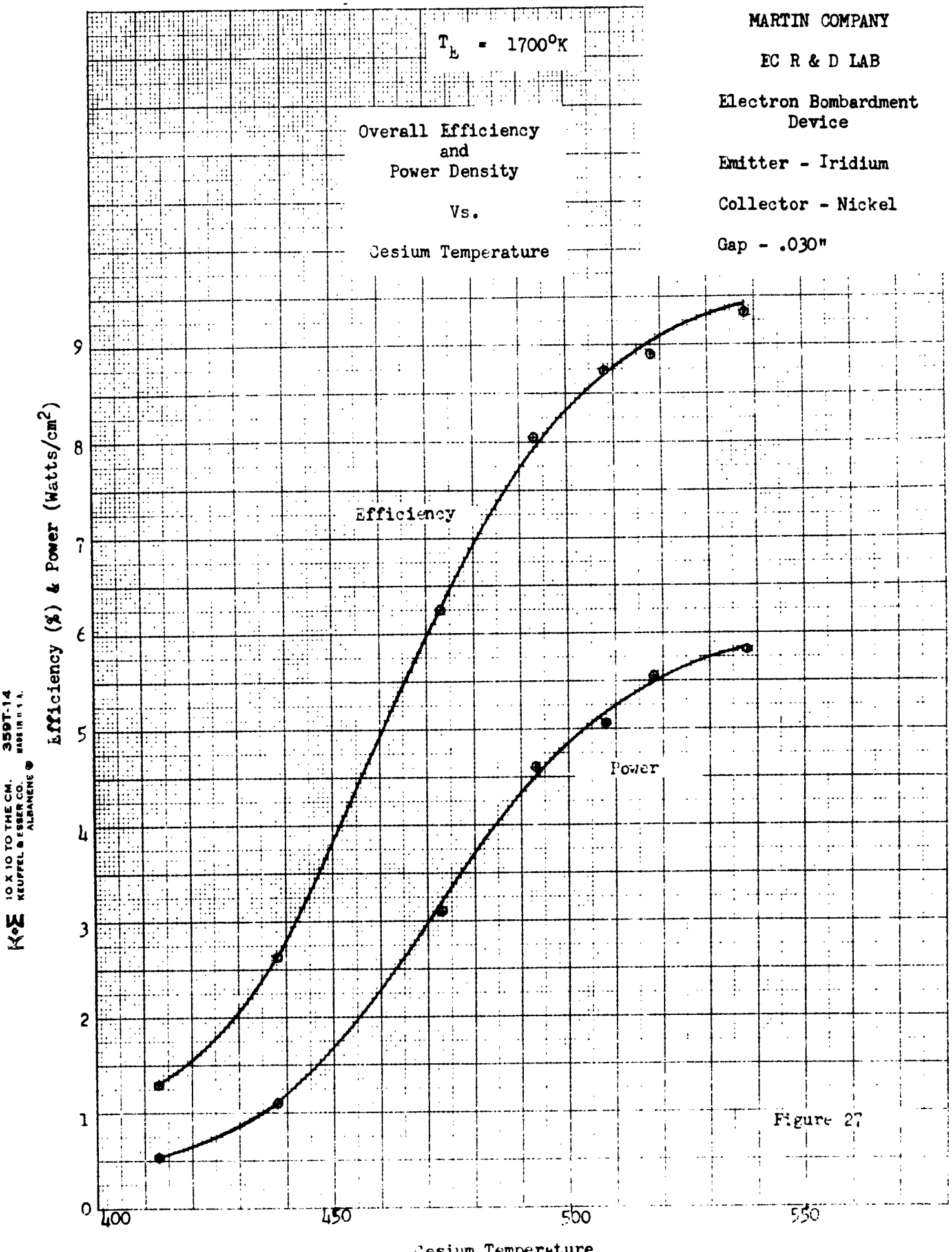
T_E = 1700°K
Overall Efficiency
and
Power Density
Vs.
Cesium Temperature
MARTIN COMPANY
EC R & D LAB
Electron Bombardment
Device
Emitter - Iridium
Collector - Nickel
Gap - .030"
Efficiency
Power
Efficiency (%) & Power (Watts/cm²)
Cesium Temperature
0
1
2
3
4
5
6
7
8
9
400
450
500
550
10 X 10 TO THE CM. 359T-14
KEUFFEL & ESSER CO. MADE IN U.S.A.
ALBANENE

Figure 27

Figure 28

(section IV. E)

Comparison of the best measured output power density and efficiency of the iridium emitter to those of the rhenium emitter.

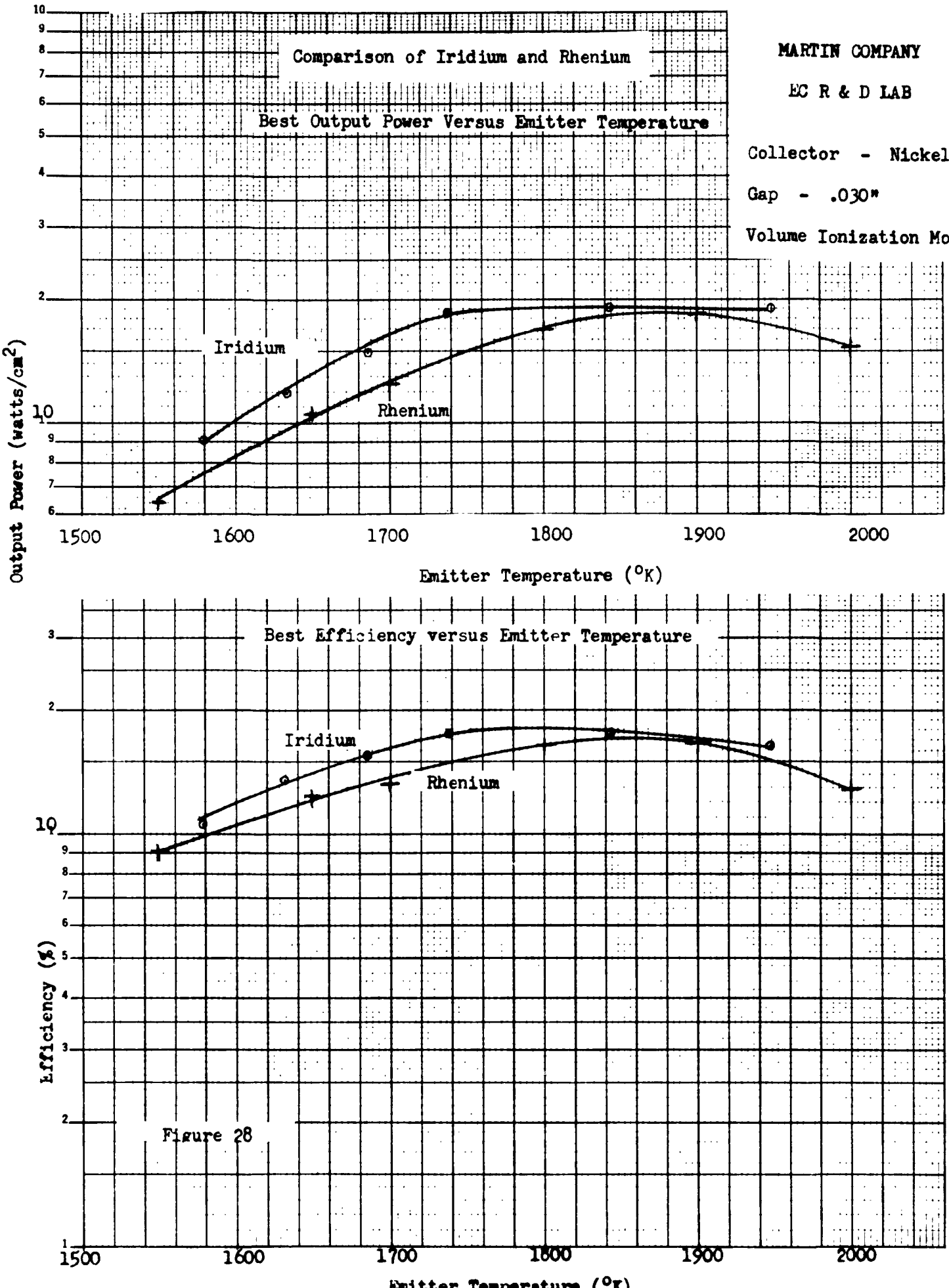
Comparison of Iridium and Rhenium
Best Output Power Versus Emitter Temperature
MARTIN COMPANY
EC R & D LAB
Collector - Nickel
Gap - .030"
Volume Ionization Mode
Iridium
Rhenium
Output Power (watts/cm²)
Emitter Temperature (°K)
Best Efficiency versus Emitter Temperature
Iridium
Rhenium
Efficiency (%)
Emitter Temperature (°K)

Figure 28

Figures 29 - 31

(section VI)

Comparison of test results of the filament devices to those of the electron bombardment heated device. The emitter temperature is 1700 ± 20°K. The liquid cesium temperatures are:

T_L = 526°K Fig. 29

T_L = 473°K Fig. 30

T_L = 495°K Fig. 31

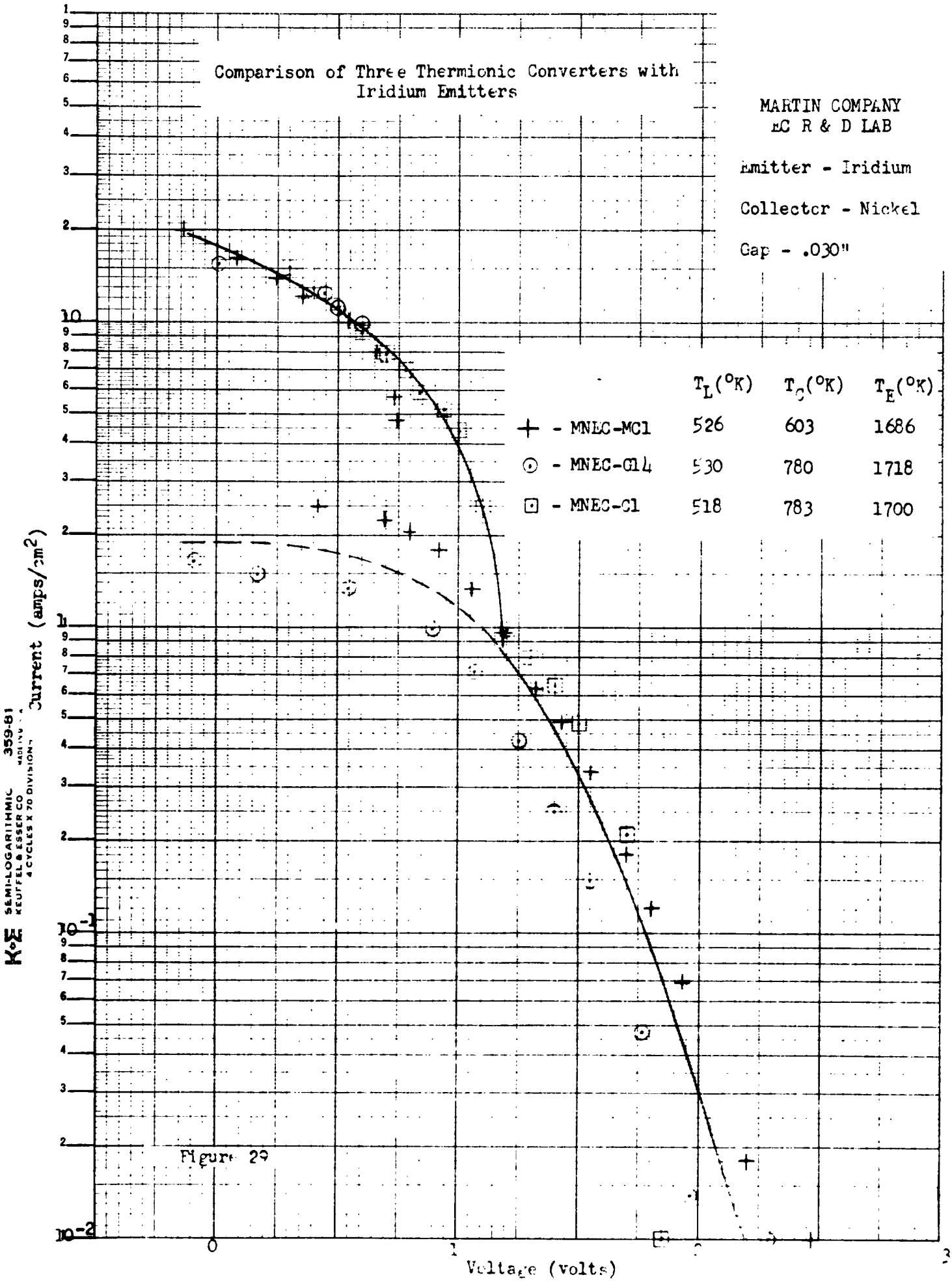
Comparison of Three Thermionic Converters with Iridium Emitters
MARTIN COMPANY
EC R & D LAB
Emitter - Iridium
Collector - Nickel
Gap - .030"
T_L(°K) T_C(°K) T_E(°K)
+ - MNEC-MC1 526 603 1686
⊙ - MNEC-C14 530 780 1718
⊡ - MNEC-C1 518 783 1700
Current (amps/cm²)
Voltage (volts)
KE SEMI-LOGARITHMIC 359-81
KEUFFEL & ESSER CO
4 CYCLES X 70 DIVISIONS

Figure 29

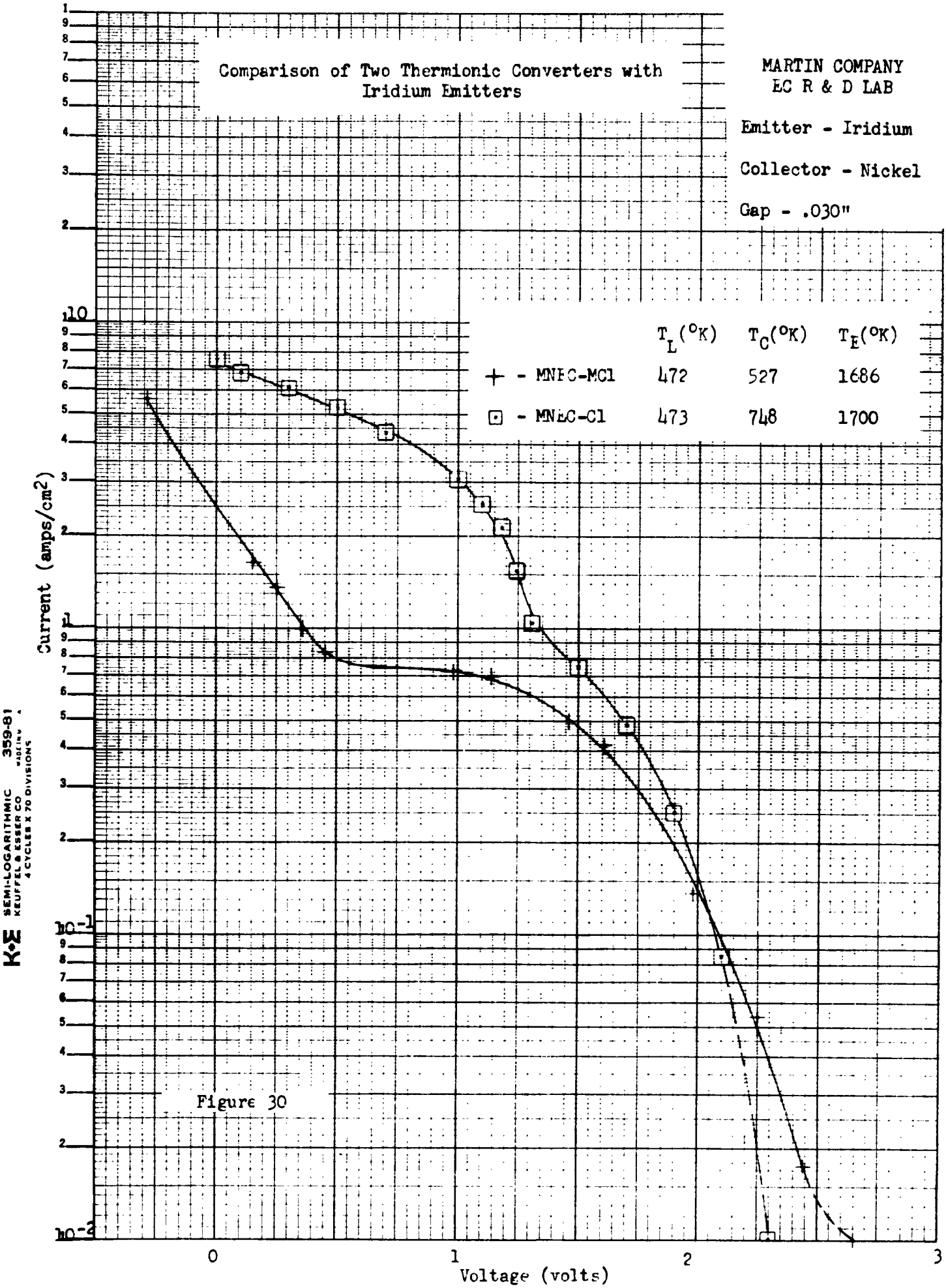
Comparison of Two Thermionic Converters with Iridium Emitters
MARTIN COMPANY
EC R & D LAB
Emitter - Iridium
Collector - Nickel
Gap - .030"
T_L(°K) T_C(°K) T_E(°K)
+ - MNEC-MCl 472 527 1686
⊡ - MNEC-Cl 473 748 1700
Current (amps/cm²)
Voltage (volts)
SEMI-LOGARITHMIC 359-81
KEUFFEL & ESSER CO
4 CYCLES X 70 DIVISIONS

Figure 30

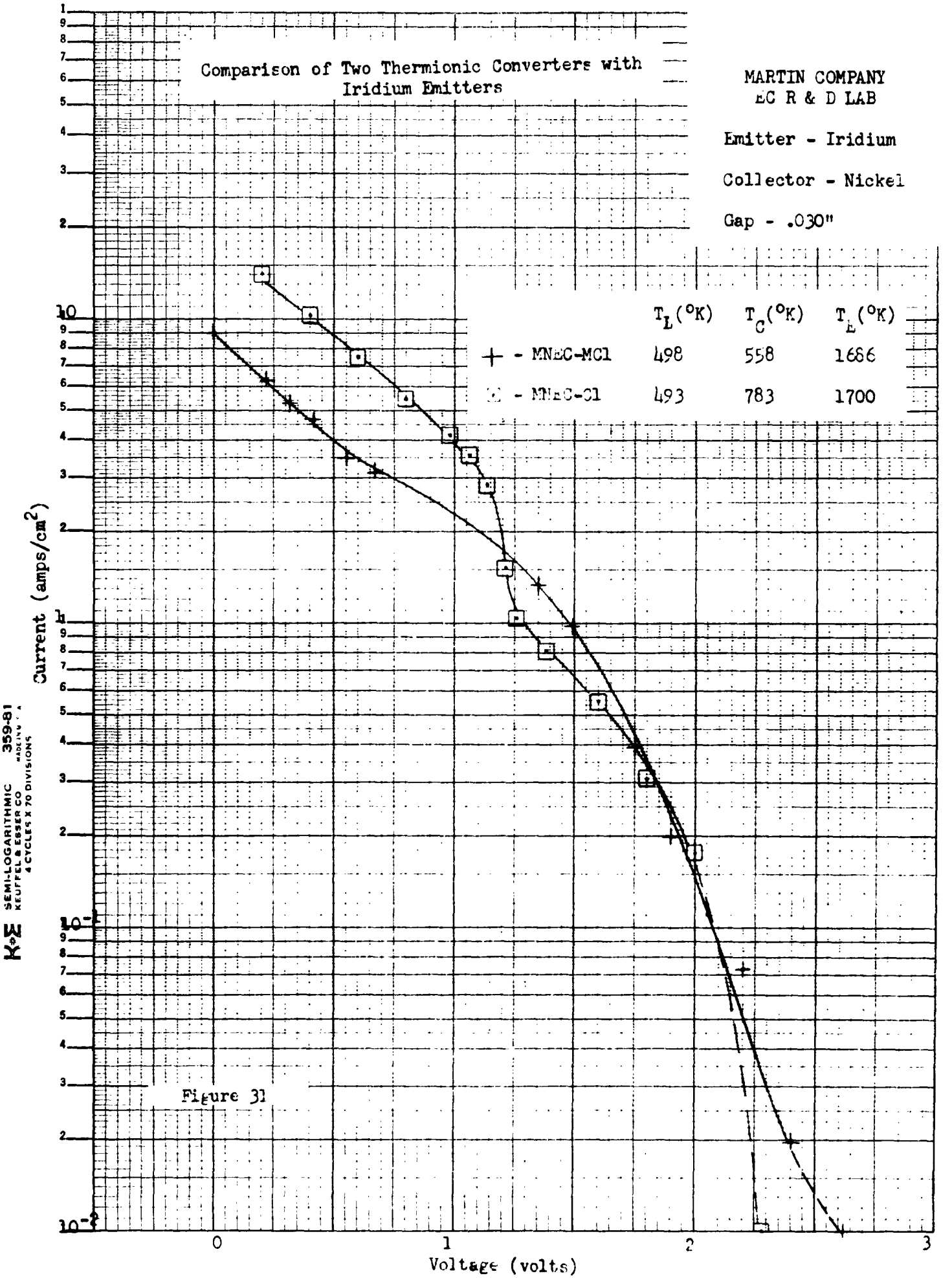
Comparison of Two Thermionic Converters with Iridium Emitters
MARTIN COMPANY
EC R & D LAB
Emitter - Iridium
Collector - Nickel
Gap - .030"
T_L(°K) T_C(°K) T_E(°K)
+ - MNEC-MC1 498 558 1686
○ - MNEC-C1 493 783 1700
Current (amps/cm²)
Voltage (volts)
0
1
2
3
SEMI-LOGARITHMIC 359-81
KEUFFEL & ESSER CO
4 CYCLES X 70 DIVISIONS

Figure 31

Figures 32 - 36

(section IV - 10)

Characteristic current versus voltage curves for the platinum emitter.

T_L = 487°K	Fig. 32
T_L = 514°K	Fig. 33
T_L = 568°K	Fig. 34
Comparison of two tests at T_L = 568°K and T_E = 1765°K. The cross on the characteristic curve indicates the extent of the curve of run B	Fig. 35
Reproduction of a photograph of the oscilloscope trace	Fig. 36

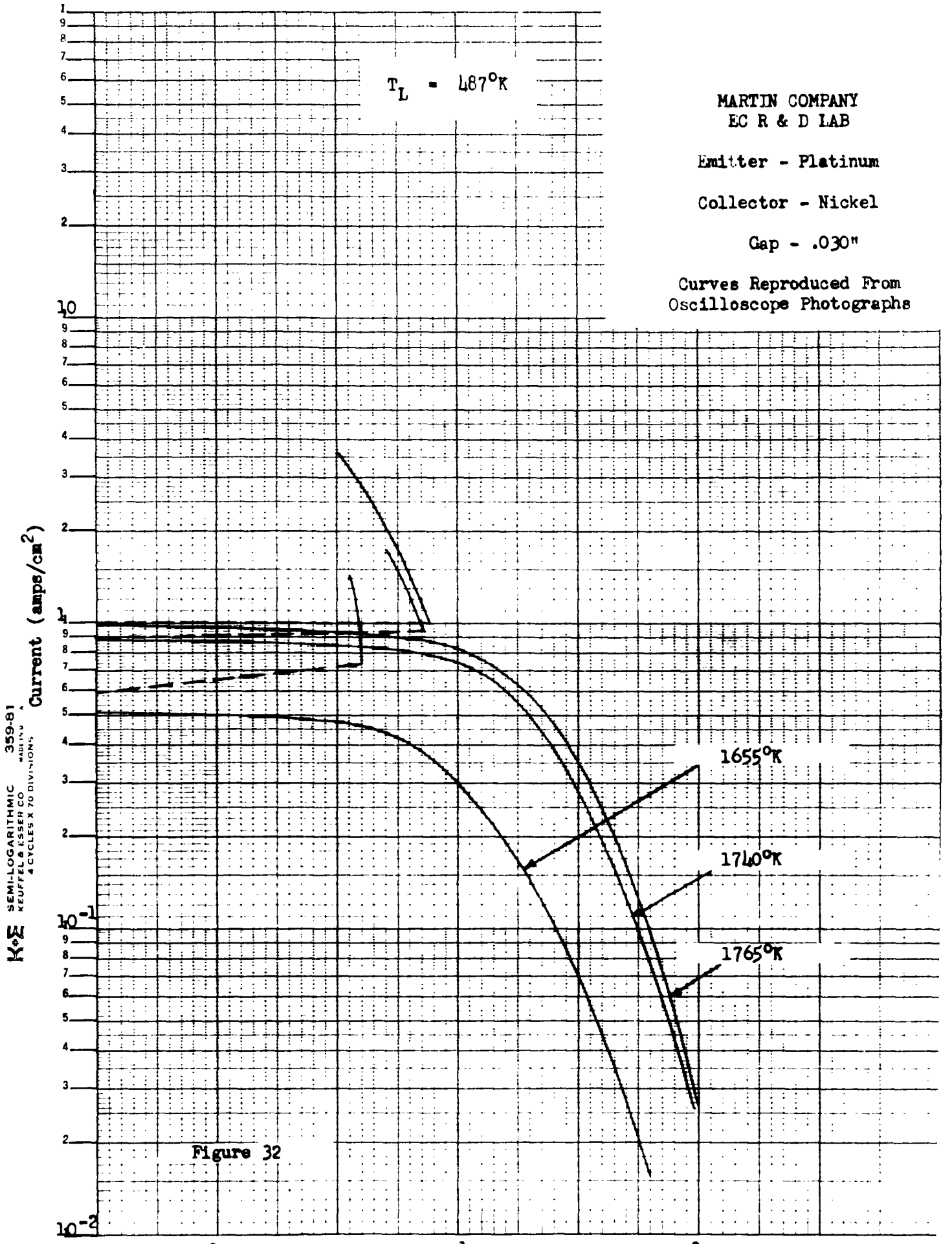
T_L = 487°K
MARTIN COMPANY
EC R & D LAB
Emitter - Platinum
Collector - Nickel
Gap - .030"
Curves Reproduced From
Oscilloscope Photographs
Current (amps/cm²)
1655°K
1740°K
1765°K
K&E 359-81
SEMI-LOGARITHMIC
KEUFFEL & ESSER CO
4 CYCLES X 70 DIVISIONS
10
1
10^{-1}
10^{-2}
0
1
2

Figure 32

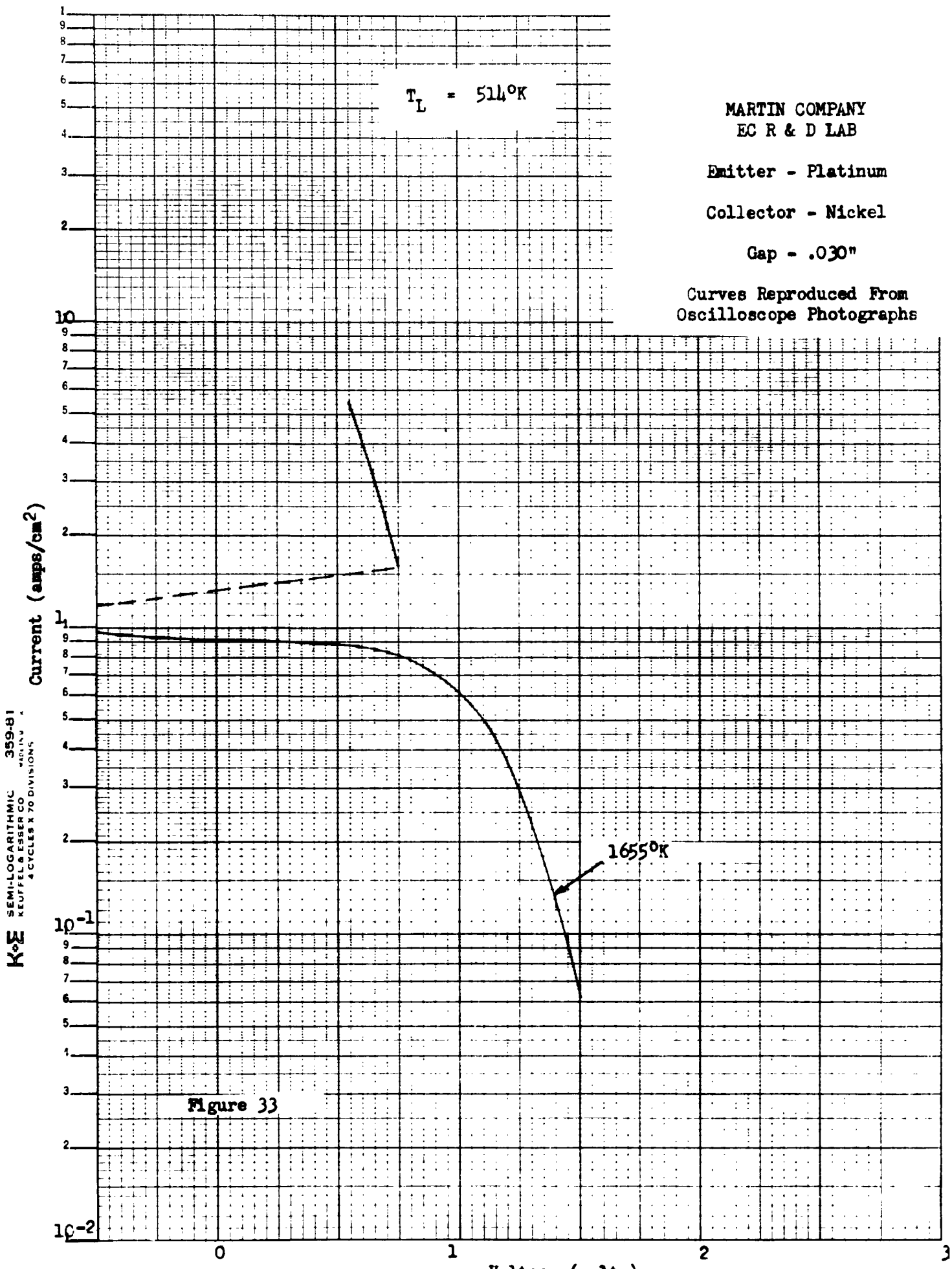
T_L = 514°K
MARTIN COMPANY
EC R & D LAB
Emitter - Platinum
Collector - Nickel
Gap - .030"
Curves Reproduced From
Oscilloscope Photographs
1655°K
Current (amps/cm²)
Voltage (volts)
SEMI-LOGARITHMIC 359-81
KEUFFEL & ESSER CO
4 CYCLES X 70 DIVISIONS

Figure 33

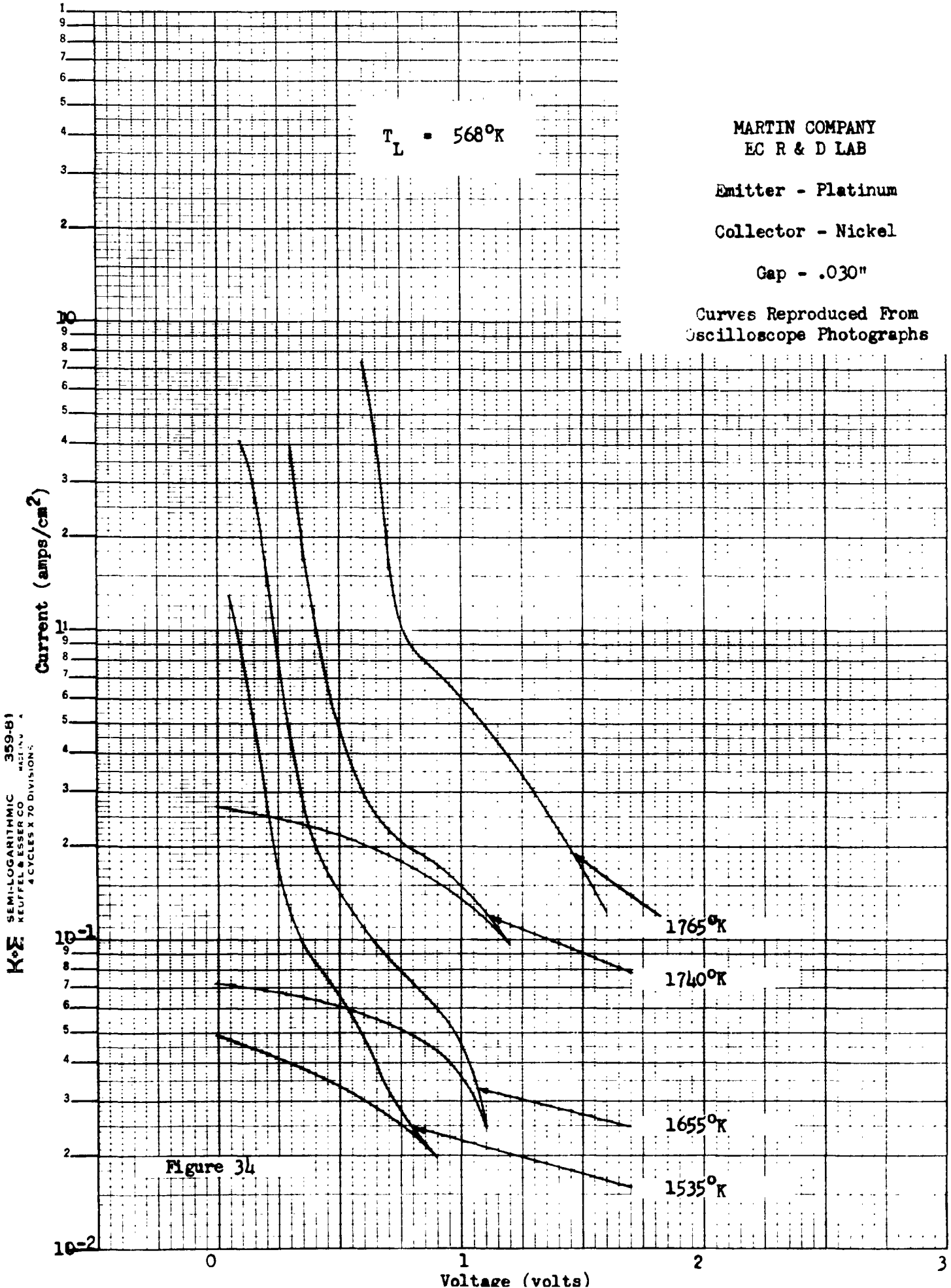
T_L = 568°K
MARTIN COMPANY
EC R & D LAB
Emitter - Platinum
Collector - Nickel
Gap - .030"
Curves Reproduced From
Oscilloscope Photographs
Current (amps/cm²)
Voltage (volts)
1765°K
1740°K
1655°K
1535°K
0
1
2
3
10
10⁻¹
10⁻²
K&E 359-81
SEMI-LOGARITHMIC
KEUFFEL & ESSER CO
4 CYCLES X 70 DIVISIONS

Figure 34

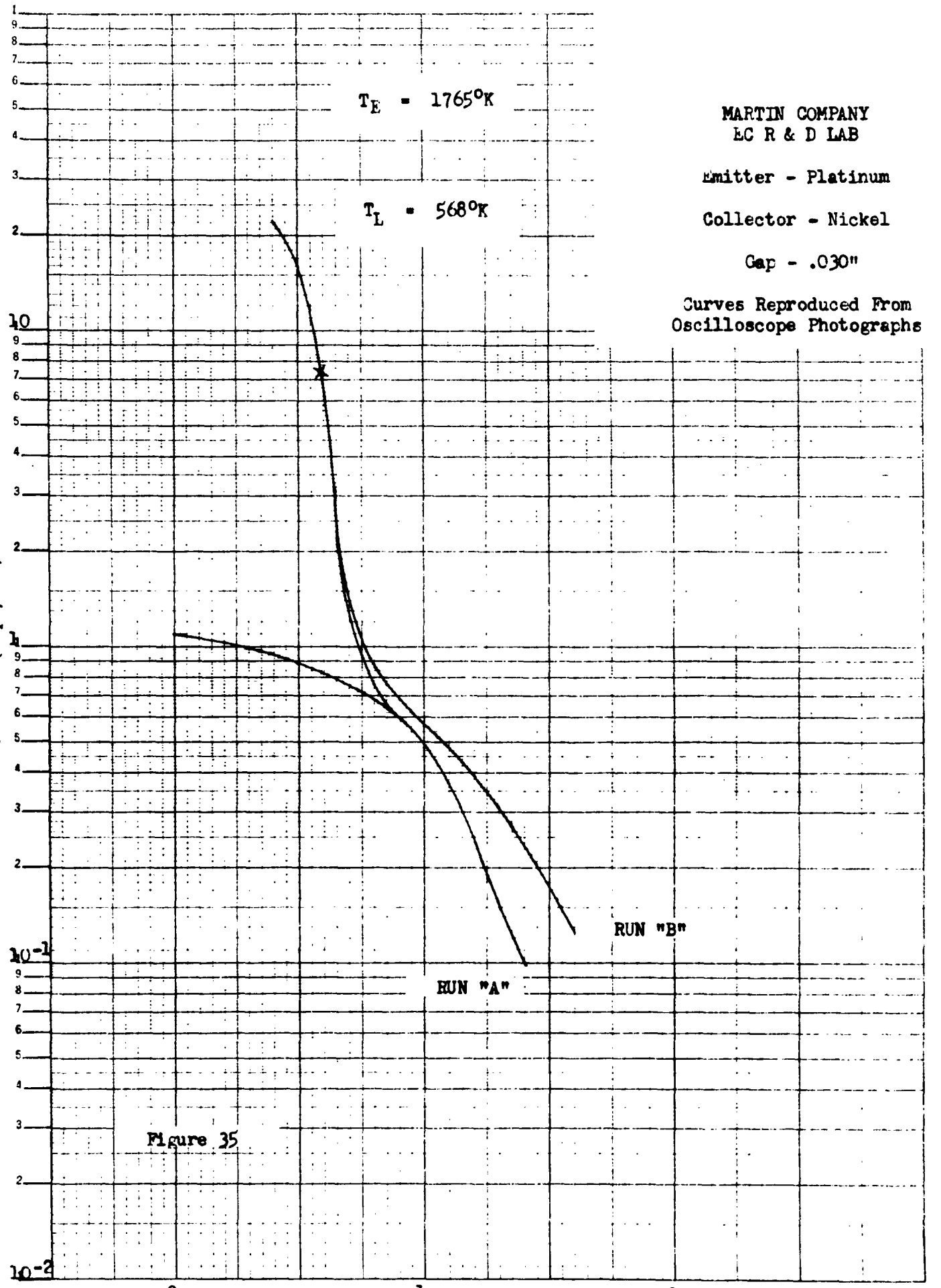
T_E = 1765°K
T_L = 568°K
MARTIN COMPANY
EC R & D LAB
Emitter - Platinum
Collector - Nickel
Gap - .030"
Curves Reproduced From
Oscilloscope Photographs
Current (amps/cm²)
RUN "B"
RUN "A"
10
1
10⁻¹
10⁻²
0
1
2
3

Figure 35

MARTIN COMPANY
EC R & D LAB

Emitter - Platinum

Collector - Nickel

Gap - .030"

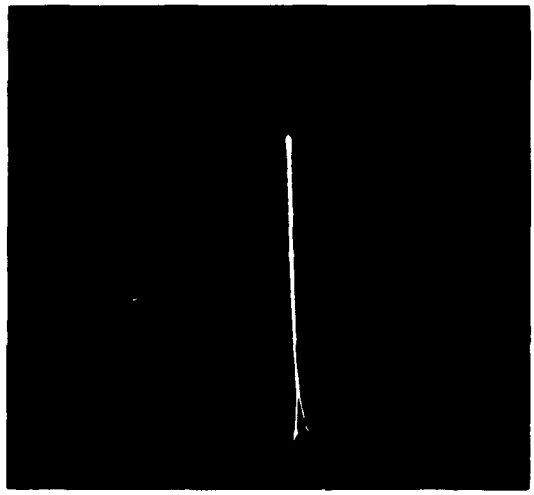

T_E = 1740°K

T_L = 568°K

T_C = 907°K

Vertical - 0.2 amp/cm

Horizontal - 0.5 volt/cm

Zero at bottom

Figure 36

Oscilloscope Trace of Current - Voltage Curve

Figures 37 - 39

(section V. A,B)

The electron bombardment heated device with iridium emitter.

Sketch of the components	Fig. 37
Photograph of device	Fig. 38
Photograph of device prepared for test	Fig. 39

Cylindrical Indirectly Heated Device
With Iridium Emitter

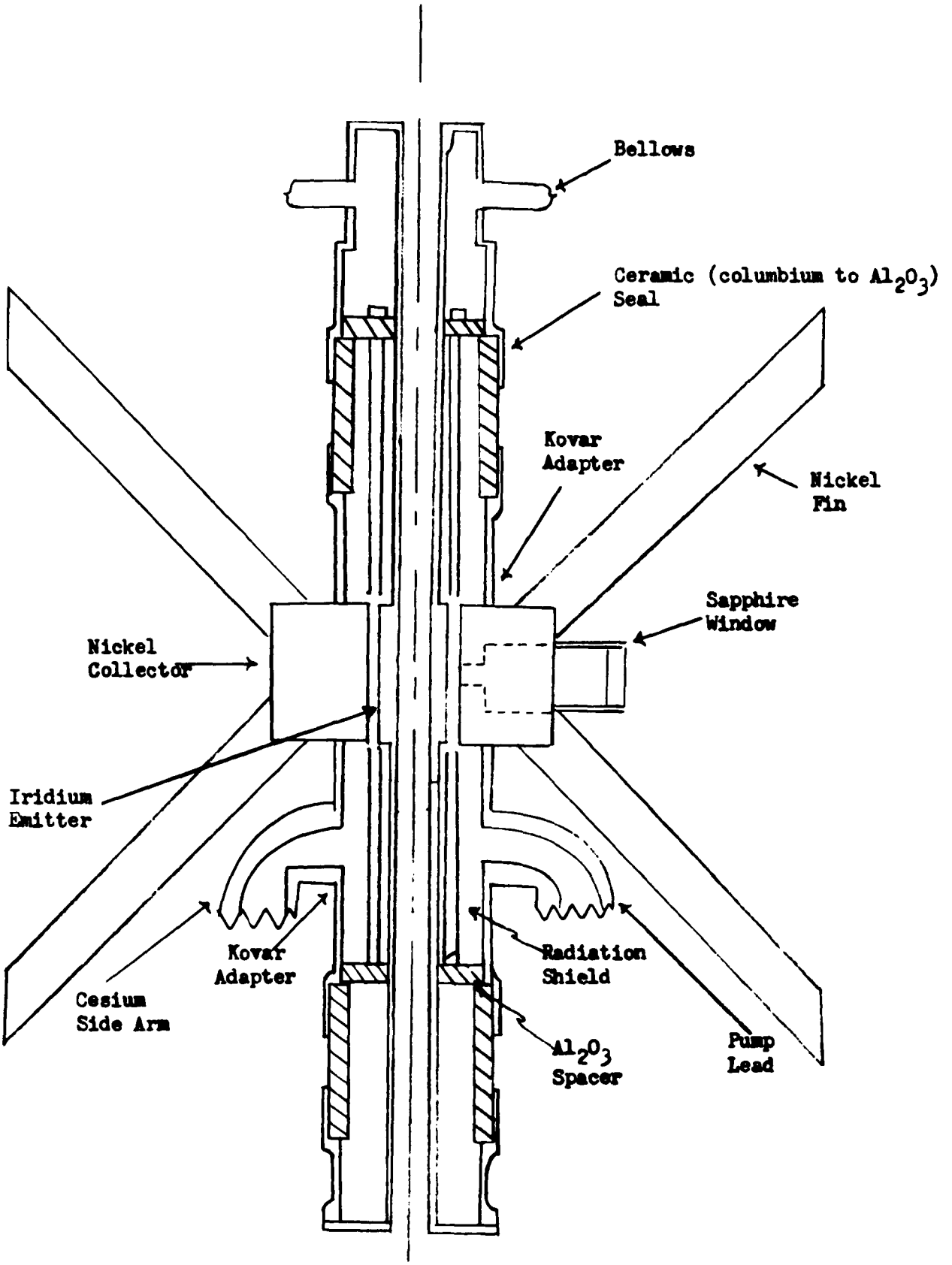

Scale: 2:1

Figure 37

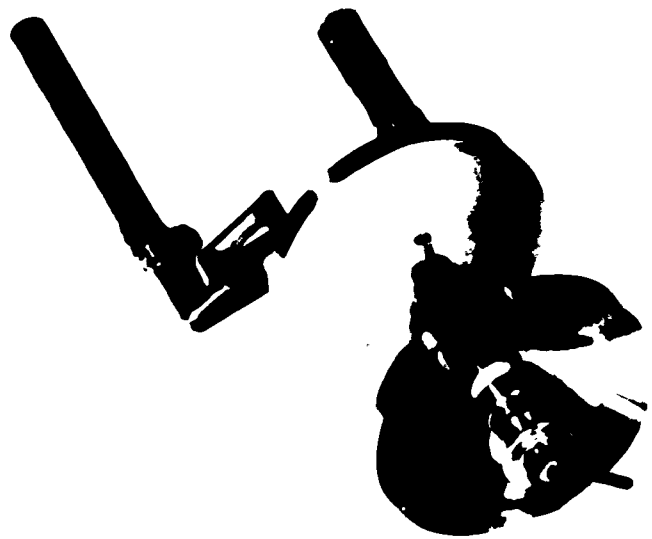

CYLINDRICAL INDIRECTLY HEATED DEVICE WITH IRIDIUM EMITTER

Figure 38

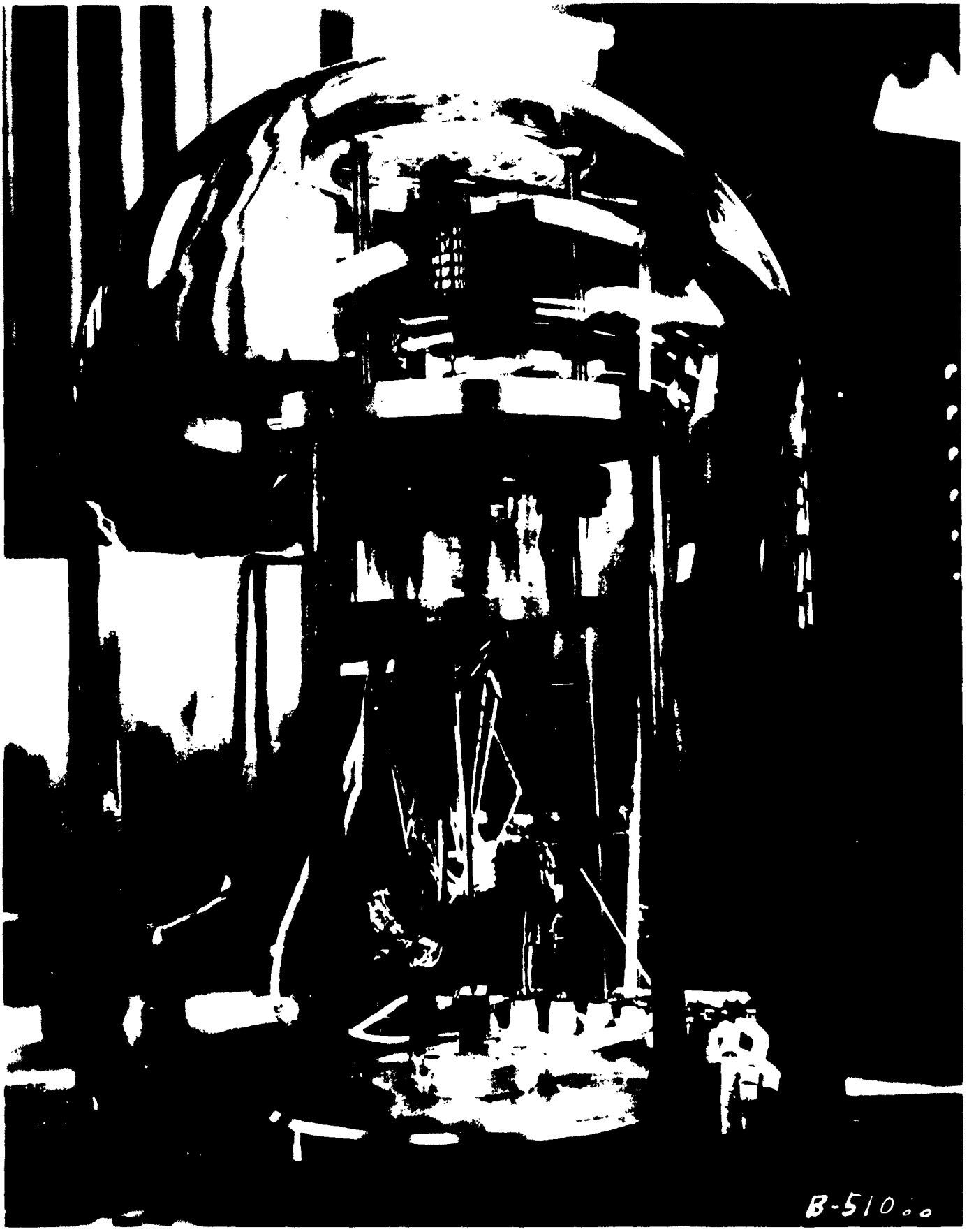

Figure 39

Figures 40 - 41

(section VIII)

Filament devices

Scale sketch of metal envelope device	Fig. 40
Photograph of glass envelope device	Fig. 41

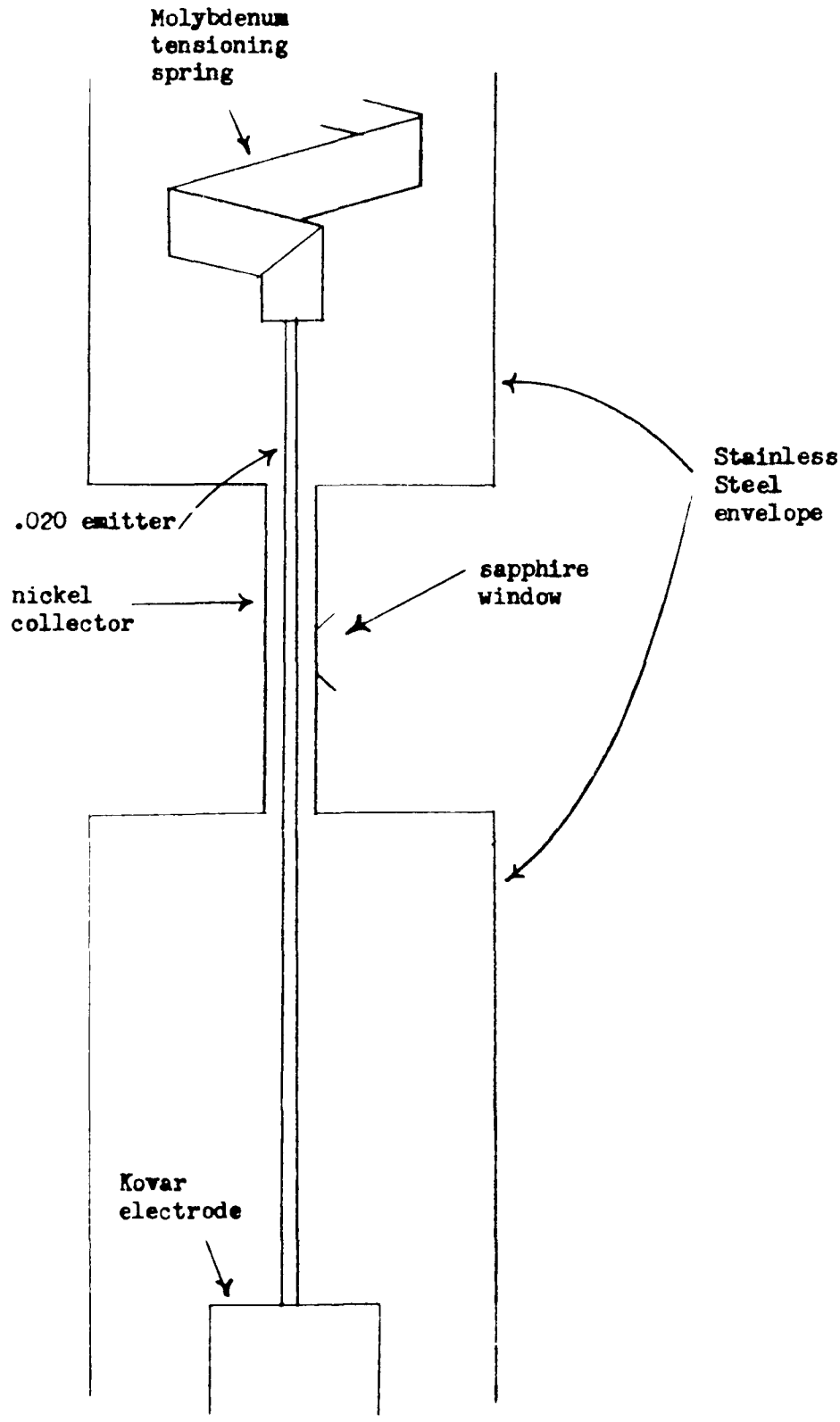

Figure 40

Scale drawing of a filament device with 0.020" filament as emitter. The emitter is positioned between a molybdenum tensioning spring and a kovar electrode so that there is a uniform temperature in the portion of the emitter which faces the collector. Not shown are ceramic-to-metal seals of both ends of the device and side-arms for evacuation and for the cesium reservoir.

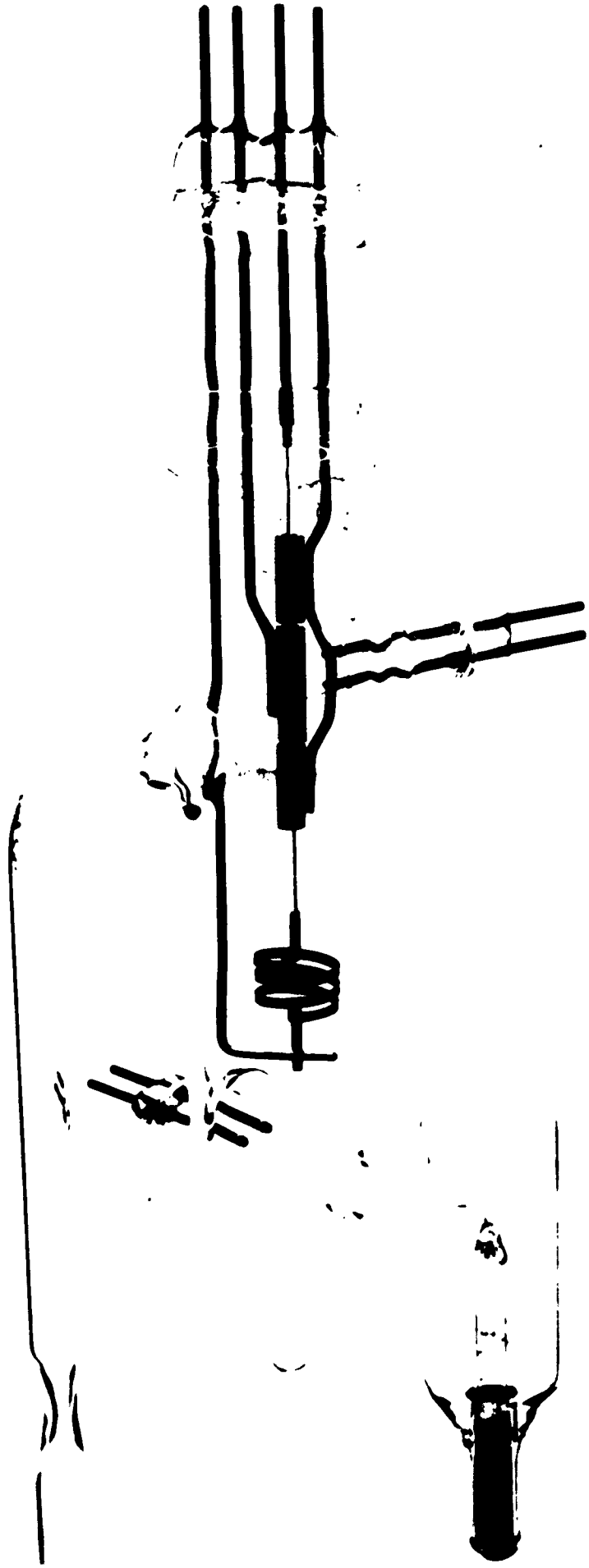

Figure 41

Figure 42 - 43

(section VIII)

Figures illustrating the comparison of the theory to the experimental results.

Mode diagram for the volume ionization mode of operation	Fig. 42
Comparison of measured characteristic curve to theoretical curve	Fig. 43

Figure 42 - 43

(section VIII)

Figures illustrating the comparison of the theory to the experimental results.

Mode diagram for the volume ionization mode of operation	Fig. 42
Comparison of measured characteristic curve to theoretical curve	Fig. 43

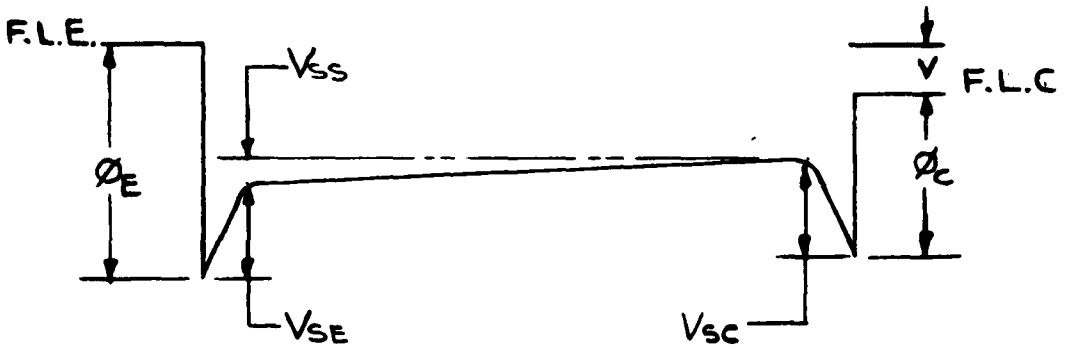

Fig. 42. Mode Diagram For Volume Ionization Mode of Operation of the Thermionic Plasma Energy Converter

MARTIN COMPANY

EC R & D LAB

Emitter - Iridium

Collector - Nickel

Gap - .030"

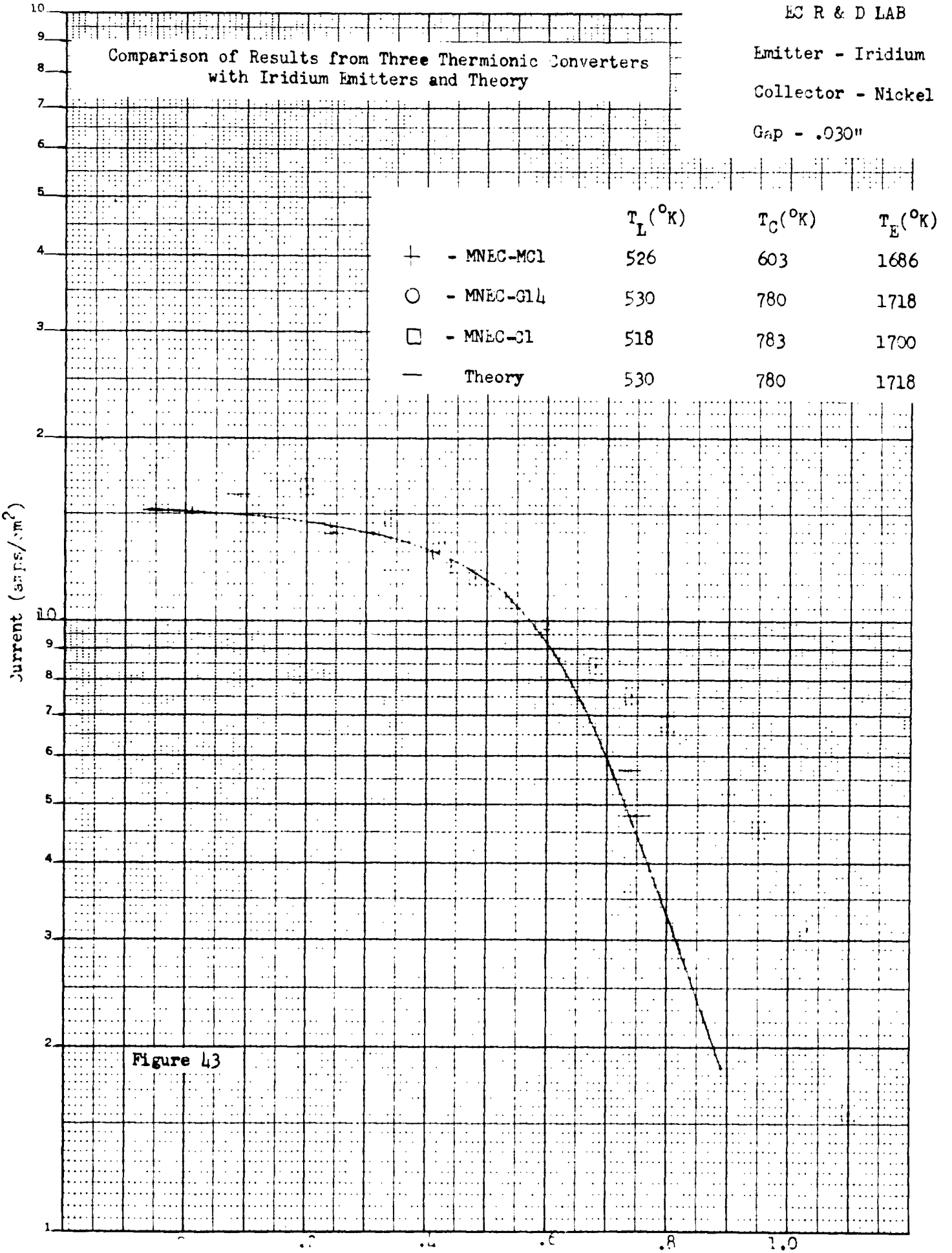

Figure 43

DISTRIBUTION LIST

	No. of Copies
Office of Naval Research Power Branch (Code 429) Department of the Navy Washington 25, D. C.	4
Office of Naval Research Power Branch (Code 429) Department of the Navy Washington 25, D. C. Attn: Comdr. J. J. Connelly	1
U. S. Naval Research Laboratory Technical Information Division Washington 25, D. C.	6
U. S. Naval Research Laboratory Washington 25, D. C. Attn: Code 6430	1
Commanding Officer Office of Naval Research Branch Office Box 39 Navy #100 Fleet Post Office New York, New York	2
Office of Technical Services Department of Commerce Washington 25, D. C.	1
Armed Services Technical Information Agency Arlington Hall Station Arlington 12, Virginia	10
National Aeronautics & Space Adminstration 1520 H. Street, N. W. Washington 25, D. C. Attn: James J. Lynch	1
National Aeronautics & Space Adminstration Lewis Research Center 2100 Brookpart Road Cleveland 35, Ohio Attn: Frank Rom Roland Breitwieser Bernard Lubarsky	1 1 1
Chief of Naval Operations (OP-07G) Department of the Navy Washington 25, D. C.	1

	No. of Copies
Commandanr, U. S. Marine Corps Code CSY-3 Headquarters, Marine Corps Washington 25, D. C.	1
Chief, Bureau of Ships Department of the Navy Washington 25, D. C.	
Attn: Code 342B	1
Code 1500, LCDR J. H. Weber	1
Code 350, LCDR F. Anders	1
Division of Reactor Development U. S. Atomic Energy Commission Washington 25, D. C.	
Attn: Auxiliary Power Branch	1
Direct Conversion Branch	1
Army Reactions & Waters Systems Branch	1
Aeronautical Systems Division ASRMFP-2 Wright Patterson Air Force Base Ohio	1
Air Force Cambridge Research Center (CRZAP) L. G. Hanscom Field Beford, Massachusetts	1
Power Information Center University of Pennsylvania Moore School Building 200 South 33rd Street Philadelphia 4, Pennsylvania	1
Director of Special Projects (SP-001) Department of the Navy Washington 25, D. C.	10
Los Alamos Scientific Laboratory P. O. Box 1663 Los Alamos, New Mexico	
Attn: Dr. George M. Grover	1
Argonne National Laboratory 9700 South Cass Avenue Argonne, Illinois	
Attn: Aaron J. Ulrich	1
Director, Advanced Research Projects Agency The Pentagon Washington 25, D. C.	
Attn: Dr. John Huth	2

	No. of Copies
U. S. Army Signal R & D Laboratory Fort Monmouth, New Jersey Attn: Emil Kittil	1
Mr. A. F. Underwood Manager, General Motors Research Labs 12 Mile and Mound Road Warren, Michigan Attn: Dr. F. Jamerson	1
Atomics International P. O. Box 309 Canoga Park, California Attn: Dr. R. C. Allen	1
General Atomic P. O. Box 608 San Diego 12, California Attn: Dr. R. W. Pidd	1
Republic Aviation Farmingdale Long Island, New York Attn: A. Schock	1
Allied Research Associates, Inc. 43 Leon Street Boston 15, Massachusetts Attn: Dr. P. Goodman	1
Ford Instrument Company 3110 Thomas Avenue Long Island City, New York Attn: T. Jarvis	1
Armour Research Foundation 10 W. 35th Street Chicago 16, Illinois Attn: Dr. D. W. Levinson	1
Jet Propulsion Laboratory California Institute of Technology 4800 Oak Grove Drive Pasadena, California	1
RCA Laboratories David Sarnoff Research Center Princeton, New Jersey Attn: Dr. P. Rappaport	1
Thermo Electron Engineering Corporation 85 First Avenue Waltham 54, Massachusetts Attn: Dr. George Hatsopoulos	1

	No. of Copies
Hughes Research Laboratories 3011 Malibu Canyon Road Malibu, California Attn: Dr. R. C. Knechtli	1
Thomson Rano Wooldridge, Inc. 7209 Platt Avenue Cleveland 4, Ohio Attn: Wm. J. Leovic	1
General Electric Research Laboratory Schenectady, New York Attn: Dr. V. C. Wilson	1
Westinghouse Electric Company Research Laboratories Beulak Road, Churchilboro Pittsburgh, Pennsylvania Attn: Dr. Max Gavbuny	1
Massachusetts Institute of Technology 77 Massachusetts Avenue Cambridge, Massachusetts Attn: Dr. White	1
The Marquardt Corporation ASTRO Division 16555 Saticoy Street Van Nuys, California Attn: A. N. Thomas	1
Texas Instruments, Inc. P. O. Box 5474 Dallas 22, Texas Attn: Dr. R. A. Chapman	1
University of Denver Colorado Seminary Denver Research Institute Denver 10, Colorado Attn: Dr. Charles B. Magee	1
Radio Corp. of America Electron Tube Division Lancaster, Pennsylvania Attn: F. G. Block	1
Electro-Optical Systems, Inc. 125 N. Kinedo Avenue Pasadena, California Attn: A. Jensen	1

	No. of Copies
General Electric Company P. O. Box 846 Atomic Product Division Vallecitos Laboratory Pleasenton, California Attn: Robert Scott	1
General Electric Company Power Tube Division 1 River Road Schenectady 5, New York Attn: Mr. Wm. Miller	1

Martin Marietta Corporation, Nuclear Division
Baltimore 3, Maryland
STUDY PROGRAM ON CESIUM VAPOR-FILLED THERMIONIC CONVERTERS HAVING IRIDIUM EMITTERS, Yearly Technical Report for the Period 1 November 1961 through 29 October 1962, by M. E. Talaat, D. S. Trimmer and A. J. Kennedy. December 1962. MND-2934, 87 pages, including figures.
Contract Nonr-3639(00) Unclassified Report

An extensive mapping of the performance of cesium vapor-filled energy conversion devices was obtained for the high vacuum work function emitter materials, iridium and rhenium, for the interelectrode gap of .030". Characteristic current-versus-voltage curves and summaries of the output power density and efficiency are given for the emitter temperature range of 1550-2000°K and the cesium temperature range of 475-600°K. The data shows a systematic superiority of iridium to rhenium.

Tests with a platinum emitter device confirm the trend of good performance in cesium vapor with high vacuum work function emitter materials.

Data is given showing a highly precise agreement between two filament emitter iridium devices and an electron bombardment heated device with iridium emitter. At the emitter temperature of 1700°K, liquid cesium temperature of 525°K, and the interelectrode gap of .030", the output power density of the three devices was 5.6 ± 0.2 w/cm^2 and the energy conversion efficiency was 14.25 ± 1.25%.

The program includes a theoretical study of cesium adsorption phenomena on the electrode surfaces and of plasma phenomena in the interelectrode gap. The theory is used to predict the characteristic voltage-current curve in the volume ionization mode of operation, and is applied to the test data.

UNCLASSIFIED

1. Direct Energy Conversion
2. Thermionics
I. M. E. Talaat
II. D. S. Trimmer
III. A. J. Kennedy
IV. Martin Marietta Corporation Report MND-2934
V. Nonr-3639(00)

MARTIN

UNCLASSIFIED

Martin Marietta Corporation, Nuclear Division
Baltimore 3, Maryland
STUDY PROGRAM ON CESIUM VAPOR-FILLED THERMIONIC CONVERTERS HAVING IRIDIUM EMITTERS, Yearly Technical Report for the Period 1 November 1961 through 29 October 1962, by M. E. Talaat, D. S. Trimmer and A. J. Kennedy. December 1962. MND-2934, 87 pages, including figures.
Contract Nonr-3639(00) Unclassified Report

An extensive mapping of the performance of cesium vapor-filled energy conversion devices was obtained for the high vacuum work function emitter materials, iridium and rhenium, for the interelectrode gap of .030". Characteristic current-versus-voltage curves and summaries of the output power density and efficiency are given for the emitter temperature range of 1550-2000°K and the cesium temperature range of 475-600°K. The data shows a systematic superiority of iridium to rhenium.

Tests with a platinum emitter device confirm the trend of good performance in cesium vapor with high vacuum work function emitter materials.

Data is given showing a highly precise agreement between two filament emitter iridium devices and an electron bombardment heated device with iridium emitter. At the emitter temperature of 1700°K, liquid cesium temperature of 525°K, and the interelectrode gap of .030", the output power density of the three devices was 5.6 ± 0.2 w/cm^2 and the energy conversion efficiency was 14.25 ± 1.25%.

The program includes a theoretical study of cesium adsorption phenomena on the electrode surfaces and of plasma phenomena in the interelectrode gap. The theory is used to predict the characteristic voltage-current curve in the volume ionization mode of operation, and is applied to the test data.

UNCLASSIFIED

1. Direct Energy Conversion
2. Thermionics
I. M. E. Talaat
II. D. S. Trimmer
III. A. J. Kennedy
IV. Martin Marietta Corporation Report MND-2934
V. Nonr-3639(00)

MARTIN

UNCLASSIFIED

Martin Marietta Corporation, Nuclear Division
Baltimore 3, Maryland
STUDY PROGRAM ON CESIUM VAPOR-FILLED THERMIONIC CONVERTERS HAVING IRIDIUM EMITTERS, Yearly Technical Report for the Period 1 November 1961 through 29 October 1962, by M. E. Talaat, D. S. Trimmer and A. J. Kennedy. December 1962. MND-2934, 87 pages, including figures.
Contract Nonr-3639(00) Unclassified Report

An extensive mapping of the performance of cesium vapor-filled energy conversion devices was obtained for the high vacuum work function emitter materials, iridium and rhenium, for the interelectrode gap of .030". Characteristic current-versus-voltage curves and summaries of the output power density and efficiency are given for the emitter temperature range of 1550-2000°K and the cesium temperature range of 475-600°K. The data shows a systematic superiority of iridium to rhenium.

Tests with a platinum emitter device confirm the trend of good performance in cesium vapor with high vacuum work function emitter materials.

Data is given showing a highly precise agreement between two filament emitter iridium devices and an electron bombardment heated device with iridium emitter. At the emitter temperature of 1700°K, liquid cesium temperature of 525°K, and the interelectrode gap of .030", the output power density of the three devices was 5.6 ± 0.2 w/cm^2 and the energy conversion efficiency was 14.25 ± 1.25%.

The program includes a theoretical study of cesium adsorption phenomena on the electrode surfaces and of plasma phenomena in the interelectrode gap. The theory is used to predict the characteristic voltage-current curve in the volume ionization mode of operation, and is applied to the test data.

UNCLASSIFIED

1. Direct Energy Conversion
2. Thermionics
I. M. E. Talaat
II. D. S. Trimmer
III. A. J. Kennedy
IV. Martin Marietta Corporation Report MND-2934
V. Nonr-3639(00)

MARTIN

UNCLASSIFIED

Martin Marietta Corporation, Nuclear Division
Baltimore 3, Maryland
STUDY PROGRAM ON CESIUM VAPOR-FILLED THERMIONIC CONVERTERS HAVING IRIDIUM EMITTERS, Yearly Technical Report for the Period 1 November 1961 through 29 October 1962, by M. E. Talaat, D. S. Trimmer and A. J. Kennedy. December 1962. MND-2934, 87 pages, including figures.
Contract Nonr-3639(00) Unclassified Report

An extensive mapping of the performance of cesium vapor-filled energy conversion devices was obtained for the high vacuum work function emitter materials, iridium and rhenium, for the interelectrode gap of .030". Characteristic current-versus-voltage curves and summaries of the output power density and efficiency are given for the emitter temperature range of 1550-2000°K and the cesium temperature range of 475-600°K. The data shows a systematic superiority of iridium to rhenium.

Tests with a platinum emitter device confirm the trend of good performance in cesium vapor with high vacuum work function emitter materials.

Data is given showing a highly precise agreement between two filament emitter iridium devices and an electron bombardment heated device with iridium emitter. At the emitter temperature of 1700°K, liquid cesium temperature of 525°K, and the interelectrode gap of .030", the output power density of the three devices was 5.6 ± 0.2 w/cm^2 and the energy conversion efficiency was 14.25 ± 1.25%.

The program includes a theoretical study of cesium adsorption phenomena on the electrode surfaces and of plasma phenomena in the interelectrode gap. The theory is used to predict the characteristic voltage-current curve in the volume ionization mode of operation, and is applied to the test data.

UNCLASSIFIED

1. Direct Energy Conversion
2. Thermionics
I. M. E. Talaat
II. D. S. Trimmer
III. A. J. Kennedy
IV. Martin Marietta Corporation Report MND-2934
V. Nonr-3639(00)

MARTIN

UNCLASSIFIED